Geant4 Studies On Various Scintillation Detection Systems And Dose Values At Different Radiation Types

HAKAN TILAVER

Master of Science by Research

University of York
Physics

September 2022

Abstract

In this thesis, various applications of Geant4 simulation studies were investigated by using various scintillation detector systems in different radiation types. In the first chapters, after focusing on the theoretical background of radiation, radiation detection and general information about scintillation detection systems and electronics, naturally occurring radioactive sources and nuclear and oil/gas installations that have enormous effects on human health are mentioned.

In the thesis, first of all, the energies, absorption doses and dose distributions of monoenergetic Alpha, Beta (Electron and Positron) and Gamma particles deposited in the water phantom were obtained with the Gate simulation program. Since even a small portion of this absorbed radiation energy can have very large biological consequences, dose values in water-equivalent phantom for use in tissues located in and around the target tumor volume for radiotherapy are discussed.

After determining the dose values, the study on the interaction of the CsI(Tl) scintillator, which is frequently used in nuclear physics applications, with the Co-60 radioactive source is explained. In the experimental measurement and simulation model, the Co-60 radiation source was positioned at different angles to the CsI(Tl) detector block in order to investigate which interaction type is more dominant in a certain energy range. In this way, the most ideal angle value was determined and the most suitable radiation source location was determined in the new type detector systems designed afterwards.

In the last part of the thesis, a three-layer phoshwich type detector system that can be used in molecular imaging system and nuclear and oil/gas installations has been investigated. The interaction percentage of each layer for different radiations (alpha, beta and gamma) was calculated by simulation of three-layer hollow cylindrical scintillators. A three-layer detection system consisting of ZnS(Ag), EJ212 and LaBr(Ce) scintillation materials was used and Am-241, Sr-90 and Cs-137 radiation sources were irradiated with the help of Geant4 based GATE simulation program.

Moreover, a new cylindrical simulation, which can be used in nuclear decommissioning as well as medical imaging, was modeled and the detection percentages of some of the naturally occurring radiation sources (K-40 and Pb-210) were obtained, and comparisons were made between systems and previous studies in the literature.

Contents

List of Figures

List of Tables

Acknowledgements

First of all, I am very grateful to my supervisor, Professor David Jenkins, for his invaluable advice and suggestions and for his unconditional support throughout this research thesis. I am indebted to my Research Master for his extraordinary encouragement and wonderful advice. Without his directives, this thesis would not have been possible.

I would also like to thank Pankaj Joshi for all his help during the first few months of my graduate studies and beyond, especially during the experiments in the laboratory. I must also thank Julien Bordes for his great advice for his help and helpful feedback on Geant4 simulations.

I am also very grateful for the help I have received from various people with many different expertise. Access to such people is the direct result of the close community of nuclear physics groups in York. I've been very productive with these inspiring people. My tap member Prof. Steve Tear and GSC Chair Prof. Alison Laird has always given me all their support and encouragement. I would also like to thank the Department of Physics and support technicians for providing equipment and technical advice.

Finally, I am grateful to my dear family, who supported me throughout my university education. And, I should also thank my relatives who made me ambitious when I was stressed and tired during my graduate research.

Author’s Declaration

I declare that this thesis is a presentation of original work, and I am the sole author. This work has not previously been presented for an award at this, or any other, University. All sources are acknowledged as References.

Chapter 1

1. INTRODUCTION

In physics, from the late 19th century to the beginning of the 20th century, classical physics theories were thought to be sufficient to explain all physical events and interactions in nature. Mechanical events are explained by Newton's laws, electrical and optical events are explained by Maxwell's equations, and thermodynamic events are explained using Statistical Mechanics theory. However, some experiments (Photoelectric Effect, Compton Scattering, Blackbody Radiation, Diffraction and Interference of Electron, etc.) made at the beginning of the 20th century could not be explained within the framework of these theories. New theories were needed to explain these experimental results. One of these theories is the "Quantum Mechanics" theory, which is used to explain the micro world (such as particles, atoms and molecules). With the emergence of quantum mechanics, interactions between particles, atoms, molecules, electron-nucleus, nucleus-nucleus in many fields of physics such as Nuclear Physics, Atomic and Molecular Physics and Particle Physics have been investigated by analyzing the wave function obtained from the Schrödinger equation's solution in the presence of an external potential.

One of the most useful ways to understand the nature of atoms, molecules or elementary particles is the scattering method. Basically, in the scattering problem - scintillators were used in this study - the direction and energies of the particles scattering from the atoms of these materials are studied by sending another particle with a certain energy onto the target particle or the material fixed at a certain point (Scintilators). Usually, as an unstable nucleus that is radioactive undergoes a change to become more stable, it emits radiations that can be measured with suitable measuring instruments. In this way, it is possible to monitor the substance involved in any event through radioactive isotopes. High-energy radiation can pass through various materials. This transition depends on the radiation energy, the type and thickness of the material. A radiation passing through matter leaves some of its energy in the matter and some changes occur in its properties. By detecting these changes, it is possible to obtain some information about the material through which the radiation passes. Because radiation can affect both living and non-living matter. Its effect on living things is in the form of some structural and functional changes, sometimes even fatal [1].

In the thesis project, firstly, cubic Water Phantom was started to work in order to determine the dose and absorbed energy values, then it was continued to work with a rectangular prism shaped Cesium Iodide (CsI) scintillation crystal to determine the most suitable and dominant angle and to observe the relevant scattering. And finally, a hollow cylindrical Phoswich detector systems were designed and related scatterings were investigated for different application areas (especially Naturally Occurring Radioactive Materials-NORM). Here, in fact, our main goal in the scattering problem caused by the interaction of these particles with these potentials is to find the transition and reflection coefficients by using the wave function obtained from the solution of the wave equations. These coefficients allow us to determine what probabilities and energies the particle scatters as a result of its interaction with the potential. Because it would be appropriate to say that all the ionizing radiation detectors used in the systems designed here are frequently used in applications such as nuclear energy, nuclear safety, nuclear decommissioning and medical imaging, and nuclear and particle physics [2].

Here, since all ionizing radiation detectors used in the systems designed through this thesis work have a wide range of uses in applications such as nuclear energy, nuclear safety, nuclear deactivation and medical imaging, nuclear and particle physics, radiation leaks in nuclear power plants anywhere in nature and its consequences amount can be calculated in a very short time and at the same time, and it will be possible to measure the presence of naturally occurring radioactive materials in the relevant study area. In this way, it will be possible to take faster measures on the effects on the lives of people working in these environments or exposed to this radiation.

Particle detectors used in the laboratory environment for all these purposes and photosensors required for signaling are increasing their importance in the literature day by day. Because these tools and equipment are needed in all high energy physics experiments. Many computer programs are used to develop these materials. These materials, which are first simulated in the computer environment, are then prepared in the laboratory environment and real products are tried to be obtained. The most important of these computer programs used is the Monte-Carlo-based Geant4 simulation program created with the C++ programming language. After the Geant4 simulation program proved its usability in many areas, it continued its development and Gate simulation program was created to enable it to be used in medical applications.

1.1 Overview of the Thesis

In the first part of this thesis, after introducing the roadmap related to the aim of the thesis project, the tools and equipment used in the project are briefly mentioned.

In the theoretical considerations of the second part, after the fundamental concepts of radiation and radioactive particles, which form the main body of the thesis project, are introduced, alpha, beta particles and gamma rays are mentioned, then the interactions of these alpha particles, beta particles and gamma rays with materials are mentioned.

In the third chapter, particle detectors and scintillation crystals, which are needed and used in the interaction of these particles with the material, are mentioned. Photosensors, which are frequently mentioned in the literature, are included for signaling purposes.

In the fourth chapter, after giving information about Naturally Occurring Radioactive Materials (NORM) as another application area of the thesis, at the end of this chapter, some Geant4 and Gate simulation studies using alpha, beta particles and gamma rays, which played a guiding role in this thesis work, are briefly mentioned.

The Monte-Carlo Method is briefly mentioned in the Material and Method part of the fifth chapter. Then, information is given about Geant4 and Gate simulation programs created by this method. After giving information about the important radiation sources and scintillation crystals that were decided for the thesis study and used in the simulation, simulation studies were carried out. Then there are the Geant4 and Gate simulations created for this thesis project.

In the Results section, which is the sixth chapter, after the relevant data and results obtained as a result of each simulation study are presented separately, some comments and discussions on the results of these data and graphics are given separately for each study.

In the Conclusion part of the seventh chapter, the thesis was completed by focusing on the solutions to which problems by using which physical systems in which ways. At the end of the thesis, there are references, appendices, coding and abbreviations.

Chapter 2

2. THEORETICAL CONSIDERATIONS

2.1 Fundamental Concepts

Here, first of all, the definition of radiation and some of its properties are briefly explained below. The energy of electromagnetic waves and the energy of high-speed particles are called radiation. And these propagate in the form of particles or waves. It is used for electromagnetic waves that do not need any material field for their propagation. However, since water and sound waves need a field to propagate, they are not considered radiation. They radiate from a source in all directions. When radiation is emitted in a vacuum field, its energy is conserved and the intensity of this emitted radiation acts according to the inverse square law. However, in the case of non-point sources such as a laser beam, light bulb filament, or microwave antenna, the inverse square law can be broken [3, 4].

2.2 Electromagnetic Radiation

Electromagnetic radiation is the diffusion of energies from Atoms that occur in different situations. Electromagnetic radiation is a combination of electric and magnetic fields. As mentioned above, they do not need any material space to spread. Their speed in vacuum is the speed of light. If they pass through a material medium, they leave their energy to the medium they enter, and therefore their speed will be reduced. In quantum physics, EM waves have both a wave structure and a particle structure. These particles are called photons. Photon energy is represented by the relation $\boldsymbol{E = h\nu}$. The ν in this relation is called the frequency. ν, frequency is given by the equation $\boldsymbol{\nu = c/\lambda}$ [5,6].

When electromagnetic radiation is mentioned, ionizing and non-ionizing radiation are encountered in the literature. These radiations; radio waves, microwave signals, infrared rays, visible rays, ultraviolet rays, X rays and gamma rays.

As can be seen in Figure 2.1, there are frequency differences as these beams pass from one to the other.

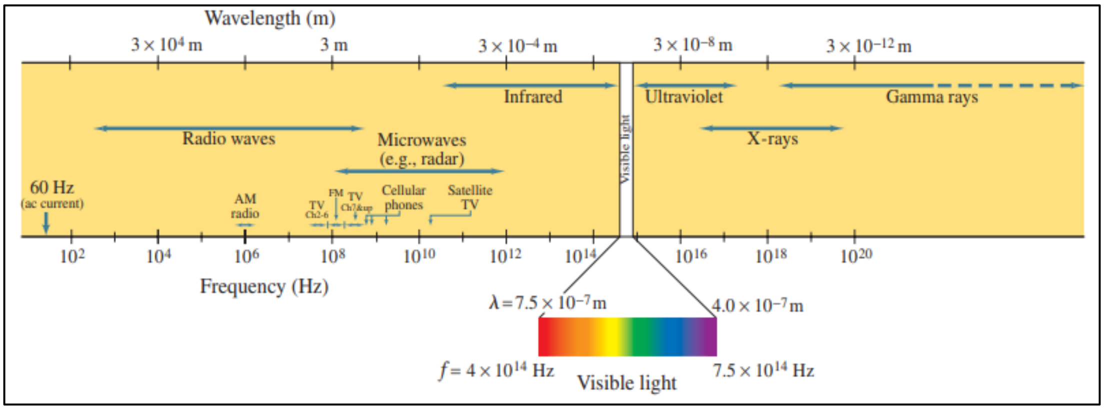

Figure 2. 1: *Electromagnetic Radiation Spectrum. Adapted from Ref. [7].*

2.3 Ionized and Non-Ionized Radiations

When looking at their energies, radiations are divided into two as ionizing and non-ionizing radiations, depending on whether they ionize an atom or not. A condition called ionization is the removal of electrons from atoms, and usually the outer orbital electrons are removed from the atoms.

Protons and neutrons, gamma rays, x-rays, alpha particles and beta particles are the particles that cause ionizing radiation. Ionizing and non-ionizing radiations can be harmful to living things and cause significant changes in nature. Ionizing radiation usually causes more harm to living things than non-ionizing radiation because of the energy they deposit.

Radiation can occur in the form of excitation and ionization in terms of its physical effect. Since the chemical structures of atoms and molecules are disrupted in ionization, they interact with cellular structures and cause the formation of free radicals. As a result, there is a change in the biological structure and damage occurs in the genetic structures of the chromosomes. This leads to the death of the cell. Due to this interaction, cancer occurs and ionizing radiation is used in its treatment. Non-ionizing radiations are also harmful because they store thermal energy in living things. An example is microwave ovens. Ionizing radiation detectors are frequently used in many applications such as nuclear energy, nuclear safety, nuclear decommissioning and medical imaging [3].

2.3.1 Use of Ionizing Radiation in Medical Diagnosis and Treatment

Radiation is used in diagnosis and treatment due to some of its properties. They are used in medical applications for images (radiology) and to destroy cells and cancers with radiation (radiology). The I^{131} isotope (oral and intravenous) is used for thyroid imaging and kidney monitoring. The Tc^{99m} isotope is used in brain scanning; If there is a tumor in the brain, this element concentrates there and the activity increases there. Similar to these activities, high-energy particles were sent to the water phantom and the relevant dose and the energy values deposited in the water were calculated in the study. Because it is aimed to obtain the closest results similar to the human body. X-ray or computerized imaging CAT and PET techniques are used with these radioisotopes injected into the human body in reality [4].

2.3.2 Excitation and Ionization

If the energy transferred to the orbiting electron exceeds the energy level of the electron, the electron jumps to a higher energy level. In this case, the electron is excited. If enough energy is given to this electron, it will completely get rid of the effect of the nucleus and move away. In this case, the atom is ionized. In order to reveal this situation more clearly, Co-60 radiation source was sent on the CsI scintillation crystal in the material-method section and the most dominant interaction type was tried to be determined by focusing on the interactions at the most ideal angle.

Some events where there is an energy level change for the orbital electrons of the atom cause radiation emission in the visible region and UV region. If there is enough energy for ionization, this is attributed to X-rays. The discrete energy levels of electrons in an atom also apply to nucleons in the nucleus. In this respect, let's briefly talk about the structure of the kernel [5].

2.4 Nucleus Forces

Protons and neutrons are bound with each other in the nucleus by nuclear forces that overcome the Coulomb repulsion. They are effective at a distance of about $10^{-15}m$.

As can be seen in Figure 2.2, the binding energies of nucleons to the nucleus is in the order of MeV, which is 1000 times the binding energy of electrons to atoms. Accordingly, the energy required in nuclear reactions is 10^6 times higher than in chemical reactions [6, 7, 8].

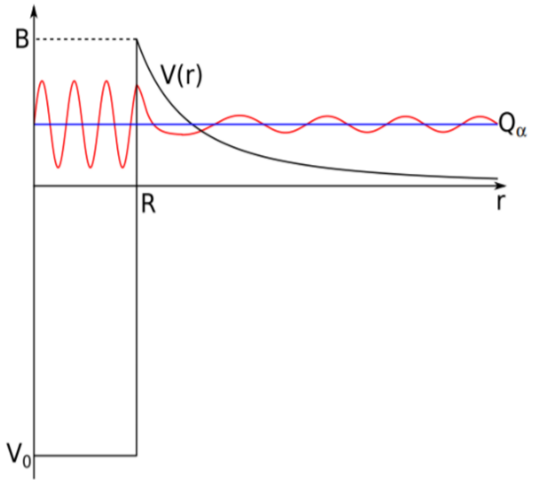

Figure 2. 2: *General schematic of alpha tunnelling showing the nuclear square well potential with depth, V_0 and the Coulomb barrier height, B. The potential falls off as a function of radius, V(r), outside the nuclear radius, R. The decay Q value, Q_α is indicate. Adapted from Ref. [8].*

2.5 Nuclear Binding Energy

The total weight of the masses of the individual nucleons in the nucleus is less than the mass of the nucleus. The mass difference is converted into binding energy according to the equation $\boldsymbol{E} = \boldsymbol{mc^2}$.

One twelfth of the mass of a ^{12}C atom is defined as an atomic mass unit (u). One atomic mass unit complies to an energy value of 931.5 MeV.

In nuclear reactions, mass loss is released as nuclear energy. Therefore, the binding energy of the formed products increases [5].

An example of a nuclear reaction and the released nuclear energy are shown below:

$$ {}_0^1n + {}_1^1H \rightarrow {}_1^2H_1 + \gamma \tag{1} $$

2.6 Nuclear Stability

The energy released from the reaction in equation (1) above is carried by the photon emitted as a result of the reaction and is 2.224 MeV. This value is the binding energy of the product particle deuteron.

The attractive nuclear forces are the same between $p-p, n-n \: or \: n-p$.

In the nucleus, these forces attract nucleons to each other, while protons repel each other with the Coulomb force. If the Coulomb repulsion exceeds the nuclear force, that nucleus is stable.

As can be seen in Figure 2.3, light nuclei are much more stable when the stability line is N=Z. However, when the stability line is N>Z, it can be said that heavy nuclei are much more stable. More neutrons are needed to counter the additional Coulomb repulsion. Nuclei with $Z > 83$ are unstable [6].

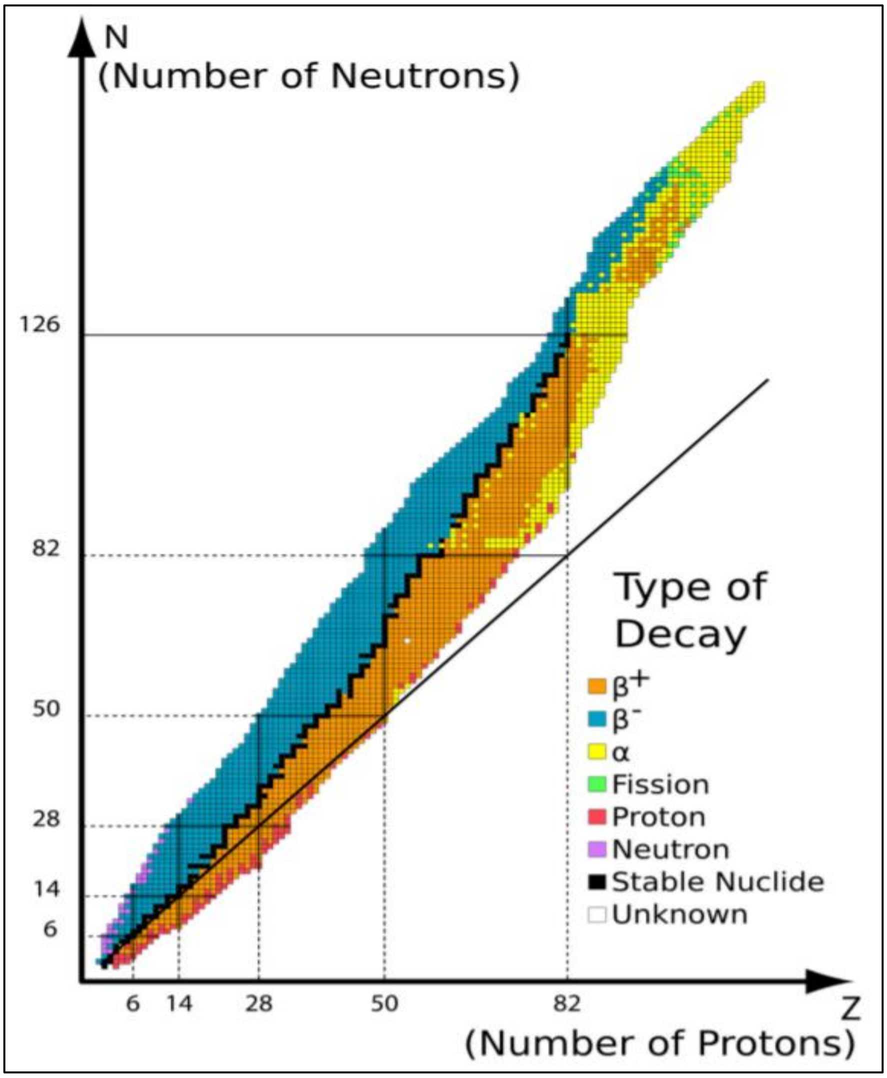

Figure 2. 3: *An 'isotope chart' representing each known isotope with a square colored box. The horizontal axis corresponds to the increasing atomic number Z, while the vertical axis represents the increasing neutron number N. Black squares are stable isotopes. Light blue squares are isotopes that undergo* β^- *decay, while orange ones are isotopes that undergo* β^+ *or electron capture* (EC) *decay. The yellow squares are mainly isotopes that decay by α emission, while the green squares are isotopes that mostly decay by spontaneous fission. Purple squares are isotopes that decay by fast neutron emission, while red squares are those that decay by fast proton emission. Adapted from Ref. [8].*

2.6.1 Periodic Table and Radioactive Detection

Elements are divided into groups according to their physical and chemical properties in periodic table. The grouping of nuclei arranges to show the nuclear properties of a particular nucleus. A nucleus is represented by its mass and atomic number.

Radioactive decay is the event that a nucleus loses its mass or energy to become more stable. The word radionuclide is also used to indicate that an atom is radioactive [7].

Common types of decay can be listed as follows:

- *Gamma Emission*
- *Alpha Particles Decay*
- *Beta Particles Decay*
- *Electron Decay*
- *Positron Decay*

2.7 Radioactivity

Rays emitted from radioactivity can be classified into three different types as Alpha (α) , Beta (β) and Gamma (γ).

As can be seen in Figure 2.4, because of their large mass, α-particles can travel short distances, but cause many ionizations before being stopped. They cannot pass through dead skin and can be blocked with a thin paper. So they cannot do external radiation damage. So they cannot do external radiation damage.

β particles penetrate to different depths in different substances depending on their energy. For example, they can go up to $3\ mm$ from aluminum. Most of these cannot pass through the skin, but those with high energy can.

Gamma rays can penetrate a lead plate several centimeters [6, 8].

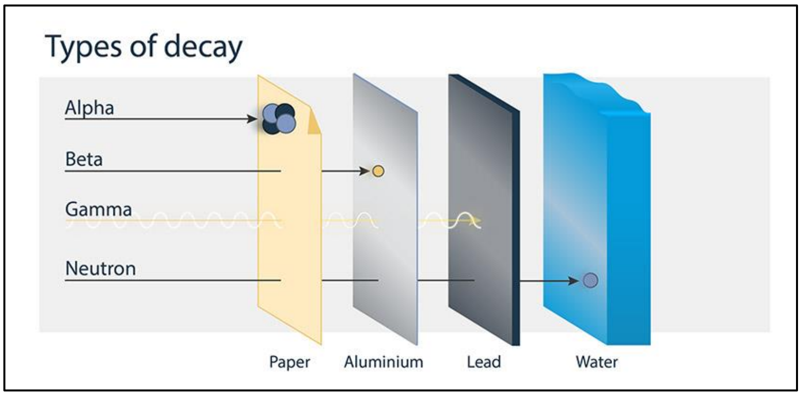

Figure 2. 4: *Representation of the relative ranges of different types of ionizing radiation in various substances (here, let's assume incoming radiation with an energy of about 1 MeV). Alpha particles are even stopped by, say, 10 s micron material (a sheet of paper). Beta particles are blocked by about 1 mm of Aluminium. Gamma rays are blocked by a few centimeters of lead. Adapted from Ref. [8].*

2.7.1 Alpha Particles

Alpha particles are high-energy Helium nuclei. When the proton/neutron ratio is too small, they are emitted from the nucleus of the radioactive isotope. They have a positive charge and consist of 2 protons and 2 neutrons [6].

As a result of alpha fission, the atomic number of the radioactive isotope decreases by two while its mass number decreases by four.

$$_{Z}X^{\mathrm{A}} \rightarrow \ _{Z-2}Y^{\mathrm{A\text{-}4}} + \ _{2}\alpha^{4} \tag{2}$$

Alpha particle fragmentation theory was first proposed in 1928 by Gamow, Gondon and Gurney. According to the theory, there are nucleons in the nucleus. Two neutrons ($_{1}n^{0}$) and two protons ($_{1}H^{1}$) combine as alpha. In other words, there are alpha groups in nuclei. These neutrons and protons exchange energy with other nucleons.

It is known that there is Coulomb repulsion between charged particles. But these repulsive forces are small compared to nuclear forces. Nuclear forces are close range forces. Alphas exist in the nucleus at a certain E_0 energy level and move in a region of the nucleus surrounded by the potential energy barrier, U. In the case where $E_0 < U$, it can be said classically that the particle does not have the energy to cross the potential energy barrier. However, according to quantum physics, the wave of the particle has the ability to overcome this obstacle as if there were a hole. This is called the tunnel event. At the same time, the probability of this particle escaping from the nucleus per unit time is called the fragmentation constant and is denoted by λ [7, 8].

2.7.2 Beta Particles

Beta radiation is particles emitted by most radioisotopes, sometimes alone, but often in conjunction with gamma radiation. Although they have a positive or negative charge, beta particles are generally symbolized for negative particles in the literature [6].

These particles first emanate from the Nucleus and then react with a substance, after these events, their energy decreases and eventually they become free electrons. These Electrons are symbolized as β^-. The positively charged beta particles are called "positrons" and are symbolized as β^+.

Positrons have a very short lifetime at the microsecond level and can be destroyed by the emission of a $0.51\ MeV$ gamma photon pair. This radiation is also called “annihilation radiation” [7].

While neutrons in the nucleus transform into protons, electrons are formed as a result of this transformation. Positrons are formed as a result of the conversion of protons in the nucleus into neutrons [8]. These formations are represented by equations below.

For Electrons:

$$n \rightarrow p + \beta^- + v^+ + Energy \tag{3}$$

For Positrons:

$$p \rightarrow n + \beta^+ + v^- + Energy \tag{4}$$

2.7.3 Gamma Rays

Gamma radiation, an electromagnetic radiation, is produced by atomic nuclei as a result of radioactive decay. These gamma rays have the highest frequency radiation and are among the most dangerous to human life among other ionizing radiations.

Gamma rays are in the high-energy or high-frequency part of the electromagnetic spectrum. Gamma-ray emission is usually associated with an electromagnetic transition between quantized excited states of a given nucleus. Observations on the structure of various binary and even binary nuclei with different masses and different fundamental structures show that the respective transition energies are in the range of keV to MeV. In principle, transition energies can range from a few eV to $10s\ MeV$.

Although this represents a significant overlap with the energy range of x-rays (in the keV region), the tradition is to distinguish these two types of ionizing radiation based on their origin, i.e. gamma ray is emitted by a nucleus and x-rays are rearrangements of electrons in the atomic Shell [6, 7, 8].

2.8 Interaction of Ionising Radiation with Materials

Considering the behavior of various types of ionizing radiation in their interactions with matter, these types of radiation define direct ionizing radiations as alpha particles and electrons, while gamma rays are defined as indirect ionizing radiation.

To understand how the various types of ionizing radiation interact with materials in all situations (solid, liquid, and gas), one must first understand how detectors are selected in nuclear physics and applications, and then how they work. Normally, alpha particles can be blocked with a piece of paper, beta particles with a thin sheet of metal, and gamma rays can be blocked with a lead wall of a certain thickness, which is often encountered in the literature.

By means of materials, alpha and beta particles that cause atoms to ionize, which directly ionize, and scattered gamma rays, which indirectly ionize, can all be distinguished from each other.

When looking at the content of conservatism in materials, it is necessary to look at how gamma rays can effectively lose all their energy through certain interactions, but how heavy ions such as alpha particles lose their energy through many interactions with the constituents of matter. Considering these interactions, Geant4 simulation program, which is a Monte-Carlo-based simulation program that is frequently used in detector and particle interaction design today, provides important contributions to a wider range of scientists [6, 8].

2.8.1 Alpha Particles Interactions

Alpha particles interact with Coulomb forces, and they do so between the positive charges of the atom and the negative charges of the orbital electrons. When charged particles enter any absorbing field, they interact with more than one electron at the same time. In this type of interaction, electrons are subjected to the attractive Coulomb force as they move around the particle.

Depending on the range of the interaction, this exposure may be enough to either move the electron to a higher shell in the absorber atom - this is called excitation - or to remove the electron from the atom altogether - this is called ionization. The energy transferred to the electron corresponds to the energy of the charged particle, and therefore the velocity of the charged particle decreases at the end of the interaction [6].

The paths followed by heavily charged particles in the deceleration processes are shown schematically in the Figure 2.5 below.

Since alpha particles are not significantly deflected in any encounter and interactions occur in all directions at the same time, tracks tend to be fairly flat except for the very end. Therefore, charged particles are categorized within a certain distance range in a given absorber.

The results of these interactions in the absorber material are either excited atoms or ion pairs.

Each ion pair consists of a free electron and a positively charged ion, corresponding to an absorbing atom from which an electron has been completely removed. Ion pairs have a natural behavior to recombine to form neutral atoms, but in some types of detectors this is suppressed and used as a detector response.

In close interactions, the electrons can collide so great that they have enough kinetic energy to form more ions after leaving their parent atom [8].

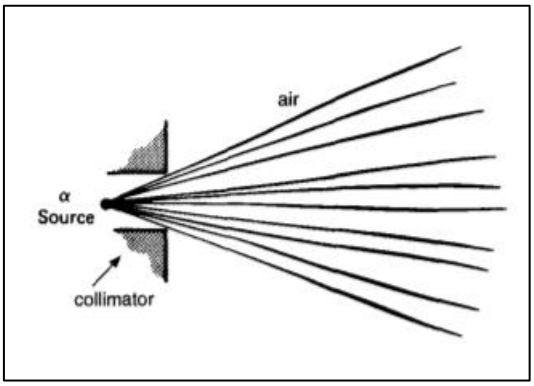

Figure 2. 5: *Pathways that heavily charged particles follow during deceleration processes. Adapted from Ref. [6].*

2.8.2 Fundamentals of Stopping Power Theory

Since the first experiments on the interaction of alpha particles with thin golden leaves, the slowing down of ions in matter is a complex issue in theory and has occupied the scientific world.

In order to make sense of the physics underlying this experiment, the stopping power at a certain energy was developed to be $S(E) = -\frac{dE}{dx}$. In this way, the energy loss per unit length for a given energy can be calculated with an accuracy of a few % for light ions such as protons, deuterons and alpha particles in the energy range $> 1\ MeV/u$.

Alpha particles are even stopped by, say, 10s micron material. on a sheet of paper, beta particles are stopped by about 1 mm of aluminum. Gamma rays are blocked by a few centimeters of lead.

During the movement of charged particles in materials, they interact with atomic electrons and lose their energy. This causes the excitation and ionization of atomic electrons. The energy loss of charged particles such as protons and alpha particles in materials is given by the Bethe–Bloch equation. Looking at the relative form of this equation derived by Fano;

$$-\frac{dE}{dx} = \frac{4\pi e^4 Z_2}{m_e v^2} Z_1^2 \left[ln \frac{2mv^2}{\langle I \rangle} - ln(1-\beta^2) - \beta^2 - \frac{C}{Z_2} - \frac{\delta}{2} \right] \quad (5)$$

where v is the velocity of the particle, $\beta = v/c$, me is the rest mass of the electron, and $\langle I \rangle$ is the average excitation potential per electron. The last two terms in the equation are the shell correction term $\frac{C}{Z_2}$ of the ion velocity in the target material and the density effect correction term $\frac{\delta}{2}$. This correction term corrects the assumption that electrons are much greater than their velocity, and corrects the difference between the electromagnetic fields in empty space and the dielectric field of the target for polarization effects at the target [6, 8].

Some corrections have been proposed to this equation, in order to be able to explain higher order terms. By defining a preliminary factor and writing $\kappa = 4\pi r_0^2 m_e c^2$, the Bethe–Bloch formula can be expressed as:

$$-\frac{dE}{dx} = \frac{\kappa Z_2}{\beta^2} Z_1^2 [L_0(\beta) - Z_1 L_1(\beta) - Z_1^2 L_2(\beta) + \cdots] \quad (6)$$

The terms on the right hand side of equation (5) are included in the term $L_0(\beta)$. But there are also two fixes L_1 and L_2 . Here, L_1—*Barcass correction* and L_2—*Bloch correction*.

The Barkas correction is sensitive to the sign of the stopping particle's charge, which takes into account the experimentally found differences between the arresting of negatively and positively charged ions. This small difference is due to the disruption of the electron cloud in the target environment caused by the charge of the intercepting particle.

The Bloch correction represents higher order terms required to fit the data, which violates the assumption that interacting particles can be treated as completely free particles [6, 8].

2.8.3 Low-velocity ions

It is known that the basic Bethe-Bloch theory is valid for high velocities, but the increased neutralization of ions at low velocities must also be taken into account. Since it is clear that individual ions cannot have fractional charges, this should be considered statistically. Northcliffe defined it as the mean value of the load-state distribution, the statistical net charge Z_1^* as follows;

$$\frac{Z_1^*}{Z_1} = 1 - \exp\left\{\frac{-v_1}{v_0 Z_1^{\frac{2}{3}}}\right\} \quad (7)$$

where v_1 is the velocity of the stationary particle and v_0 is the Bohr velocity $\frac{e^2}{\hbar}$. Obviously, at high velocities, $Z_1^* \cong Z_1$. This effect is much more significant for heavy ions than for light ions. It can be thought of as substituting Z_1^* for Z_1 in equation (6) to reproduce the experimentally observed stopping power [6, 8].

2.8.4 Range

The expression Δx, which is the stopping range of a particle in a substance, can be expressed by the integral of the inverse of the stopping power of the incoming particle from its energy to zero, that is, S(E):

$$\Delta x = \int_0^{E_0} \frac{1}{S(E)} dE \tag{8}$$

where E_0 is the initial kinetic energy of the particle [8].

2.8.5 Bragg Peak

Looking at equation (5), it can be seen that the stopping power, $-\frac{dE}{dx}$, has a dependency on $\frac{1}{v^2}$ at the beginning of the equation.

Here, as soon as the ion has a low velocity, this indicates that the stopping power increases drastically at the end of the stopping process. This indicates that most of the energy is accumulated somewhere towards the end of the portion that leads to the Bragg peak. In Figure 2.6, the Bragg peak can be easily seen.

Multiple energy dissipation mechanisms can be seen in that along their path some of the carbon ions are broken down into lighter ions with different energies and correspondingly varying spacings [6, 8].

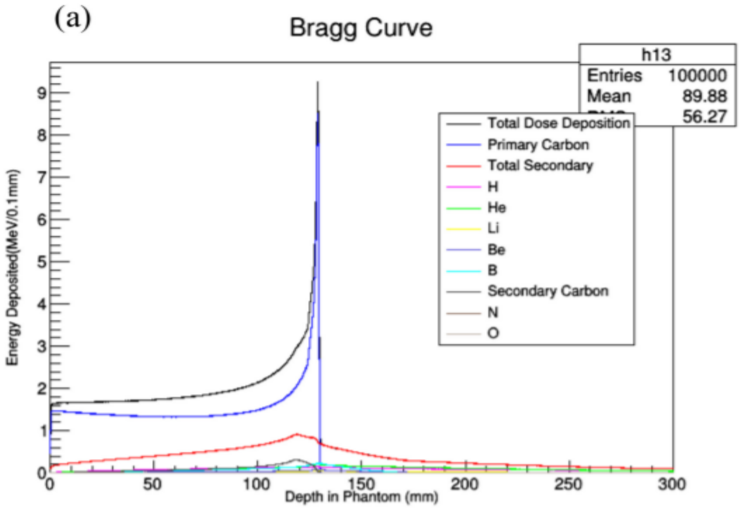

Figure 2. 6: *Monte-Carlo-based GEANT4 simulation of the Bragg peak of a 290 MeV/u ^{12}C beam sent to a PMMA (Polymethyl Methacrylate) phantom. Adapted from Ref. [8].*

2.8.6 Straggling

Theories are statistical in nature, just as mentioned above. This means that in order to reveal the collisions that any stationary particle undergoes in detail, it is necessary to look at all of these, since each particle will have a free orbit to itself. Because of the difficulty of this situation, it makes more sense to look at a statistical distribution around a central value. The square root of the variance in the particle range is expressed as *Straggling*. Because the collision can occur both in the direction of the incoming particle beam and laterally. Due to the fact that the target materials are not uniform and homogeneous, it is quite difficult to precisely calculate all these deviations by experiment [6, 8].

2.8.7 Channeling

A special case that should be considered in terms of energy losses in the interaction of heavy ions with substances is channelization. This channeling occurs in oriented crystals such as the $Si\langle 110\rangle$ surface with a honeycomb structure.

If ions, for example, can align correctly with holes in an accelerator crystal structure, they can then follow trajectories where they interact weakly with the electron gas in these channels and do not encounter the atoms head-on. In this case, energy losses are also strongly reduced.

Figure 2.7 shows an example of accelerated charged ^{79}Br ions channeled through an oriented Si 110 crystal. Here the energy loss experienced in the transition of the crystal is about $50\ \%$ of the nominal value expected for a randomly oriented surface. Here, more than $90\ \%$ of the ions exit the oriented crystal in the initial +33 charge state, while a much wider final charge distribution is obtained with the randomly ordered crystal [6, 8].

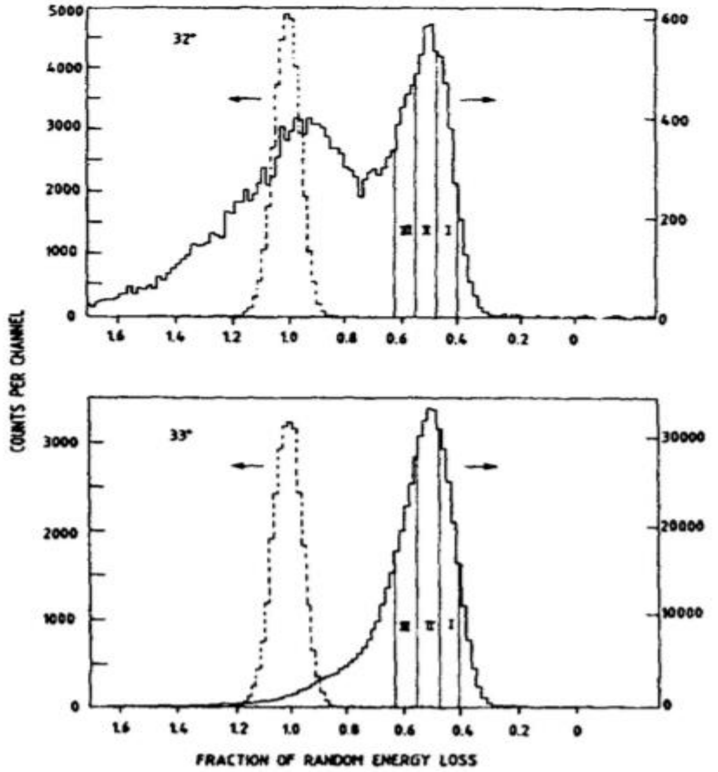

Figure 2. 7: *Energy loss spectra of + 32 (upper) and + 33 (lower) ions of* ^{79}Br *falling on thin silicon foils at 15.6 MeV/u energy. The solid line is the data for an aligned 8 µm thick* $Si\langle 110\rangle$ *crystal, while the dashed line is the data for a 1 µm thick randomly oriented Si crystal. As can be seen, this channeling effect in the oriented crystal leads to a reduction in energy loss up to about* 50% *of the randomly oriented foil value. Adapted from Ref. [8].*

2.8.8 Delta Electrons

In many nuclear physics experiments in the literature, it is seen that an accelerated beam of heavy ions hits a thin target foil, and by interacting with this energy beam, delta electrons, which are secondary electrons removed from atoms in the target foil, are produced. However, these electrons are in the energy range of $10 - 100\ keV$, depending on the beam-target type and the energy of the beam. Since electrons and their spectra do not contain nuclear physics knowledge, they are generally considered a problem for measurement [6, 8].

2.8.9 Beta Particles Interactions

In interaction with matter, the interactions of electrons and positrons and these particles are similar because they are point-like and have equal (but opposite charge). The only difference is that the positron particle is an unstable particle that can disappear at the end of its range when it forms the exotic positronium system with an electron. Let's take a look at the interaction of these two particle types with matter separately [6, 8].

2.8.10 Electrons

The interaction of electrons with material is qualitatively dissimilar from that of light and heavy ions. A heavy ion has a relatively direct path through matter, losing energy in many individual collisions/interactions. But the interaction of electrons with matter is very different in that atomic electrons play a significant part in the stopping process, and these collisions involve two particles of obviously the same mass, rather than one large and one light particle, as in stop ions. This leads to wide-angle multiscattering. And at the same time, there is a high probability of backscattering. For this reason, the probability that the electron (or positron) sent into a material will scatter out of that material is a non-zero probability. A second property is that collisions between stopped electrons and atomic electrons can result in a large transfer energy per collision. From this, there may not necessarily be many smooth steps in the de-excitation process, but it can be observed relatively few large divergence and energy loss events that cause a great deal of clutter.

In Figure 2.8, it can be seen the complexity of electron/positron interactions with materials for the positron state with 600 keV energy resting in a 5 mm thick plastic scintillator [8].

The energy loss of electrons in matter is due to two reasons:

- It is the loss of energy through excitation and ionization due to inelastic Coulomb collisions with the bound atomic electrons of the stopping medium.
- Energy loss due to emission of bremsstrahlung radiation in the field of nuclei and atomic electrons.

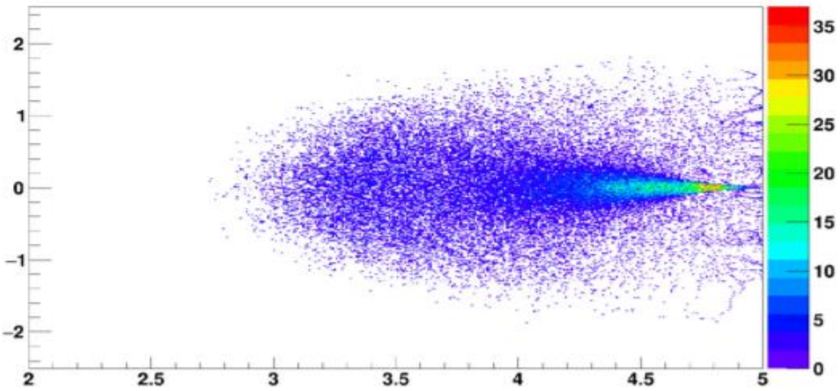

Figure 2. 8: *A Monte-Carlo-based Geant4 simulation of positron spacing with a maximum energy of 600 keV fired as a pencil beam onto a 5 mm thick plastic scintillator. Depth spacing is on the x-axis (scale in mm), lateral spacing is on the y-axis (scale in mm). The maximum spacing of positrons is about* $2.2\ mm$*, while most positrons stop within the first* $0.5\ mm$*. Adapted from Ref. [8].*

The two components that cause the energy loss above give us the total energy loss:

$$\left(\frac{dE}{dx}\right)_{total} = \left(\frac{dE}{dx}\right)_{excitation} + \left(\frac{dE}{dx}\right)_{radiation} \tag{9}$$

where $\left(\frac{dE}{dx}\right)_{excitation}$ is a modified version of the Bethe–Bloch formula:

$$\left(\frac{dE}{dx}\right)_{excitation} = \frac{2\pi e^4 Z}{m_0 v^2}\left[\ln\left(\frac{m_0 v^2}{2I^2(1-\beta^2)}\right) - ln\left(2\left(2\sqrt{1-\beta^2}-1+\beta^2\right)\right) - \frac{\left(1-\sqrt{1-\beta^2}\right)^2}{8}\right], \tag{10}$$

where I is the mean ionization potential and $\beta = v/c$.

The energy loss from Bremsstrahlung is expressed as follows.

$$\left(\frac{dE}{dx}\right)_{radiation} = NE_0\Phi_{radiation} \tag{11}$$

where

$$\Phi_{radiation} = \frac{1}{E_0}\int_0^{v_0} hv\frac{d\sigma}{dv}dv \tag{12}$$

Here, E_0 is the electron's initial energy, and v is the emitted bremsstrahlung photon's frequency.

It can be said that the bremsstrahlung energy loss is proportional to the initial energy of the electron and is proportional to Z^2 for the stopping material.

The energy loss from collision/ionization is linearly related to Z and increases logarithmically with electron energy. If the stopping powers from the two processes are equal, i.e. where a critical energy (Ec) has to be defined, it would be more accurate to equate these two components to each other;

$$\left(\frac{dE}{dx}\right)_{excitation} = \left(\frac{dE}{dx}\right)_{radiation} \tag{13}$$

In this case, the critical energy comes out as follows;

$$E_{critical} \approx \frac{1600 m_e c^2}{Z} \tag{14}$$

2.8.11 Positrons

Positrons can disappear or stop at the end of their range, and when they stop they can form the positronium, that is, they can form, in a way, an electron-positron atom.

There are two forms of positronium: para-positronium and ortho-positronium.

The Para-positronium transforms into two 511 keV gamma rays, and these two gamma rays have a half-life of 125 picoseconds.

The ortho-positronium transforms into three gamma-ray photons that share the mass of positronium at 1,022 MeV' with a much longer lifetime of 142 ns.

Looking at the experimental results, it seems that the first process tends to dominate in most cases, but the ratio between the two annihilation modes depends on the environment in which the positronium is formed [8].

2.8.12 Cherenkov Radiation

If a charged particle passes through a dielectric field at a speed much greater than the speed of light, it emits Cherenkov radiation, an electromagnetic radiation. An example of Cherenkov radiation is the characteristic glow of blue light seen in underwater nuclear reactors [6, 8].

Here, the energy lost by the particle may not be important sometimes, but Cherenkov radiation helps us in particle detection. The threshold velocity for Cherenkov to occur is defined in terms of the refractive index of the medium;

$$v_{th} = \frac{c}{n} \tag{15}$$

Cherenkov radiation propagates at half an angle θ with respect to the particle's direction;

$$cos\theta = \frac{1}{\beta n} \tag{16}$$

where $\beta = \frac{v}{c}$.

The relative kinetic energy of a charged particle is given as:

$$KE_{relative} = (\gamma - 1) m_0 c^2 = \left(\frac{1}{\sqrt{1-\frac{v^2}{c^2}}} - 1\right) m_0 c^2 \tag{17}$$

where m_0 is the particle rest mass ve n is refractive index.

2.8.13 Gamma Rays Interactions

Gamma rays interact discontinuously with atoms and molecules in the material field they enter. As can be seen in Figure 2.9, gamma rays have three main types of interaction in the energy range of 10 keV to several MeV. These; The Photoelectric Effect, Compton Scattering and Pair Production.

As a result of these interactions, either all or part of the gamma radiation energy is converted into the kinetic energy of any electron. At the same time, another result of this interaction is the formation of positron-electron pairs.

Finally, these energized electrons and/or positrons interact with a detector selected depending on the material of the experiments and produce an electrical signal. Gamma rays also exhibit an interaction called Rayleigh scattering (elastic scattering), but this interaction is not used much because it does not allow for any gamma radiation detection.

As mentioned above, all these interactions depend on the energy and density of the material into which the radiation enters, that is, on the atomic number [6, 8].

The practical way to show how gamma radiation can more easily enter matter is to define an average free path λ corresponding to the reduction. At the intensity of the gamma-ray flux penetrating the material, I_0 is given as:

$$I = I_0 \exp\left(-\frac{t}{\lambda}\right) \tag{18}$$

$$\lambda = \frac{1}{\left(\frac{\mu}{\rho}\right)} \tag{19}$$

where t is the thickness and λ is the thickness in units of mass per unit area. And ρ is the material density (gcm^{-3}) and μ is a material-specific linear attenuation coefficient (in cm^{-1}). As can be seen in Figure 2.10, the absorbency of the material depends on the shortness of the absorption length. In this way, it can be said that a radiation detector made from a material with a high atomic number will have higher efficiency than a detector made from materials with a low atomic number.

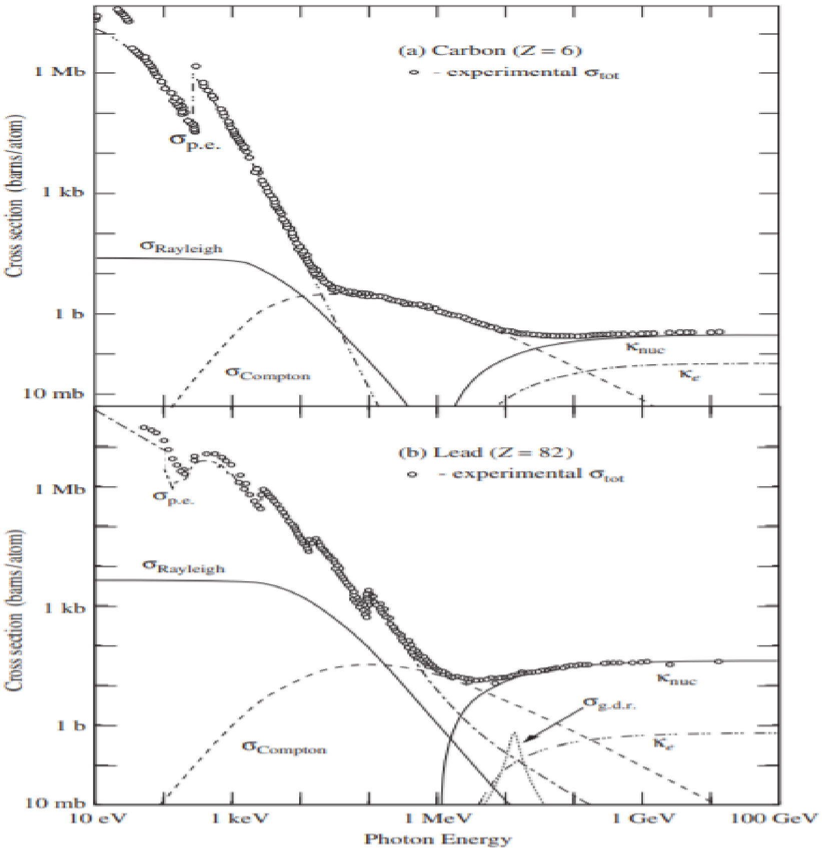

__Figure 2. 9:__ Total cross-sections for all photon types of interaction of gamma radiation as a function of energy in Carbon Z=6 (top) and Lead Z=82 (bottom). Adapted from Ref. [8].

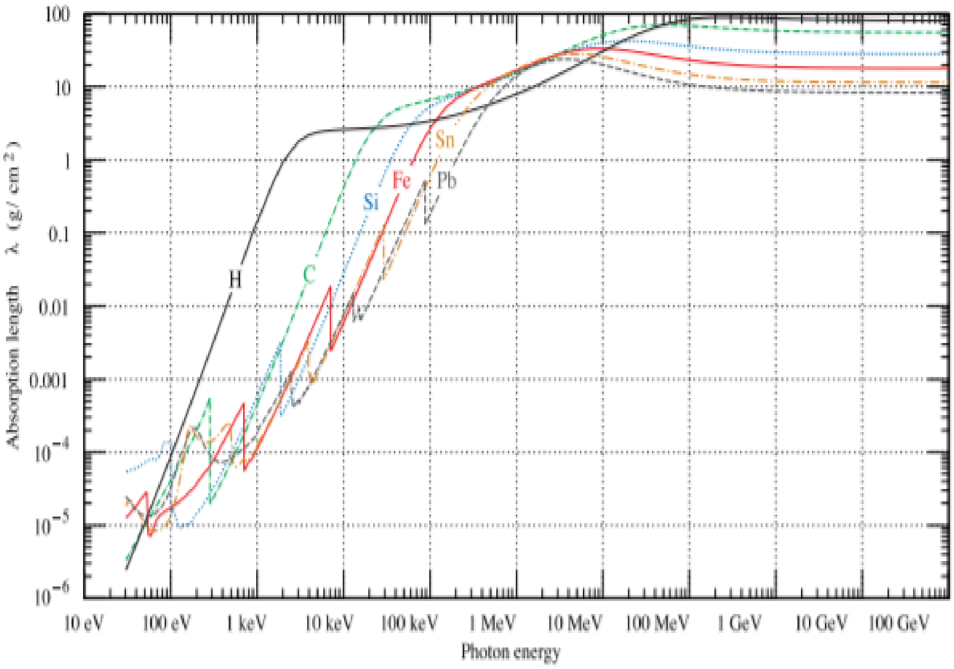

__Figure 2. 10:__ The photon mass attenuation length as a function of the gamma-ray energy entering the material, ie the plot of λ for different elements from lead to hydrogen. Adapted from Ref. [8].

2.8.14 Photoelectric Absorption

The photoelectric effect is generally used for low energy gamma rays (below $100\ keV$). As can be seen in Figure 2.11, in the case of the photoelectric effect, when a gamma ray in its interaction imparts its energy to an atomic electron, it transfers its energy to the electron of the K shell, which is usually the most tightly bound shell of an atom, if the energy of that gamma ray exceeds the binding energy of the K shell electron. But if the energy of this Gamma ray is lower than the binding energy of the K shell, it is likely to interact with higher shells (L Shell e.g.) [8].

The atomic electron that comes out of the shell is now called a photoelectron, that is, it becomes energetic. Then an expression of energies can be written as follows;

$$E_e = E_\gamma - E_b \tag{20}$$

E_b is the binding energy of the electron.

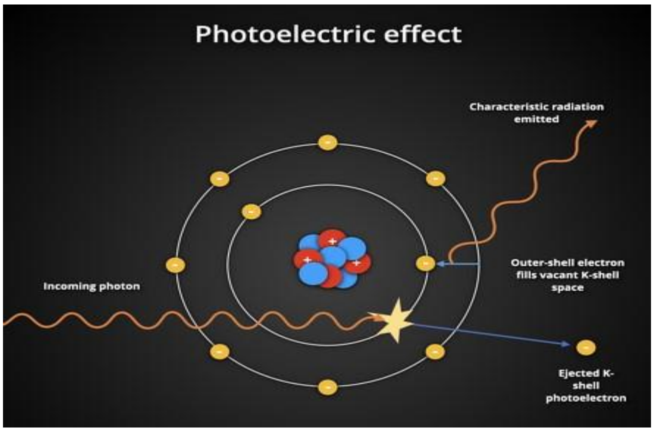

Figure 2. 11: *The Photoelectric Effect processes. Adapted from Ref. [48].*

As a result of the photoelectric effect, a gap is left in one of the atomic shells, for example the K-shell.

Electrons descend through atomic energy levels to fill this gap, which causes the absorption of characteristic x-rays or Auger electrons.

The probability of the photoelectric effect is proportional to the atomic number Z of the stopping material. This ratio is as much as Z^5 [6, 8].

2.8.15 Compton Scattering

Gamma ray radiation gives some of its energy to the electron and it scatters, this is called Compton scattering. The possible interaction energies of this scattering are approximately $50\ keV$ and above $800\ keV$ for carbon and lead atoms. For example, for the Germanium atom used for the gamma radiation detector, this energy threshold is around $100\ keV$.

In addition, this scattering manifests itself before the pair formation reaches the initial energy of 10 MeV, and this energy range creates a very wide study area for nuclear physics.

In Figure 2.12 you can see a typical diagram of this scattering. After the photon of gamma radiation entering the material gives some of its energy to the electron, it is scattered at an angle of θ. Since the electron is initially effectively stationary, the initial energy and momentum of the photon are conserved - according to the law of conservation of momentum in physics - and this momentum and energy are divided between the energies and momentum of the scattered gamma photon and the electron [6, 8].

The scattering of a photon with energy $h\upsilon_0$ from an electron with energy $h\upsilon_1$ can be roughly depicted as follows;

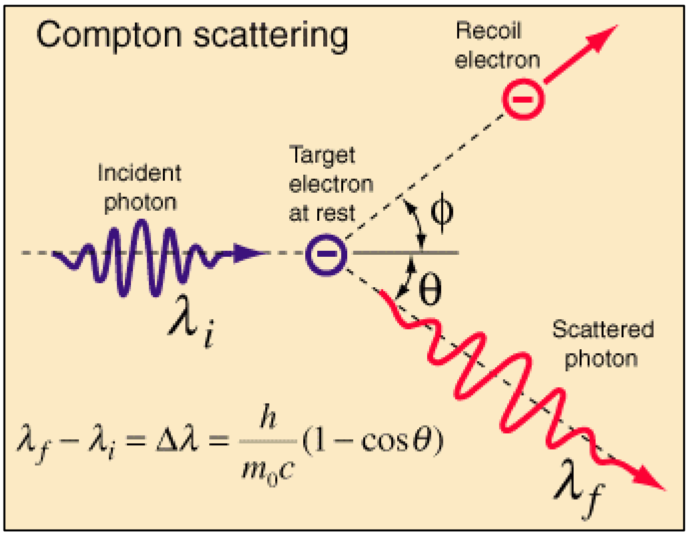

Figure 2. 12: *The Compton Scattering processes. Adapted from Ref. [49].*

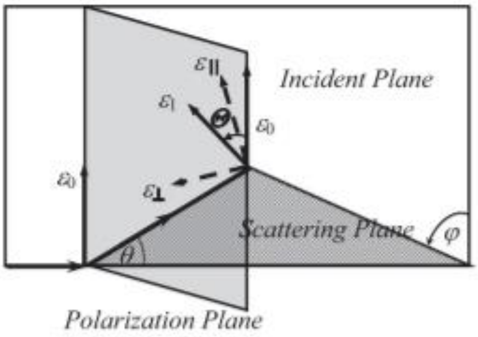

Figure 2. 13: *Compton scattering planes, scattering photon and electric vectors and representation of related angles. Adapted from Ref. [8].*

$$\frac{h\upsilon_1}{h\upsilon_0} = \frac{1}{1+\frac{h\upsilon_0}{m_0c^2}(1-cos\theta)} \tag{21}$$

where h is Planck's constant and m_0c^2 is the energy of the rest mass of the electron.

It can be said for sure that if the gamma photon is scattered 180^0, that is, if $cos\,\theta = -1$ in the equation, then it can be understood that the electron is given maximum energy.

To look at the probability of scattering, it can be looked at the Klein-Nishina formula;

$$\frac{d\sigma}{d\Omega}=\frac{r_0^2}{4}\left(\frac{v_1}{v_0}\right)^2\left[\frac{v_1}{v_0}+\frac{v_0}{v_1}-2+4cos^2\Theta\right] \tag{22}$$

where Θ and ε_0 are the electric vectors of incident and scattered photons. ε_1 is the angle between these two photons. It can be seen in Figure 2.13.

Figure 2.14 shows the Klein-Nishina cross section for three different gamma ray energies as a function of the scattering angle (θ).

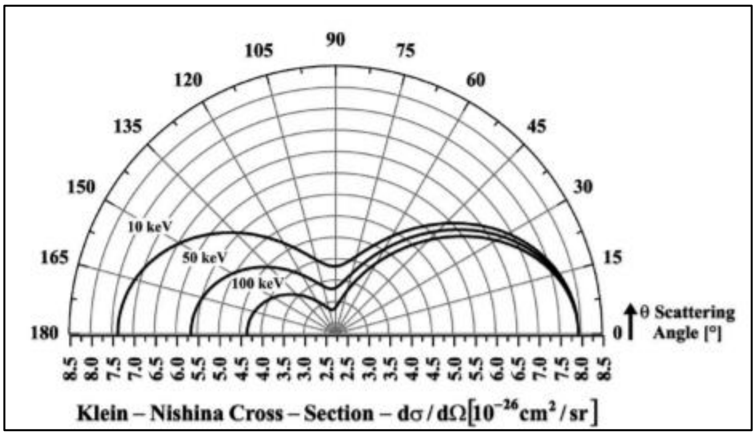

Figure 2. 14: *Cross section as a function of scattering angle of various gamma photon energies. Adapted from Ref. [8].*

The scattering cross section, which depends on the angle between the electric vectors, also depends on the linear polarization of the photon. This is one way to determine the multipolarity of gamma-photon transitions.

This multipolarity can be seen if the intensity of the incident photon is split into two components;

$$I_0=I_{||}+I_{\perp} \tag{23}$$

where $I_{||}$ is the component parallel to the polarization plane and $I_{\perp}$ is the perpendicular component.

The parallel scattering differential cross section for the incoming component is given as:

$$\frac{d\sigma_{||}}{d\Omega}=\frac{r_0^2}{4}\left(\frac{v_1}{v_0}\right)^2\left[\frac{v_1}{v_0}+\frac{v_0}{v_1}-2-4sin^2\theta cos^2\Phi\right] \tag{24}$$

It can be seen the angle values here in Figure 2.11***.***

The differential cross section of the scattering perpendicular to the incoming component is given as:

$$\frac{d\sigma_{\perp}}{d\Omega}=\frac{r_0^2}{4}\left(\frac{v_1}{v_0}\right)^2\left[\frac{v_1}{v_0}+\frac{v_0}{v_1}-2\right]. \tag{25}$$

2.8.16 Pair Production

As can be seen in Figure 2.15, the place where the positron-electron pair is produced takes place in the gravitational field of an atomic nucleus.

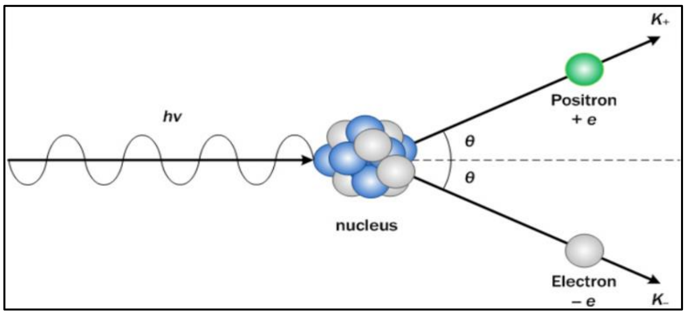

Figure 2. 15: *The Pair Production processes. Adapted from Ref. [50].*

The energy threshold required to produce the positron-electron pair is $2m_ec^2$. m_e is the mass of the electron. Two identical particles are produced, each with an energy of 0.511 keV, but with only different charges, and their total energies are 1.022 MeV. As can be seen in Figure 2.16, above events can also occur in the atomic electron field with an energy of $4m_ec^2$, but the first process, the state with an energy of 1.022 MeV, is a process with very important applications in nuclear physics.

In the literature, the basic theory of this electron-positron generation has been given by Bethe and Heitler. According to this theory, the total cross section for pair production is related to Z^2, which shows a large material dependence [6, 8]. Figure 2.16 shows the predictions of Bethe and Heitler's theory together with the experimental data.

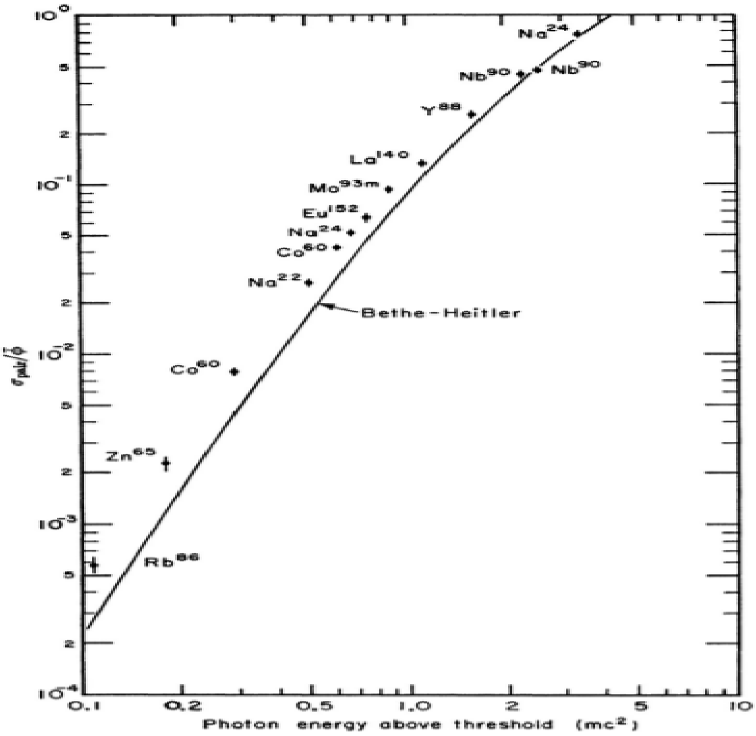

Figure 2. 16: *Cross section for pair formation as a function of the energy of a photon above the threshold energy in m_ec^2. Adapted from Ref. [8].*

Chapter 3

3. SCINTILLATION DETECTORS And PHOTOSENSORS

This section presents some information about scintillators and related photosensors from a general point of view. First, gamma-ray detection was examined. For this reason, the interaction processes of gamma rays and their relevance to materials are mentioned. Organic and inorganic scintillators are of two types to be used in the literature. Initially, after giving information about inorganic scintillators, organic scintillators were started.

In the last section, there is information about the different photosensor sources where this scintillation light is collected. These are photomultiplier tubes, avalanche photomultipliers and silicon photomultipliers.

Let us now briefly review the gamma-ray interaction. There are three main modes here at low energies; Photoelectric absorption, Compton scattering and Pair production.

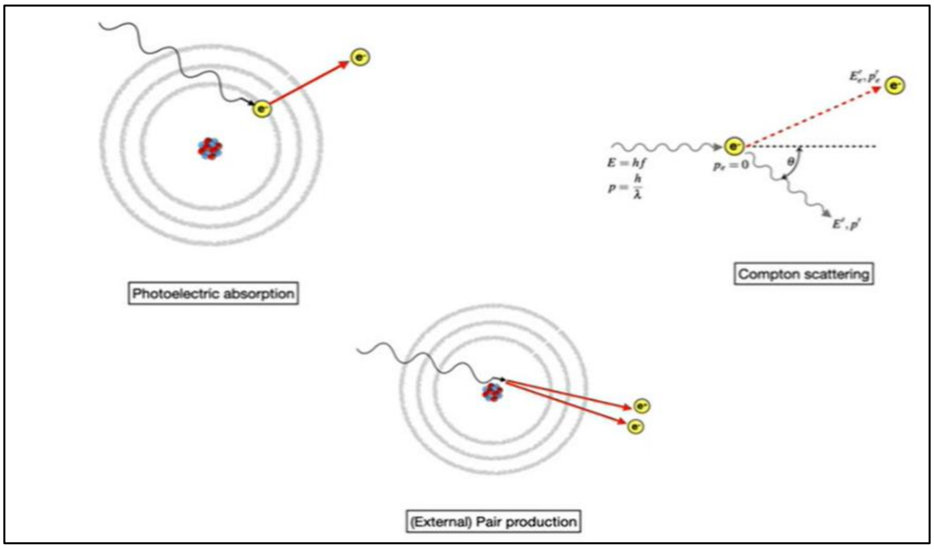

Figure 3. 1: *Modes of Gamma-Ray Interaction. Adapted from Ref. [9].*

In the first mode, Photoelectric Absorption, the gamma photon enters the material and removes an electron from the atom of that material. For the atom, the electron is a state where the kinetic energy is equal to that of the photon minus the binding energy around the electron. This process happens when the atomic number Z is either to the fourth or fifth power. Therefore, the probability of photoelectric absorption occurring depends on how high the Z-value of the material is.

The second mode is Compton Scattering. Here, a gamma ray is inelasticly scattered by an electron. When gamma-ray scattering is simulated, some—but not all—of the photon's energy appears to be transferred to the electron.

And as the third mode, it is an action where a gamma ray above one MeV energy interacts and an Electron-Positron Pair is produced. And in the subsequent interaction of this action, the positron can be captured and destroyed by an electron. As a result, photons with an energy of 511 keV can be produced.

All these mechanisms basically show how the gamma ray somehow transfers its energy to electrons and/or positrons. The probabilities of these different types of processes should be looked at.

At the bottom, there are cross-sections depending on the energy of the photon in the lead element and all kinds of interactions can be seen. As a new way of approaching these interactions from a material point of view, the focus is on the absorption lengths in these different materials. Thus, judging by the short absorption light, gamma rays are attenuated in the material. The length at which gamma rays are considered likely sheds light on elements that absorb much more light [9].

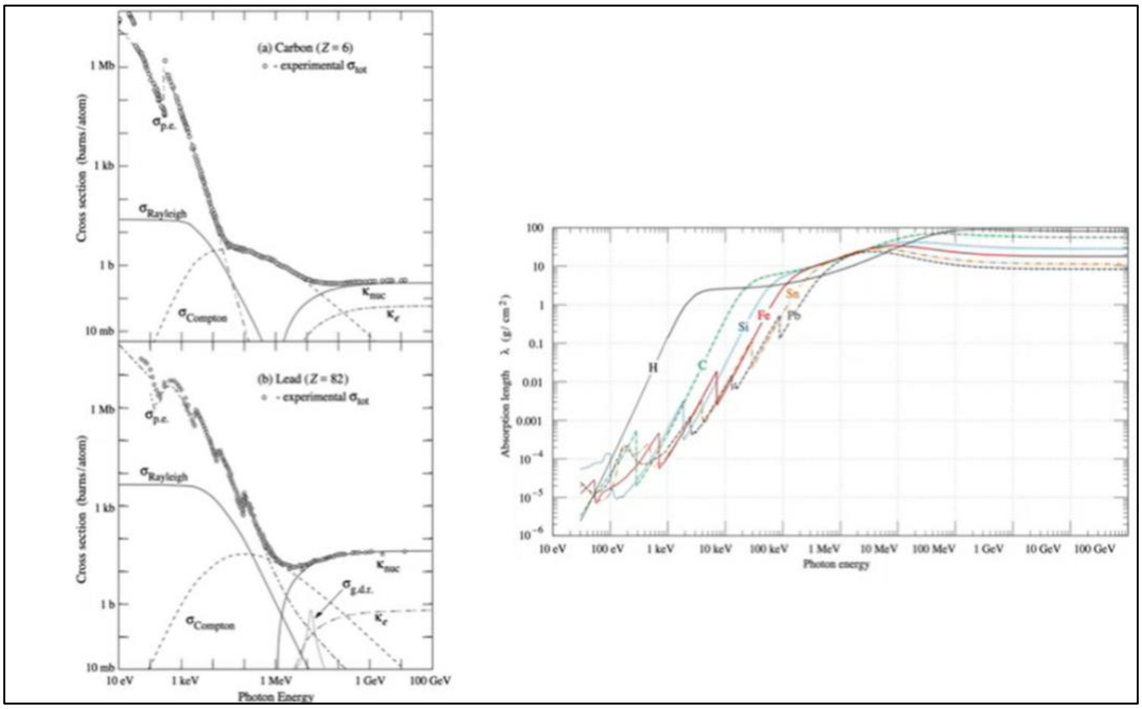

Figure 3. 2: *The possible interaction energies of the scattering are approximately 50 keV and 800 keV for Carbon and Lead atoms. Adapted from Ref. [8].*

3.1 Inorganic Scintillators

In this section, inorganic scintillators are also mentioned. These are usually crystalline or sometimes ceramic materials based on inorganic chemistry.

The mechanism behind the production of Scintillation Light is illustrated in the figure below. Here the electrons stay in the valence band. Energy is transferred to the material and electrons are excited from the valence band to the conduction band. What normally happens is that these electrons relax back into the valence band and photons are emitted.

Most conventional forms of scintillator materials are generally not very efficient scintillators. For example, Sodium Iodide as a pure material is a scintillator, but not very effective. The main development in this material area was in the 1940s and in the 1950s people noticed this by adding activation centers to the crystal. And then these activation centers began to provide an additional pathway for electrons to be excited.

And this makes the glow process more efficient and also shifts it to a more suitable wavelength, typically a visible wavelength. And this is the basis of Sodium Iodide. In fact, the mechanisms are much more complex than that [9].

The *Figure 3.3* below is a classical scintillator.

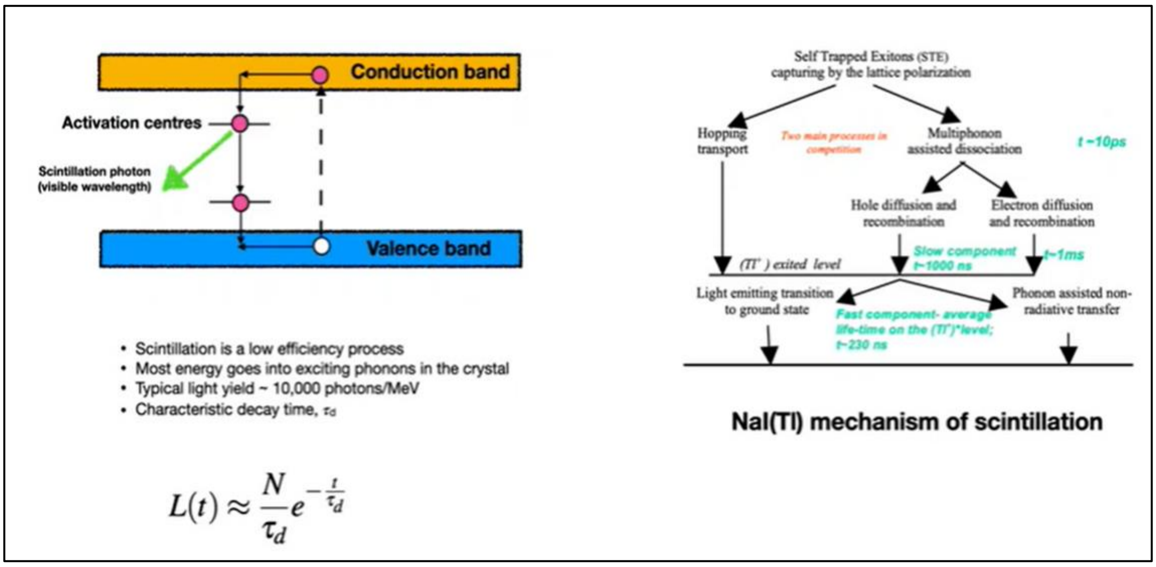

Figure 3. 3: *Inorganic Scintillators Mechanism. Adapted from Ref. [8].*

L**, luminance is a function of time.* ***T_d *is an exponent of the characteristic decay time of a crystal.*

Here are some pictures of the classical scintillator material, Sodium Iodide in the lower left, Cesium Iodide in the upper left is widely used. And some of it is Barium Fluoride.

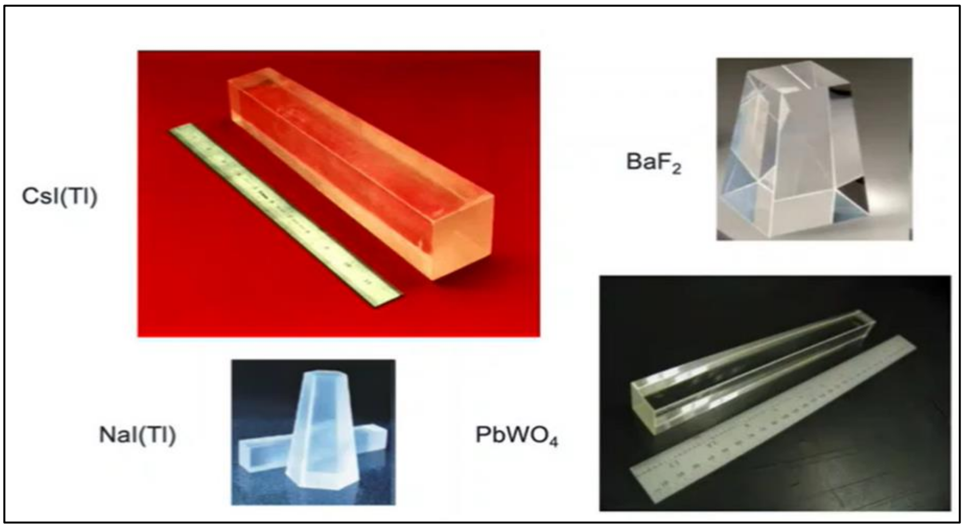

Figure 3. 4: *Common scintillators used in nuclear physics experiments and applications. Adapted from Ref. [9].*

So they are all usually crystal material, soft and clear, sometimes colorful etc. However, a very important feature is whether they are hygroscopic or not. Hygroscopic means they respond more to light.

Thus, these hygroscopic crystals can be prepared in their form coated in some way to protect them. All crystals that are Cesium Iodide are hygroscopic. However, if it is desired to process many or some of the common ones such as crystal, a glove box should be used in a laboratory setting as shown in Figure 3.5 below.

wrapped $CeBr_3$ crystal   coupled to PMT   coupled to SiPM array

Figure 3. 5: *Preparation of a Hygroscopic Crystal with the Photosensors. Adapted from Ref. [9].*

Figure 3.6 below shows what a typical scintillator should look like. If a choice is to be made as to what kind of scintillator is desired, the characteristics of interest should be as follows.

	NaI(Tl)	BaF_2	CsI(Tl)	CeF_3	BGO $Bi_4Ge_3O_{12}$	PWO $PbWO_4$	LuAG:Ce	
X_0 [cm]	2.59	2.03	1.86	1.66	1.12	0.92	1.41	Absorption coefficient
ρ [g/cm^3]	3.67	4.89	4.53	6.16	7.13	8.2	6.73	Density - key to stopping power
τ [ns]	230	0.6 620	1050	30	340	15	60	Mean decay time of scintillation light (some multiple)
λ [nm]	415	230 310	550	310 340	480	420	535	Peak wavelength (some multiple peaks)
$\eta@\lambda_{max}$	1.85	1.56	1.80	1.68	2.15	2.3	1.84	
LY [%NaI]	100	5 16	85	5	10	0.5	50	Light output relative to Sodium Iodide

Figure 3. 6: *Typical Scintillator Properties. Adapted from Ref. [8].*

- *The top Xo is the absorption coefficient. And it gives information about the absorbency of the material.*
- *Interception of gamma rays is about two things. One is the density, which is in the second row of the table, and obviously these densities vary quite a lot from material to material. The other is the atomic number Z. And let's remember photoelectric absorption at the fourth or fifth power of an effective Z number, and a higher Z number is a much more effective absorption.*
- *What is seen in the third row here is the decay time of the scintillation light. Here you can see that Sodium Iodide is about two hundred nanoseconds. Cesium Iodide has about four or five times longer duration.*
- *The wavelengths of light emissions are quite high. They are typically in the visible or near ultraviolet range. And indeed, there is usually a fairly wide range and wavelength in the light output.*
- *The next column is the refractive index of the material. Therefore, the scintillator can be very bright in terms of how many photons are produced. But if the index of refraction is too high, it is difficult to optically pair it with a photosensor or an efficient light guide.*

Here, Figure. 3.7 shows an example of Barium Fluoride with more than one light emission component is mentioned. And this is because it has a core band higher than the valence and conduction band and the more complex band structure shown below.

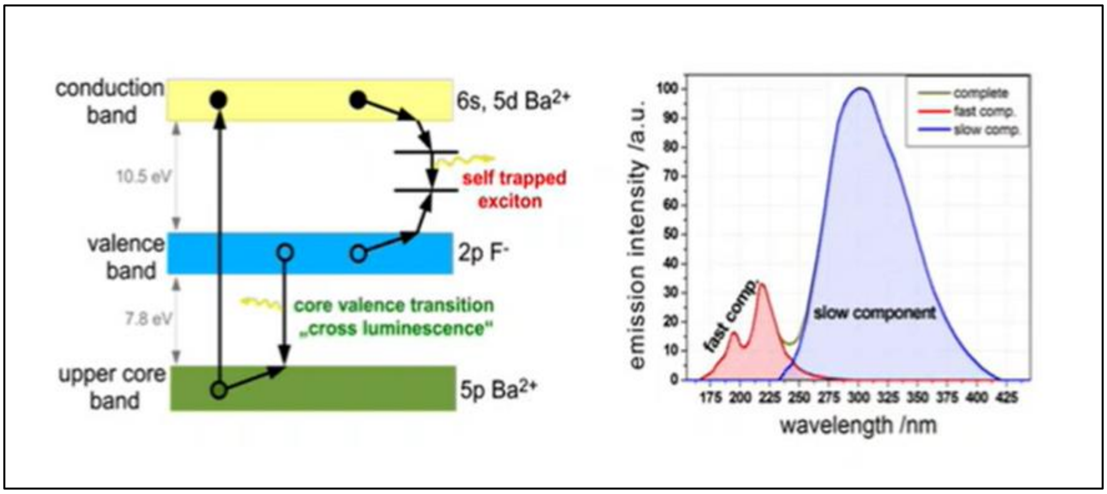

Figure 3. 7: *BaF2 Scintillation Mechanism. Adapted from Ref. [9].*

There are two possible ways down from these situations. And this leads to the emission of the first component, shown above as the red region of the wavelength diagram. The slow component is a much larger component.

This first component is used for the first time measurements because it has a decay time in itself. This is approximately half a second. But again in this example, you can see that the wavelength of these first components is very precise, like two hundred nanometers. So it becomes quite difficult to match with the photosensor.

While talking about the ideal scintillator idea in this section, the following diagram is emphasized. Ideal scintillators, as mentioned above, have a very large luminous efficiency. Ideally they have a very fast decay constant.

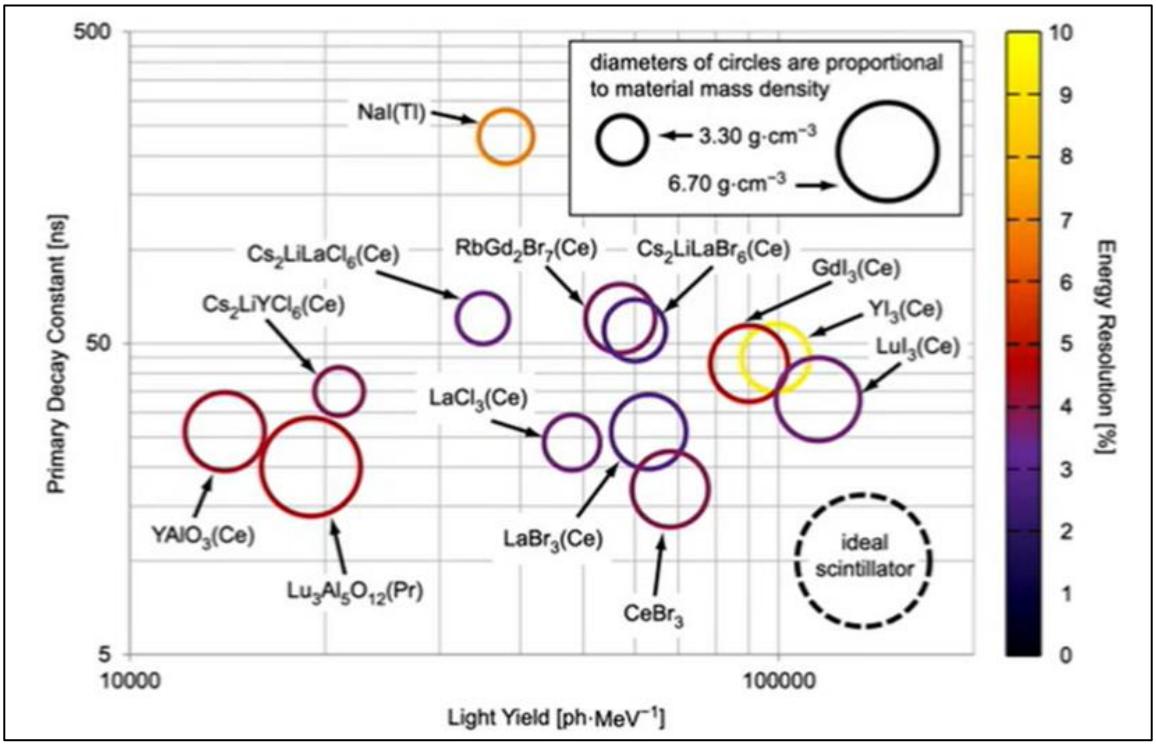

***Figure 3. 8:** The Ideal Scintillator. Adapted from Ref. [8].*

Why is fast decay time needed for light emission? There are two reasons for this. The first is to quickly get back to the baseline. That is, the detection calculation turns fast because the pulses are not stacked.

The second reason is when it comes to integrating the signal from the crystal electronically, the longer the signal that needs to be integrated, the more noise integrated into it, the higher the energy resolution. That's why the fasticate constant is important.

And this Figure 3.8 is a pretty clever diagram because it uses both colors and shapes, namely circles, and here the larger the diameter of the circle, the higher the density of the material. Ideally, high density material scintillators are dealt with. And finally, the colors represent the measured 662 keV energy resolution for these materials. Therefore, as good an energy resolution as possible is desired.

A smaller number is possible, corresponding to the dark colors in this Figure 3.8. Therefore, the ideal scintillator should be at the bottom right of the diagram. And that would be a big black circle. It will have very good energy resolution and a very fast decay time and a very high light.

It is also known to be ideally excellent materials. However, as can be seen from this Figure 3.8, there are many materials that are better than Sodium Iodide in some respects, such as those shown near the bottom middle of the diagram. Lanthanum Bromide, Cerium Bromide etc. these two materials are much better and much faster scintillator crystals. And indeed, they have much better energy resolution [9].

The Figure 3.9 below is gamma ray spectroscopy for sodium iodide and Sodium Iodide is the key parameter here.

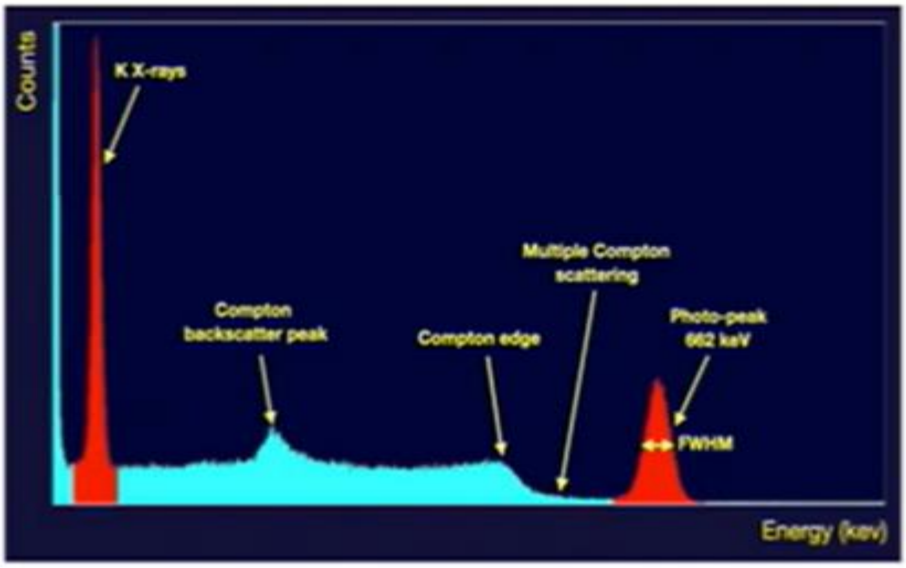

Figure 3. 9: *Gamma-Ray Spectroscopy for Sodium Iodide. Adapted from Ref. [8].*

Here is some information on what the Scintilator spectrum looks like. And that will be something you will discover in the lab and work on a bit. Here is the spectrum obtained with a silicon photomultiplier photosensor coupled with a Cesium Iodide crystal.

Let's explain more what's going on here. The new signal is a typical spectrum you get. Here, a photopic with the red peak on the right is obtained. And for the approximate peak Full Width Half Maximum is an energy resolution and this property is measured for the photopic of about 662 keV.

You can also see that there is another peak in the spectrum in another red color, and that is the X-rays from the Cesium-137 source. It can be seen that between these two red peaks there is a pale blue region associated with Compton scattering, and there is a Compton edge. The Compton backscatter peak comes from the details of the Compton scattering process and the minimum energy that can be affected by it. And then some multiple Compton scattering can also be seen between the Compton edge and the photopic. This can be understood from the diagram below [9].

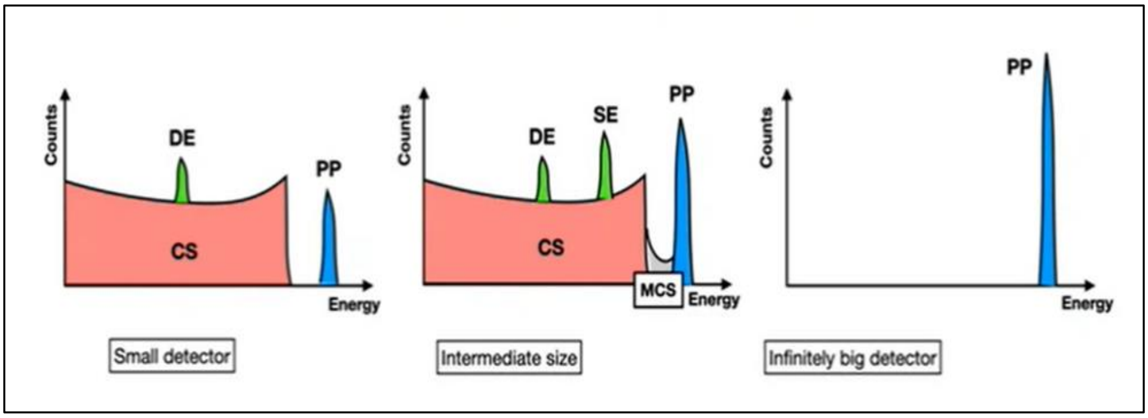

Figure 3. 10: *The spectrum obtained with a Silicon Photomultiplier Photosensor coupled with a Cesium Iodide Crystal. Adapted from Ref. [8].*

Let's say we have 1.5 MeV of energy, and then we have double generation. So if it was a very small detector like the one in the top left, it would look very small photopic and a lot of Compton scattering background would appear like in orange. On top of that, a double escapement in green is also seen. Thus the annihilation of the photon from pair generation would occur when both extinction gamma rays escape with the detector.

So this is for a very, very small detector. But if there were an infinitely large detector like the one on the far right, all these secondary photons, etc., would be captured regardless of what happens in these secondary processes that match the productions. So it will all be in the photo. So you can see a photo in a unique way. It is very difficult to design such an infinitely large detector. But the middle part is a more typical detector. As can be seen, these data are like the real data of the previous spectrum. Escape peaks can also be seen despite having a higher energy. In this way, single and double shot photopic can be obtained from the scattered background and many different scatterings in between.

Energy resolution is the key parameter here and tells what can be done with gamma ray spectroscopy. That is, how easily these peaks can be resolved and how easily the gamma-ray spectrum can be interrogated or interpreted. The figure below shows the energy resolutions for a number of different materials [9].

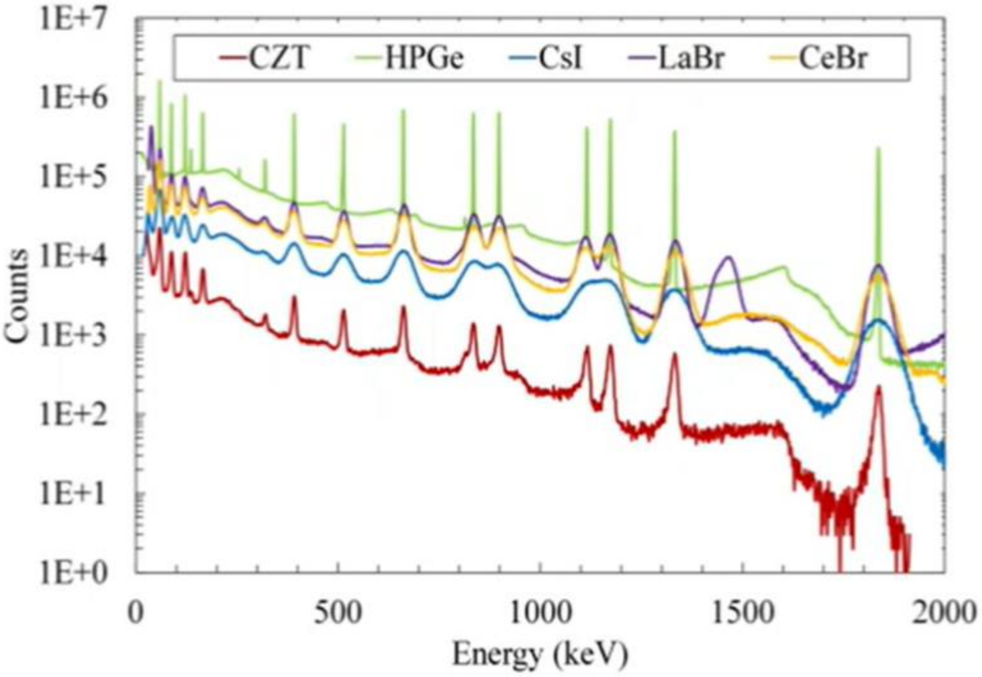

Figure 3. 11: *Cadmium Zinc Telluride, Cesium Iodide, Lanthanum Bromide, Cerium Bromide and High Purity Germanium, which are next generation scintillators with Energy Resolution. Adapted from Ref. [9].*

So here it can be seen in Figure 3.11 that the porous one is a light blue color, Cesium Iodide. Peaks in the spectrum can be seen very easily indeed. So it's basically measuring the same source with all these different detector types and seeing some peaks converge. You can have sufficient energy resolution when you use a better scintillator material such as Lanthanum Bromide and Cerium

Bromide. And of course, when you go to truly top-of-the-line gamma-ray detectors, High Purity Germanium detectors are an example, and they have very excellent energy resolution.

Also, Cadmium Zinc Telluride, shown in red in this diagram, is also a material with room temperature semiconductor detectors like Cesium. The best scintillators always have excellent energy resolution. However, they are all used for their energy solubility in a particular application. These materials are perfect no matter how good the energy resolution you need for the material you want to use. For example, most of the new simulators such as Lanthanum Bromide and similar can be 10 times more expensive than the old generation ones [9].

As can be seen in Figure 3.12, Let's talk about how energy depends on energy resolution. And here are examples of Lanthanum Bromide and Cerium Bromide as they produce more light.

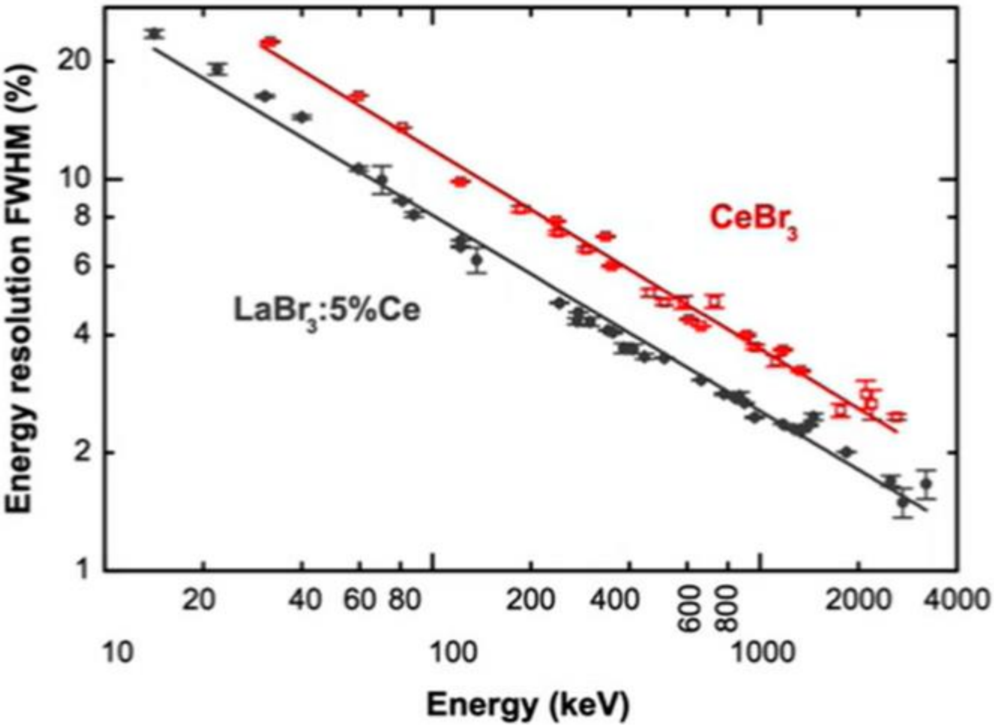

Figure 3. 12: *Energy Dependence of Energy Resolution. Adapted from Ref. [8].*

The more light you collect, the more energy accumulates in the material. The energy resolution appears to be getting better and better as a function of energy. In fact, attention is always paid to the energy resolution of 662 keV.

Now let's talk about where this energy resolution comes from. In the equation below you see the corresponding contributions, and they are four terms. One of them is related to Crystal, while the other three are related to photomultipliers. Therefore, it would be good to dwell too much on the photomultiplier contribution [9].

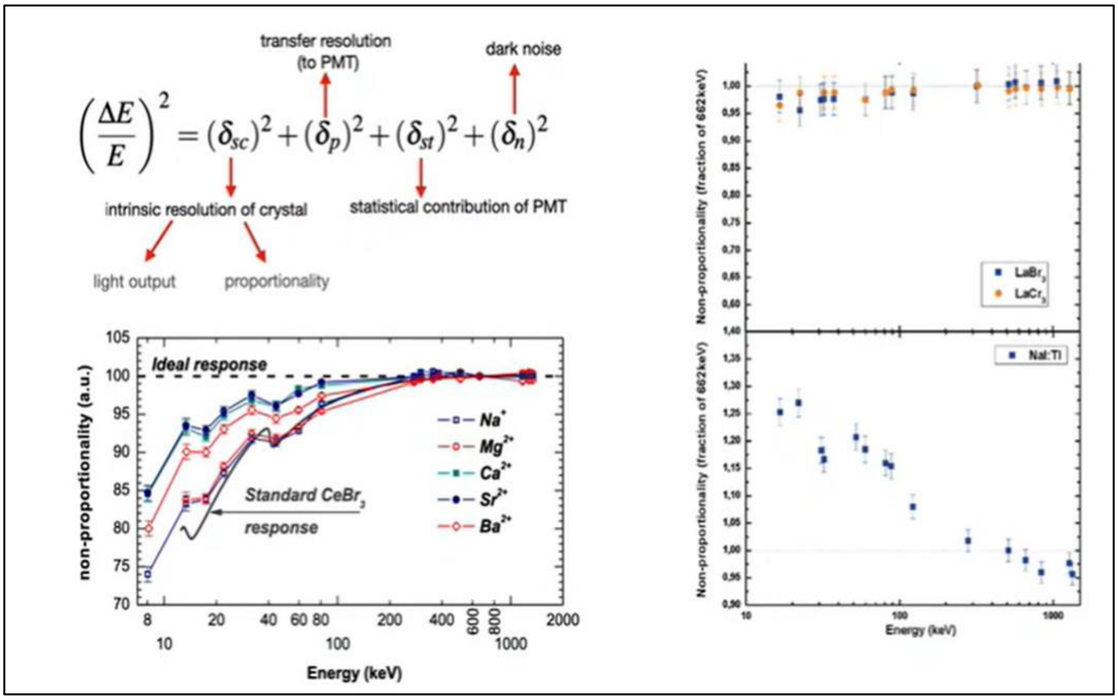

Figure 3. 13: *Contributions to Energy Resolution. Adapted from Ref. [8].*

First, let's look at the first term, the intrinsic resolution of the crystal. The intrinsic resolution of the crystal depends on the light output. It's about how much light is produced. That is, the stored energy must be proportional to the crystal. So the crystal can produce a lot of light. However, if it is not very proportional as a function of the stored energy, this lowers the energy resolution.

It can be seen this situation for Sodium Iodide with Thallium at the bottom right. As can be seen in Figure 3.13 that the disproportion of the material varies quite a lot as a function of energy. At the top, it is seen that these next-generation materials, such as Lanthanum Bromide, are very flat as a function of energy.

In other words, it can be said that this material shines much better due to the reflection of its high proportionality on its energy resolution. The scientists discovered that they improved the proportionality of the crystals with the Kodo pigment, as shown in the lower left. And that's actually what's being done right now in the above figure. The proportionality of the Lanthanum Bromide crystal has increased further thanks to the Strontium Ions.

A few physical properties of scintillator crystals also show a change in light output with temperature, and some increase in light output as they warm up to room temperature. In some, the light output is reduced. But of course, if you want to ensure stability, stabilizing people's temperatures in the scintillator detector is pretty typical, depending on the application [9].

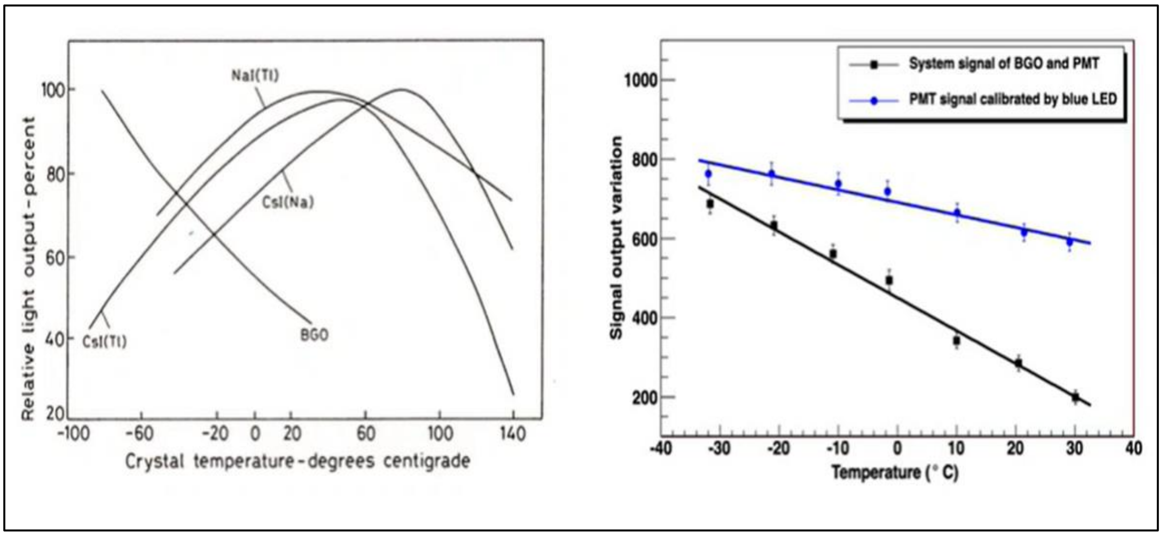

Figure 3. 14: *Variation of light output of some scintillation materials with Temperature. Adapted from Ref. [8].*

Actually, as can be seen in Figure 3.14, this is more complicated because the performance of the photo sensor that used also vary as a function of temperature. And so, it is considered how the crystalline composite system on the photo sensor and especially the scintillators can also change with temperature, which may be important in field applications.

As can be seen in Figure 3.15, for Cesium Iodide, among these different types of crystals, quite a few typical curves are seen at peak wavelengths, as mentioned earlier. It has to do with the choice of photomultiplier tube or similar. Therefore, ideally, with respect to the photosensor peak [9], the photosensitivity peak would be matched with the peak of scintillation light detection efficiency.

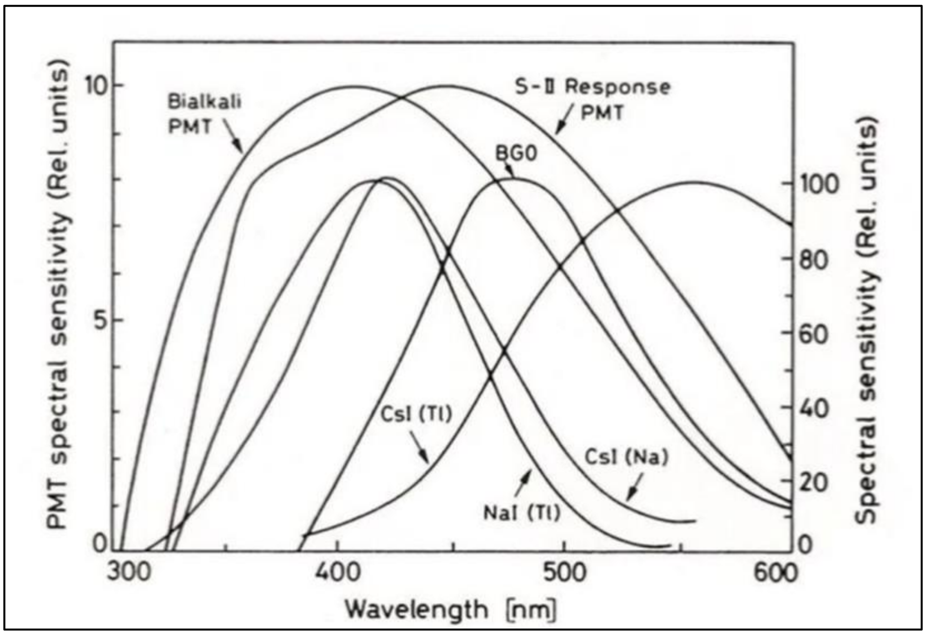

Figure 3. 15: *Peak Wavelength and Photosensor Matching. Adapted from Ref. [8].*

Here some basic parameters of an organic scintillator are summarized.

Summary of Key Parameters of Inorganic Scintillators:

- *Energy Resolution*
- *Light Output*
- *Non-Proportionality*
- *Peak Wavelenght(s)*
- *Decay Time*
- *Temperature Stability*
- *Refractive Index*
- *Density and Effective Z Efficiency*
- *Radiation Damage*

Energy resolution is number one. Normally how good a shine is the first thing to look at. And as stated above, it is about light output and disproportion, which are inherent properties of the material. The peak wavelength is important in how it is paired with the photosensor. The decay time is important as it allows the detector to count fast and also aids in energy resolution.

Ideally, a scintillator should be stable to the temperature function. It should have a relatively low refractive index. Thus, glasses etc. It can be easily paired with common optical components such as Density and effective Z value are the main determinants of the efficiency of this scintillator. Because very high radiation flux, which may occur in some industrial applications on a scintillator, causes radiation damage. If the crystal structure is damaged, the light output of the scintillator is reduced [9].

3.2 Organic Scintillators

Organic scintillators come from organic chemistry. Such materials are a feature of the atomic structure and molecular levels of atomic levels, which are light emission rather than scintillation. And this diagram shows the molecular state of a typical organic scintillator [9].

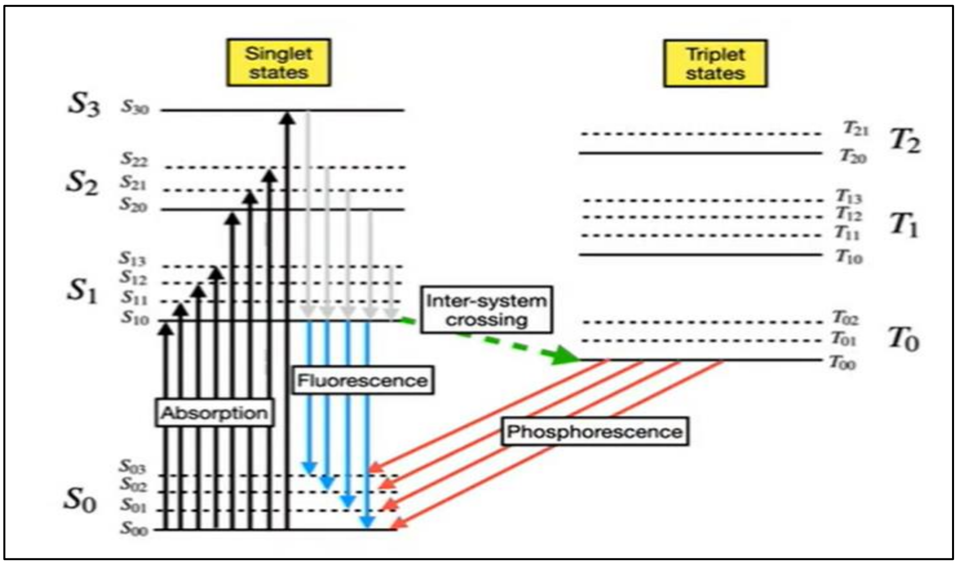

Figure 3. 16: *Organic Scintillators Mechanism. Adapted from Ref. [9].*

So organic scintillators come from organic crystals, they are similar, usually liquid scintillators and plastic scintillators. As can be seen in Figure 3.16, the idea is that initially, scintillators are in the ground state of the molecular state. This is a singlet state like S_{00} shown in the diagram. But when the scintillator accumulates energy in ionizing radiation, an absorption process occurs and excites excited singlet states up to many possible states that can be excited. These then interrupt the excitation of the first low molecular excited state, S_{10}.

From this point on, these two possible things that could happen, you can get fluorescence, which is fast scintillation light emission that takes you straight down from the S_{10} state. These are the levels S_{00}, S_{01} and so on, shown in blue.

However, there may also be another process called whole system crossover where this Singlet state goes to the lowest level of Triplet states after that Triplet state. In this case, they decay to their lowest singlet state by the phosphorescence process. And this process is essentially slower than fluorescence decay [9].

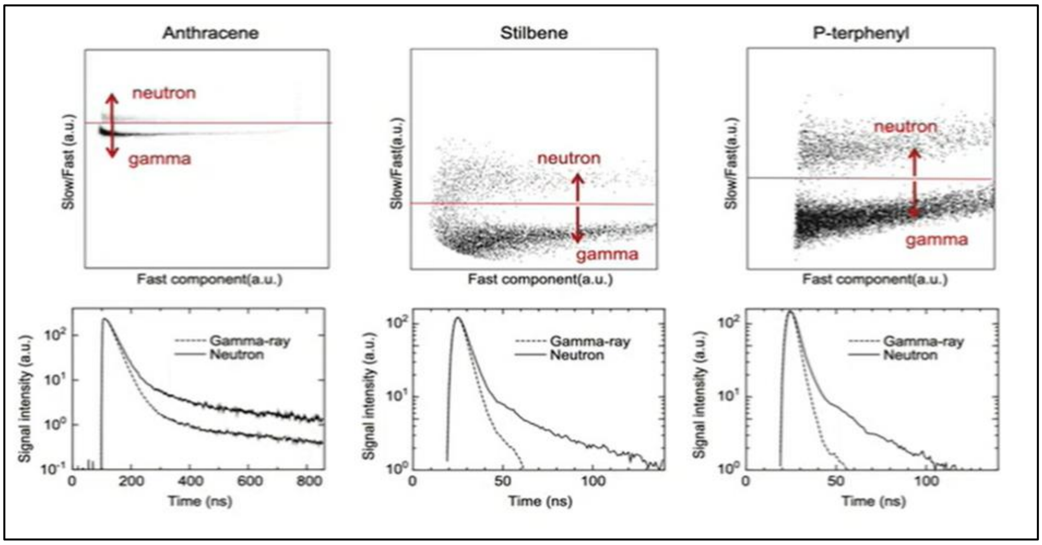

Figure 3. 17: *Examples of Organic Scintillator Crystals. Adapted from Ref. [8].*

The interesting thing about organic scintillators is that different types of ionizing radiation interact with them. Thus, gamma rays or neutrons can be seen in an organic material, whose protons tend to rebound. These protons have a different interaction and acquire more phosphorescence than your fluorescence. It may all sound very complicated, but it can be seen in Figure 3.17, that the decay curve is much faster when excited by gamma rays than when excited by neutrons. And then there's a much longer term component to the signal. By looking at the tail of the signal here, it can be told if it's a neutron or gamma ray interaction.

And this is probably one of the most useful features of organic scintillators. For example, gamma rays are high and have some resolution when used to detect fast neutrons. Whichever you spot quickly, discriminators and gamma rays need to go. Looking at the ratio of these components of light shows in the slow and fast Td histograms that the idea you can draw is the slow and fast component versus the first component. And then a distinction is made between neutrons and gamma rays [9].

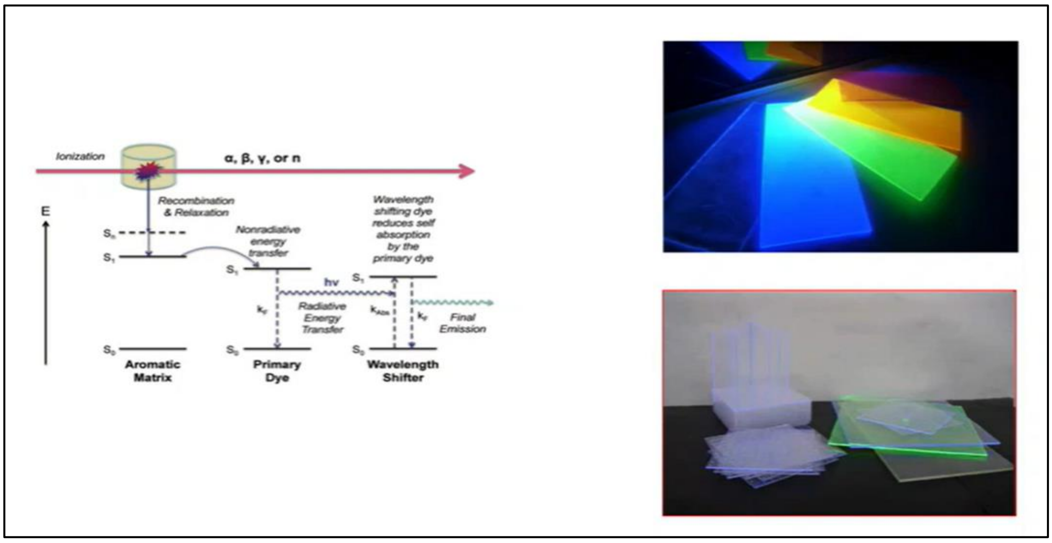

***Figure 3. 18:** Plastic Scintillators Mechanism. Adapted from Ref. [9].*

As can be seen in Figure 3.18, plastic scintillators are one of the special class scintillators that it can be worked on a lot in the laboratory. Honestly, plastic is a very nice material. Plastic can be custom molded into different shapes in our daily life. And basically, you can't put plastic into it to become an efficient scintillator. Because any plastic will sparkle. This is at a level as described by the mechanism for organic scintillators. But a normal plastic won't be a very efficient scintillator, so something has to be done to it. Thus, they are added to a primary dye that modifies the excitation through a process called non-radioactive energy transfer. And then you get a more efficient light output.

And more importantly, wavelength recognizes that light is not absorbed by the plastic itself. Otherwise, more light will come out. Above you can see some of these different types of plastic scintillators that get excited when the lights are on. You can see that they shine with their characteristic color [9].

3.3 PHOTOSENSORS

In this section, photosensors and how they work are discussed. The literature traditionally dates back to the 1940s and is still used photomultiplier tubes.

The figure below is a photomultiplier tube. Its basic idea is that high energy photons come in and produce electrons these electrons are Compton scattered electrons which excite the inorganic scintillator and then cause the proportionality of the scintillation light. Then this scintillation light is converted into an electrical signal that can do something useful. So the photomultiplier shown in red in this figure has a photocathode in front of it. And this photocathode is typically a semiconductor material. And depending on which semiconductor material you choose and the work function that material has, you can match it to the wavelength of light you're interested in. And when the wavelengths of light above a suitable range fall, these photons will produce photoelectrons, that is, they will eject the electron from the photocathode, go to the electrode shown in green, and from there fall into the first dino shown in blue. These dynodes are kept at high voltage. A higher and higher voltage is going through the dynode [9].

Thus, between each dynode, the electrodes are accelerated, typically by about one hundred volts. And so when the primary electrons fall in the first dino, some degree of collision occurs where more secondary electrons are produced. And as this electron chain goes through the dynodes, you get more and more electrons produced in the new lunch mode. This results in a huge gain in the signal.

So you get a relatively large signal emanating from a handful of photoelectrons. And it can be seen the payoff of the multipliers at the bottom of the Figure 3.19. And that gain depends on the power of the number of dynodes you have and a function of the voltage between the dynodes. And that results in a typical win of about ten to the six or seven.

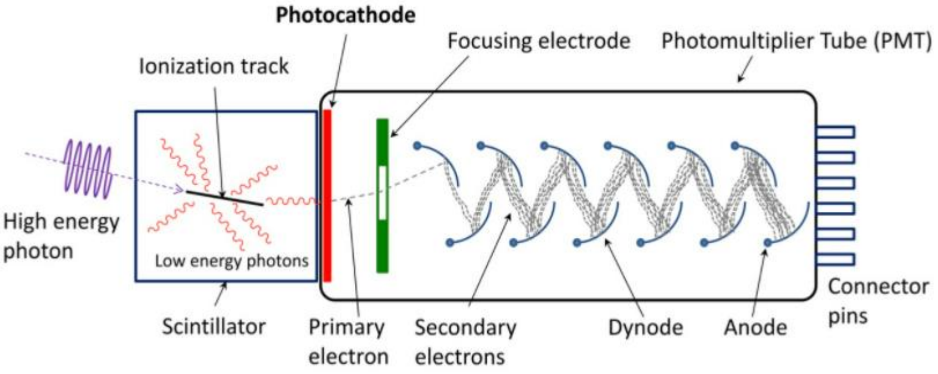

$$G = AV^{kn}$$

Photomultiplier gain, G, is a function of Voltage detween dynodes, V, and number of dynodes, n
Typical gains of order 10^6 or 10^7

Figure 3. 19: *Photomultiplier Tube (PMT) and its Gain. Adapted from Ref. [9].*

Using photodiodes and Avalanche photodiodes as an alternative to these conventional photomultiplier tubes is crucial for higher gain. The figure below is a photo diode. It is very similar to solar cells, the way sunlight is converted into electrical energy.

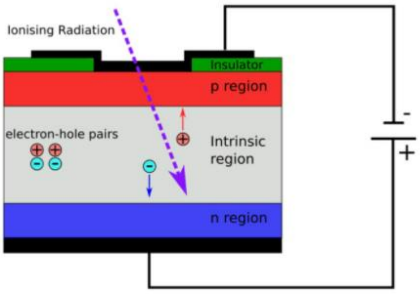

- Photodiode - gain is one so needs amplification
- APD is photodiode with large (100 V) reverse bias operating in avalanche mode
- APD gain typically of order 100 X

Figure 3. 20: *Photodiodes and Avalanche Photodiodes (APDs). Adapted from Ref. [8].*

This above Figure 3.20 shows the ionizing radiation coming into the photodiode. If there is a certain wavelength associated with these photons, they fall on this material, usually silicon is used.

That's because silicon is fascinating interior region and semiconductor and has a P and N region. So the Photon produces an Electron-Hole Pairs that are swept onto the plate.

Thus, a signal is generated through the edges. There is now a pretty good reason to use a photodiode sensor. The main reason for this is more gain. And remember, the photomultiplier tube's gain was 10^6th or 10^7th. But this photodiode is much more sensitive to electronic noise. And a photomultiplier tube has an electronic noise called the Groomes fault.

But you might think that when using a scintillator crystal, if you also cover the edges of the photodiode, more photodiodes gather more light. Because if you add too much noise you will never improve your signal. As a result, you won't be able to improve your energy resolution either.

Photodiodes are mostly used in the detection of charged particles, where a large amount of energy accumulates in the scintillator crystal. Gamma-ray interactions, which are difficult or relatively difficult to use, are more interesting in this region.

As a better device than a photo diode are avalanche photodiodes. And this is essentially the same thing as photodiodes that drive it with a large reverse bias. And so, by having this reverse bias, you get an avalanche process when the electron-hole pairs move. You get an ongoing multiplication. This means you get an effective gain of about five to a hundred.

So these devices work much better than basic photo diodes and they are also used in many applications. Mostly for charged particle detection, of course. However, they still do not have comparable gains with standard photomultiplier tubes. This is where photosensors come into play. These are silicon photomultipliers. They have comparable gain to a photomultiplier tube.

And this was a technology that was developed about 10 years ago and is now being used by medical imaging, especially positron emission tomography [9].

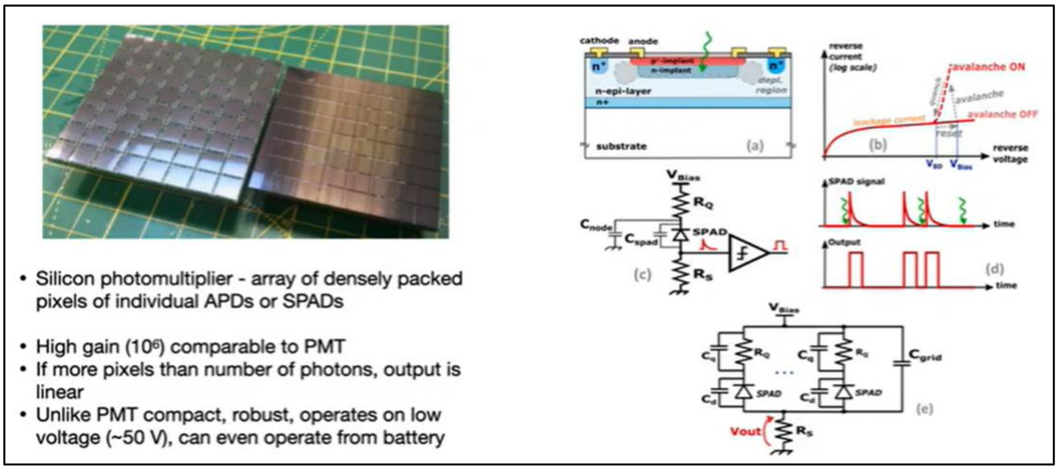

- Silicon photomultiplier - array of densely packed pixels of individual APDs or SPADs

- High gain (10^6) comparable to PMT
- If more pixels than number of photons, output is linear
- Unlike PMT compact, robust, operates on low voltage (~50 V), can even operate from battery

Figure 3. 21: *Silicon Photomultipliers (SiPMs). Adapted from Ref. [8].*

By design, it's about taking the pixels of individual avalanche photodiodes and packing them very densely into a tiny silicon sensor.

In the top left picture you see the silicon photomultipliers arranged like this chessboard. If you look through a microscope at one of these six-by-six-millimeter squares, you'll see tens of thousands of tiny avalanche photodiodes on it. And each of them sits on a sheet trigger. It produces an avalanche when a photon falls on it, and then rebounds. So, when you have more avalanche photo diodes, more small pixels on it, and photons falling on it, you see that the output signal is proportional to a number of photons. And this is very important for the spectroscopic detector.

As Figure 3.21 clearly shows, the main advantage of this type of technology is that it is significantly more compact than a photomultiplier tube. And so it is a relatively fragile tube. These things are very tiny silicon sensors.

Also, non-silicon photomultiplier tube requires high voltage, i.e. a thousand volts or more, while the silicon one typically operates with a bias of about 50 volts. So you can even run silicon photomultipliers from a battery [9].

To summarize, here is an introduction to the different types of scintillators that distinguish between inorganic crystal scintillators and organic scintillators, which are more typically used for neutron detection. Photomultiplier tube and avalanche photodiodes are still the most important technologies, after giving the necessary information about photo sensors, focusing on a few main examples. Then, information about Solid State Insertion Photodiodes, which is an avalanche photodiode, was given. Finally, the use of avalanche photodiodes called Silicon Photomultiplier is mentioned as an attempt to replace the traditional photomultiplier tube.

Some of the equipment used in the laboratory in Figure 3.22; Coated scintillation material, photosensor, oscilloscope and multi-channel analyzer program and other cables and hardware can be seen.

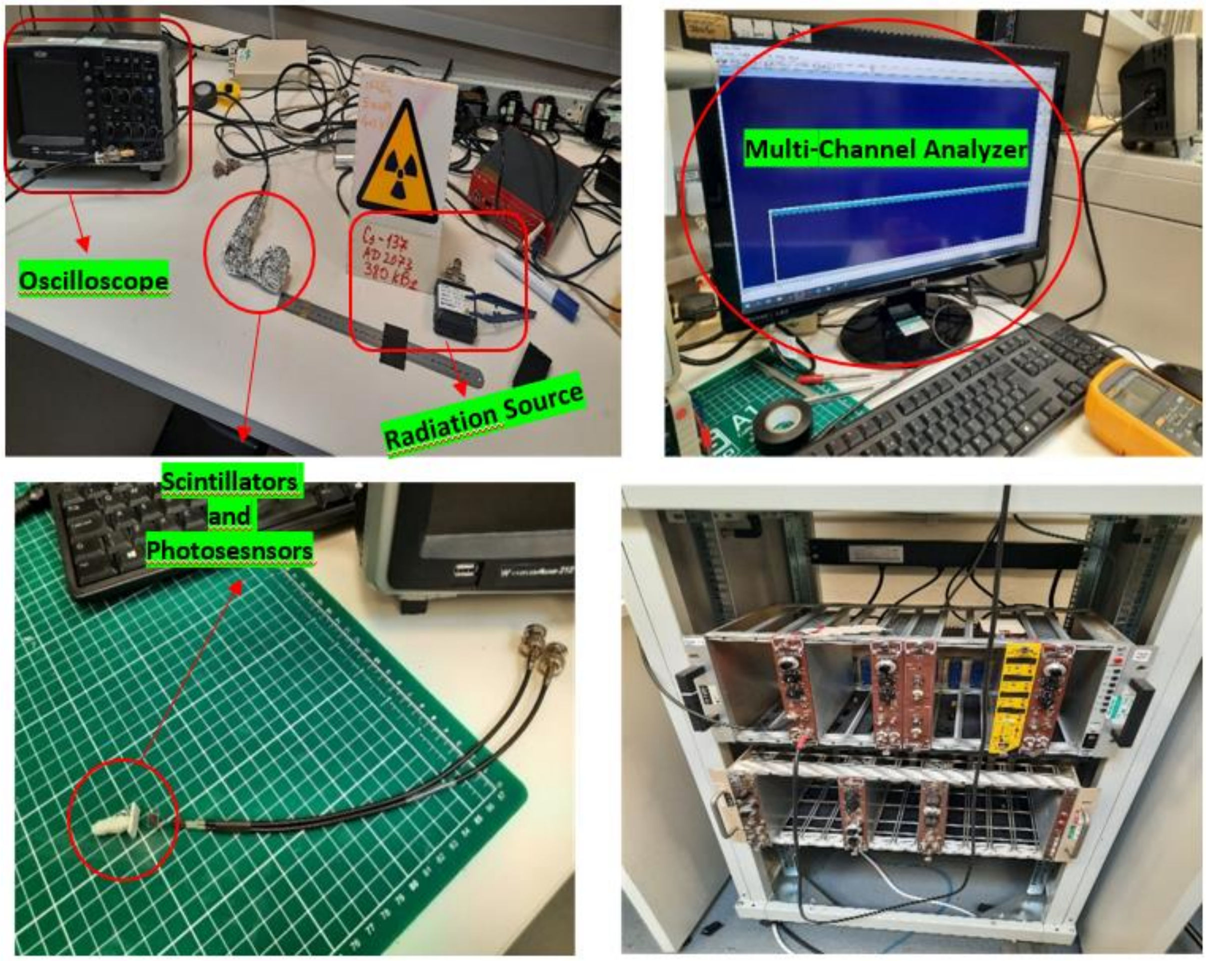

***Figure 3. 22:** Some tools and equipment used in the laboratory.*

Chapter 4

4. NATURALLY-OCCURRING RADIOACTIVE MATERIALS (NORM)

Since the formation of the earth, radioactive elements in the structure of the earth's crust and the radiations emitted by them and high-energy cosmic rays from space constitute natural radiations. Natural radioactive substances, which are found in many other environments such as soil, water, air, vegetation, nutrients and building materials, irradiate our body externally and internally. Humanity has continued to evolve over millions of years to significantly withstand the biological effects of naturally occurring radiation in the environment. However, higher levels of this type of radiation can increase health risk. All types of soil contain an average of 500 Bq of natural radioactive material per kilogram. As can be seen in Figure 4.1, the most important radiation sources in nature to protect ourselves from the possible bad effects of radiation are radionuclides in the U-238 and Th-232 decay series. For most human activities involving minerals and raw materials, exposure levels to these radionuclides are not significantly higher than normal background levels, but certain business activities can result in significantly increased exposures that may need to be controlled by regulation. The material that causes these enhanced exposures is known as Naturally Occurring Radioactive Material (NORM) [10].

Examples of NORM are long-lived radioactive elements such as uranium, thorium, and potassium, and any of their decay products, such as radium and radon. These products have always been present on Earth and its atmosphere, and are concentrated in some parts of the world where they can be mined, such as uranium ore bodies. It also exists to separate the norm, i.e., natural radioactive material, from sources of anthropogenic radioactive products, such as those produced by nuclear reactors and used in nuclear decommissioning or nuclear medicine; where the radioactive properties of a material can make it useful and suitable. But from the perspective of radiation doses for humans, such a distinction is arbitrary. The average dose of local radiations together with cosmic rays in a year is 2.4 mSv (mili Sievert) as the world average [11].

The types of radiation from Po-210 and Pb-210 in NORM are low-energy forms that cannot penetrate the skin. However, they can be harmful to health if the radioactive material is inhaled or swallowed. Management of health risk is necessary where prolonged exposure to NORM and/or high concentrations is possible. In addition, lime, dust and mud containing NORM can ignite spontaneously in some cases. This poses a fire and explosion safety risk in gas networks and facilities such as petrochemical plants that use gas as a raw material [12, 13, 14].

Other than uranium ore extraction and other fuel cycle activities, industries known to suffer from NORM problems include:

- ***Oil and Gas industry***
- *Coal industry*
- *Metal mining*
- *Mineral sand (Soil minerals, zirconium, titanium etc.).*
- *Fertilizer industry*
- *Construction industry*
- *Recycle*

4.1 NORM Resources

If it is desired to group radioactive isotopes that cause natural radiation, they can be grouped as substances on earth (terrestrial sources) as the first group and as (cosmogenic) substances produced as a result of the interactions of gases in the atmosphere with cosmic rays coming from outer space as the other group. NORM is generally expressed in one of two ways: Becquerel per kilogram (or gram) or indicates the level of radioactivity of a particular radioisotope, while parts per million (ppm) indicates the concentration of a particular radioisotope in the material [15].

4.1.1 Terrestrial NORM

Terrestrial NORM emanates from the earth's crust and consists of radioactive products that result in exposure to radiation in environments with increased human activity. The materials may be such as Uranium and Thorium or their degradation products or Potassium-40 forming part of the characteristic decay chain series. The two most important chains providing some suitable nuclides in NORM are the thorium and uranium series, as illustrated in Figure 4.1. Another important terrestrial NORM source is Potassium 40 (K-40). Due to potassium 40's long half-life (approximately 1.25 billion years), it appears to exist in certain amounts today. Beta usually decomposes into Calcium-40 and constitutes 0.012% of natural potassium, which is composed of stable K-39 and K-41. Potassium is the seventh most abundant element on earth, where K-40 averages 850 Bq/kg. It is found in many food products and thus reaches our bones and meets an important nutritional requirement. (Humans have about 65 Bq/kg of K-40 and therefore contain a small level of radioactivity with these foods. The average 70-75 kilos person has 4400 Bq of K-40 and 3000 Bq of Carbon-14.) [16].

4.1.2 Cosmogenic NORM

Cosmogenic NORM is formed by the interaction of certain gases in the atmosphere with cosmic rays from outer space. Since most cosmic rays are deflected by the earth's magnetic field or absorbed by the atmosphere, very little reaches the Earth's surface, and these cosmic radionuclides cause greater doses at lower altitudes than cosmic rays. At higher levels, dose values increase depending on both, indicating that mountain dwellers and frequent flyers are exposed to higher doses than others. For the vast majority of people, this cosmogenic Norm contributes very little to the dose values exposed – that is, a few tens of microsieverts per year. But in terrestrial NORM the situation is much different. Radon in particular contributes most of the natural dose, usually over 1000 microsieverts (1 mSv) per year. NORM and cosmic radiation account for more than 85% of the "average individual" exposure to radiation. Much of this comes from exposure related to nuclear facilities and medical procedures. (Exposure from the nuclear fuel cycle, including fallout from the Chernobyl accident, accounts for less than 0.1%.) [17].

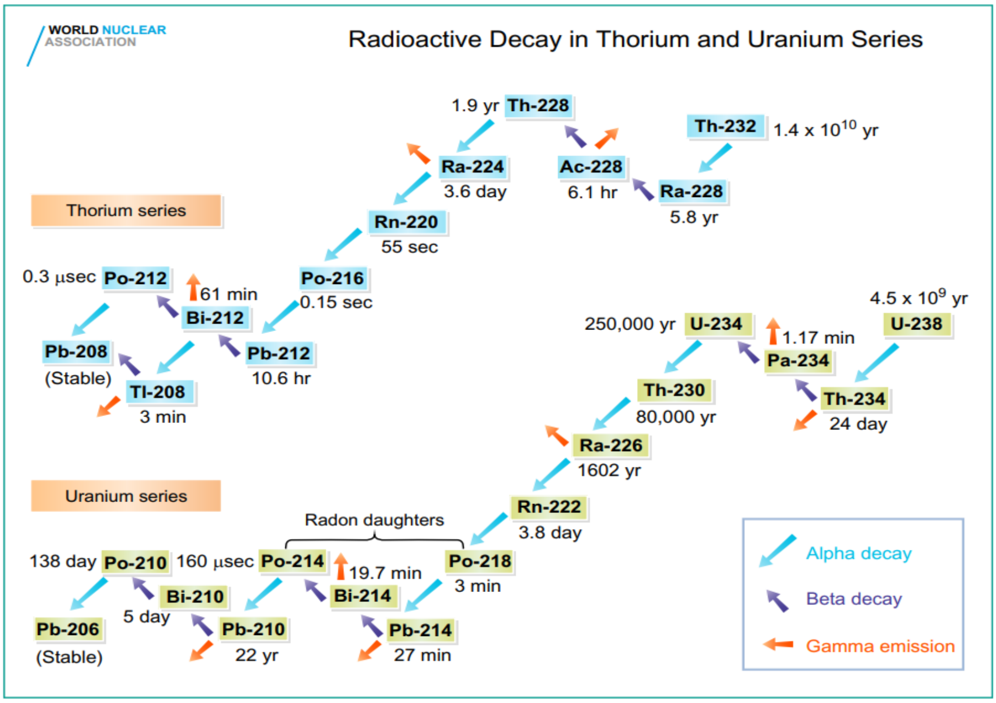

Figure 4. 1: *Radioactive decay in Thorium and Uranium series. Adapted from Ref. [16].*

4.2 NORM in Oil and Gas Production

Analysis of many oil and gas wells has shown that uranium and thorium isotopes are not mobilized from the rock formations containing them. For example, Ra-224, Ra-226, Ra-228 and Pb-210 are mobilized and occur in co-produced water during oil and gas extraction. These radioactive isotopes can then precipitate out of solution along with sulphate and carbonate deposits as lime or sludge in pipes and related equipment. Radon-222 is the abrupt decay product of Radium-226 and usually follows gas lines. It converts to Pb-210 with a few quick steps, so it can be deposited as a thin film in degassing equipment [18].

The level of radioactivity varies depending on the radioactivity of the reservoir rock and the salinity of the water co-produced from the well. The higher the salinity, the higher the probability that NORM will act. Because salinity generally increases with the age of a well, older wells tend to exhibit higher NORM levels than younger wells. Table 4.1 gives the measurement values of the concentrations and properties of NORM produced during oil and gas extraction.

If the hard scale has an activity of 30,000 Bq/kg, it is “contaminated” according to Victorian regulatory guidelines. This means that the level of Ra-226 for the Ra-226 scale is 3300 Bq/kg. For the Pb-210 scale, the level is 10,000 Bq/kg. These numbers refer to scale, not the total mass of pipes or other materials. A 2010 analytical report shows the scale of Pb-210 at 18.6 MBq/kg from a pipeline in Canada.

Another NORM problem for seawater injection systems has recently emerged: biofilm deposits that fix significant amounts of seawater uranium. Fracture for gas production (hydraulic fracturing) releases significant NORMs in some geological environments, both in drill cuts and in water. In the US Marcellus shale (a black shale) of Pennsylvania, New York, and West Virginia, activity is typically about 370 Bq/kg, with high levels of radium-226 in brine, up to 625 Bq/L and 66 Bq'. Returned to the surface in other waters up to /L. USGS figures for salt water are reported as 377 Bq/L Ra-226 and 46 Bq/L for

Ra-228. Other reports have tied the wastewater here to the drinking water standard (0.185 Bq/L) and recorded 300 times the US NRC limits for industrial wastewater discharge [19].

NORM in the oil and gas industry is a major problem for workers, especially during maintenance, waste handling and processing, and decommissioning [20].

Radionuclide	Natural gas (Bq/m^3)	Produced water (Bq/L)	Hard scale (Bq/kg)	Sludge (Bq/kg)
U-238		Trace	1–500	5–10
Ra-226		0.002–1200	100–15 million	50–800,000
Po-210	0.002–0.08		20–1500	4–160,000
Pb-210	0.005–0.02	0.05–190	20–75,000	10–1.3 million
Rn-222	5–200,000			
Th-232		Trace	1–2	2–10
Ra-228		0.3–180	50–2.8 million	500–50,000
Ra-224		0.05–40		

Table 4. 1: *NORM in Oil and Gas Production. (Source: IAEA 2003, Safety Report Series 34.)*

As shown in Figure 4.2, exposure to NORM in the oil and gas industry is usually low enough that no protective measures are required to ensure workers are below the annual radiation dose limit, as specified in IAEA standards [21].

Figure 4. 2: *Some Pipe types and sizes in the industry where Naturally-Occurring Radioactive Material measurements can be taken. Adapted from Ref. [14].*

4.3 Some Literature Studies Used In The Thesis

In studies published in 2011 and 2015 by Seiichi Yamamoto, Hiroyuki Ishibashi and Jun Hatazawa, they developed a detector system to simultaneously detect alpha and beta particles and gamma rays emitted into the environment as a result of the accident, based on the nuclear power plant accident in Fukushima Daiichi [22, 23]. This system consists of 3-layer scintillation detectors optically connected to each other and integrated with a photomultiplier tube. The first layer, made of a thin ZnS(Ag) plastic scintillator, detects alpha particles, while the second layer, made of Gd2SiO5 (GSO) (1.5 mol.% Ce) scintillator, detects beta particles. The third layer was also made from GSO (0.4% mol. Ce) scintillator to detect gamma rays. It is thought that this developed detector system will be useful not only for radiation monitoring but also for medical and molecular imaging, especially in other applications where simultaneous measurements of alpha and beta particles and gamma photons are required at nuclear power plant accident sites (Seiichi Y., Hiroyuk I., 2015; Seiichi Y., Jun H., 2011).

Nuray Yavuzkanat and Sefa Ertürk developed a new generation gamma detector system for use in medical imaging with GAGG(Ce) scintillation material, in their work published in 2019 [24]. In the study, they observed that mammography and standard breast imaging devices in hospitals were not sufficient for the diagnosis of breast cancer, especially for women over 40 years of age and overweight. From this point of view, the spatial resolution of the scintillation detector system, which is an extremely important parameter for nuclear medical imaging, is emphasized. SPECT systems with different scintillators used in imaging devices were investigated by using the GATE simulation program, which is based on GEANT4. Medical image ImageJ. image properties such as spatial resolution and mean gray values for various scintillators were compared. With this research, it has been shown that the spatial resolution value for GAGG(Ce), a relatively new scintillation material, is very close to that of SrI, one of the expensive scintillators. For medical imaging, position-sensitive SiPMs or PMTs have been used to describe the location of events. Appropriate collimators were used to obtain a meaningful image from the detector system. It is stated that the newly designed detector system can be in direct contact with liquid or water to monitor the radiation in or around the nuclear power plant, as well as detecting three different types of radiation with a single detector. Through this work, they were able to directly measure beta particles emitted by Ga-68 and F-18, which are used as PET radiotracers at the Hull PET research center. In the study that shows the design of such a detection system, it is emphasized that the detector system can be mobile and can be used for real-time monitoring in groundwater, and is also highly suitable for application to nuclear decommissioning applications with alpha-beta-gamma detection (Yavuzkanat N., Ertürk S., 2019).

In a study published in 2021 by David Jenkins and Nuray Yavuzkanat, a 3-layer scintillation detector system was studied to measure alpha and beta particles and gamma rays simultaneously and separately with good efficiency and at the same time offer cost-effective, portable and real-time monitoring [25]. In this research, the best available alpha-beta-gamma radiation detector materials and their optimum thicknesses were investigated using Geant4-based GATE simulation. As a result of this study, it was seen that for each type of radiation, a better efficiency result was obtained compared to previous studies in the literature. In this simulation study, 0.05 mm ZnS(Ag), 3.2 mm plastic scintillator and 1.75 mm BGO materials were used for the detection of alpha, beta and gamma rays, respectively. It was emphasized that this study can be used as a miniaturized radio-guided surgical beta-gamma probe, as well as a modification to nuclear medicine and robotic surgery, and it will also affect three different areas in imaging technology, homeland security and nuclear industry (Yavuzkanat N., Jenkins D., 2021).

Chapter 5

5. MATERIAL AND METHOD

5.1 Monte-Carlo Method

Monte Carlo methods have a great place in nuclear physics, statistical physics, biophysics and physico-chemistry and in processes that require many applications. The MC method, which is needed in quantum measurements and radiation modeling, which seems very complex to us, and in dose calculations related to radiation, shows itself in almost all disciplines.

Thanks to the MC method, molecular designs and statistical field theories of particle-polymer systems can also be made. At the same time, Monte Carlo methods can solve the many-body problem for quantum systems.

In the interaction of radiation with materials and in experimental nuclear physics, Monte Carlo methods are used to model radiation detection, make sense of their interactions, and compare the experimental data obtained with theoretical data.

In addition, the Monte-Carlo method is used in a wide variety of ways in astrophysics to model both the structure of galaxies and the microwave radiation emitted from any planet. Monte Carlo methods are also used on the basis of today's weather forecasts.

It can also be easily used to predict the distribution and interactions of radioactive particles. With the GEANT4 code in it, you can design, view, etc. work can be done easily [26].

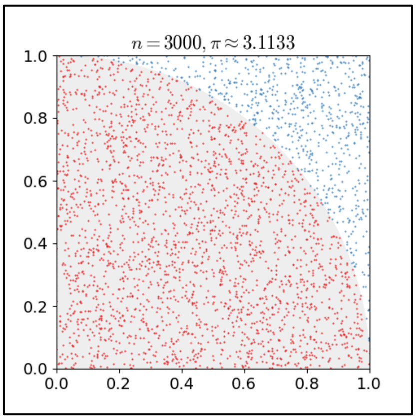

Figure 5. 1: *Monte-Carlo method applied to approximating the value of π. Adapted from Ref. [26].*

5.2 GEANT4 Simulation Toolkit

Geant4 is a software program that simulates the interaction types of radiation and radioactive particles, which are the subject of many fields of physics, and their relations with materials, inspired by the Monte-Carlo methods that were first used in the 1970s.

In a study initiated in the 1990s the simulation of detectors in the Large Hadron Collider experiment in high energy physics, the Geant4 simulation package was created using the more advanced C++ software language, with the idea of moving forward the Geant3 program obtained from the old Fortran software.

This simulation program is used in many fields of physics, as well as in engineering, medicine and space. Because the program can present to its users in a very sensitive way, how, how and what kind of interactions with which matter the particles it contains until the end of their energy. Users of the program have the opportunity to see, watch and discuss every step of the particle interaction.

This program, which allows its users to change the type of particles and the materials they will interact with as they wish, also offers the opportunity to adjust the geometries, positions and energies of particles and materials according to their respective projects. At the same time, it has a very large library that everyone can benefit from. In this library, information about related physical processes, formulas and models can be easily accessed.

Projects in the program are made in source folders called src. In this folder, there are different files suitable for each physical process and modeling. For instance; DetectorConstruction.cc, PrimaryGeneratorAction.cc, PhysicsList.cc … etc. Because the operation of the relevant simulation depends on this folder [27].

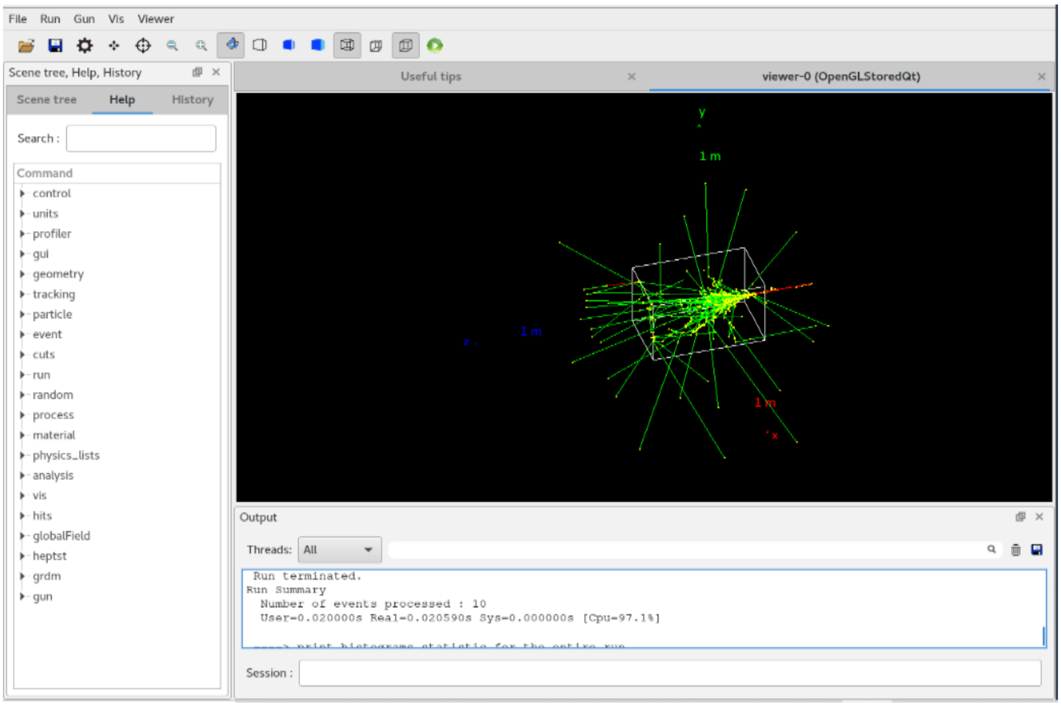

```
 Run terminated.
Run Summary
  Number of events processed : 10
  User=0.020000s Real=0.020590s Sys=0.000000s [Cpu=97.1%]
```

Figure 5. 2: *Some application areas of Geant4 Simulation Program in physics, depending on wavelength and kinetic energy. Adapted from Ref. [27].*

5.3 GATE Simulation Toolkit For Medical Applications

The GATE software program, developed by OpenGATE Collaboration for the use of Geant4 simulation program in medical applications, is a Geant4-based program that is frequently used in the field of dose calculation and medical physics, especially in radiotherapy. Thanks to the Gate simulation program, many studies such as some models in physics, complex geometries, design and optimization *of medical imaging devices, calculation of radiation dose in radiotherapy can be performed. In addition, macro codes can be worked in this simulation program without any advanced C++ knowledge and it is easier to identify the radiation source, detector and related phantom in this program compared to Geant4.*

In the Gate simulation program, important issues such as physical processes, radiation source, detector structure and material, data output, experiment collection and visualization are presented together in this program [28].

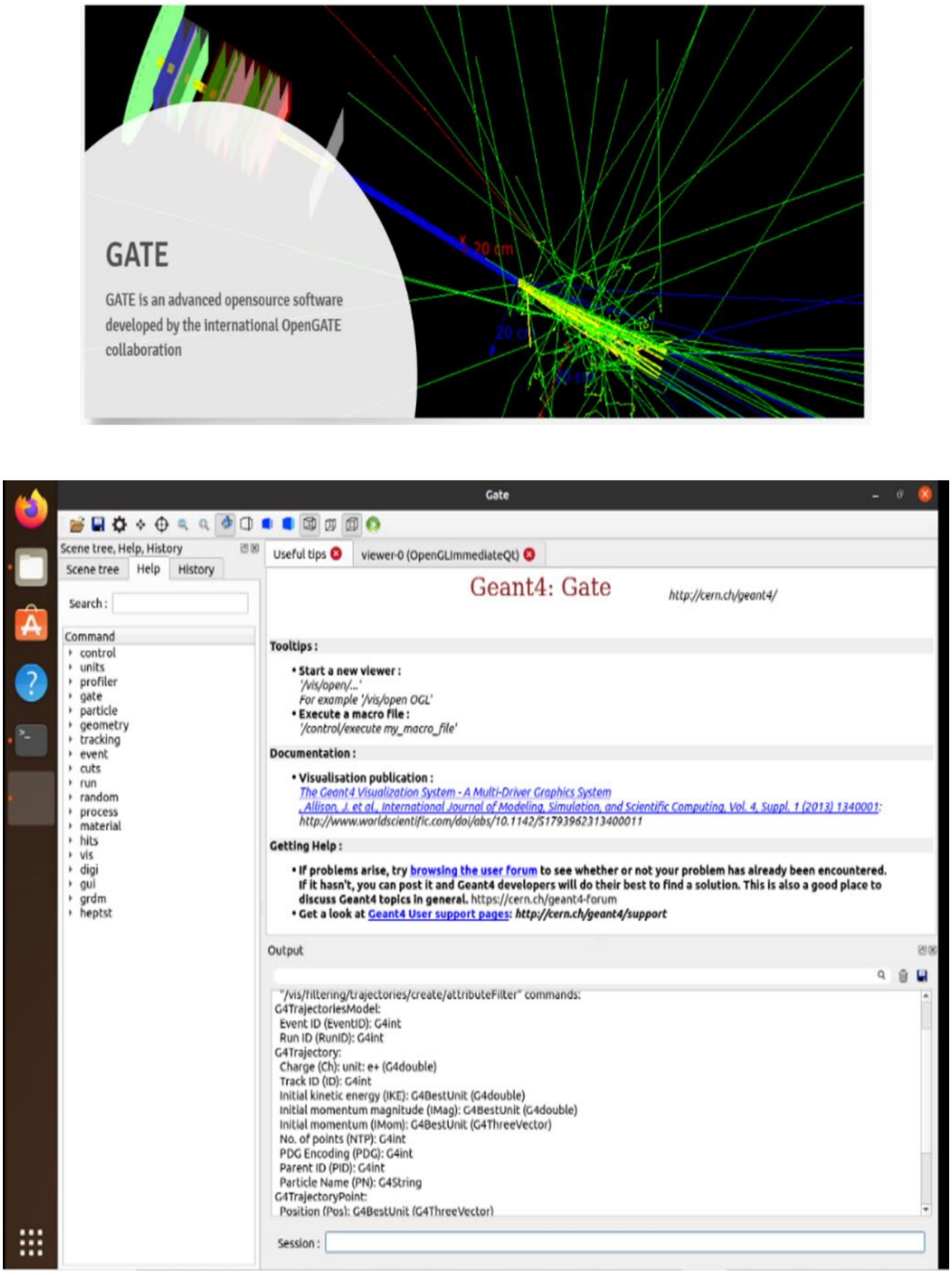
GATE

GATE is an advanced opensource software developed by the international OpenGATE collaboration

Geant4: Gate

http://cern.ch/geant4/

Tooltips :

- **Start a new viewer :**
  '/vis/open/...'
  For example '/vis/open OGL'
- **Execute a macro file :**
  '/control/execute my_macro_file'

Documentation :

- **Visualisation publication :**
  The Geant4 Visualization System - A Multi-Driver Graphics System
  , Allison, J. et al., International Journal of Modeling, Simulation, and Scientific Computing, Vol. 4, Suppl. 1 (2013) 1340001;
  http://www.worldscientific.com/doi/abs/10.1142/S1793962313400011

Getting Help :

- **If problems arise, try browsing the user forum to see whether or not your problem has already been encountered. If it hasn't, you can post it and Geant4 developers will do their best to find a solution. This is also a good place to discuss Geant4 topics in general.** https://cern.ch/geant4-forum
- **Get a look at Geant4 User support pages: *http://cern.ch/geant4/support***

```
 "/vis/filtering/trajectories/create/attributeFilter" commands:
G4TrajectoriesModel:
 Event ID (EventID): G4int
 Run ID (RunID): G4int
G4Trajectory:
 Charge (Ch): unit: e+ (G4double)
 Track ID (ID): G4int
 Initial kinetic energy (IKE): G4BestUnit (G4double)
 Initial momentum magnitude (IMag): G4BestUnit (G4double)
 Initial momentum (IMom): G4BestUnit (G4ThreeVector)
 No. of points (NTP): G4int
 PDG Encoding (PDG): G4int
 Parent ID (PID): G4int
 Particle Name (PN): G4String
G4TrajectoryPoint:
 Position (Pos): G4BestUnit (G4ThreeVector)
```

Figure 5. 3: *Output of the Gate simulation program from interacting with a radiation source and detector. Adapted from Ref. [28].*

5.4 Radiation Sources Used In The Thesis Project

5.4.1 POTASSIUM-40

Potassium-40 is the radioactive isotope of Potassium and has a long half-life of 1.25 billion years, making up about 0.012% (120 ppm) of the total potassium content.

As can be seen from Figure 5.4, Potassium-40 is a rare nuclide capable of both types of beta decay. In these decompositions, it decomposes into Calcium-40 by emitting 89.28% of beta particles at an energy of 1.31 MeV. The remaining 10.72% emits gamma at an energy of 1.46 MeV and decays to Argon-40 (40Ar). The excess of Argon concentration in the atmosphere is due to this decay (approximately 1%).

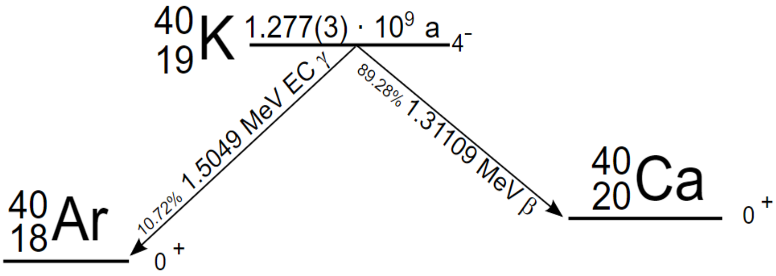

Figure 5. 4: *Possible decay rates, types, energies and decay products of potassium-40. Adapted from Ref. [29].*

The radioactive decay of 40K in the world comes in the third place after the decays of 232Th and 238U, and this situation manifests itself as a radiogenic heat source. It is therefore suggested that significant core radioactivity (1-2 TW) is due to high levels of Uranium, Thorium and Potassium [29].

5.4.2 LEAD-210

(210)Pb is a radionuclide commonly found in the earth's crust and resulting from the decay of (238)U. In the atmosphere, it is due to the decay of (222)Rn. The range of activity concentrations in air at ground level for (210)Pb is 0.2-1.5 Bq m(-3). The activity concentration of (210)Pb in drinking water from private wells is around 11-40 mBq l(-1).

(210)Pb Occurs in reservoirs of sedimentary rocks, mainly in oil and gas sources, sandstones and limestones. Since uranium and thorium are widely distributed in crustal rocks, 238U and 232Th decay strains are found in surface oil, gas, and produced water. Significant quantities of NORM containing these radionuclides are produced during the production, maintenance and shipping phases of operations. 210Pb is found in many extraction and processing sites, mud tanks, pumps and drill pipes. A naturally occurring radioisotope with a short life and a half-life of 22.2 years, as shown in Figure 5.5.

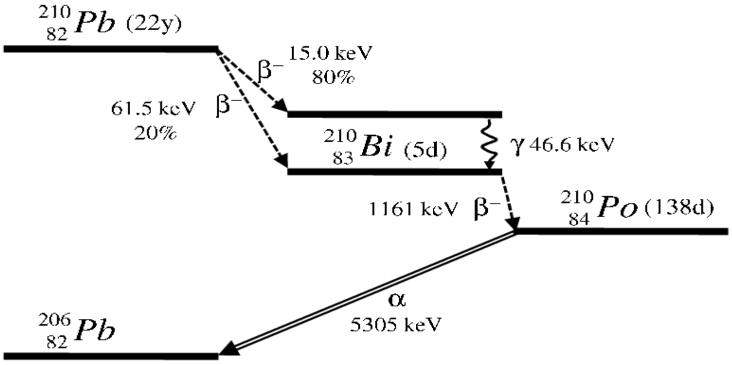

Figure 5. 5: *Decay processes of 210Pb and related energy, half-life and decay products. Adapted from Ref. [30].*

In gas production plants, Radon-222 (immediate decomposition product of 226Ra with a half-life of 3.8 days) decomposes rapidly to 210Pb. Because 222Rn is a gas and therefore highly mobile, degradation strains are deposited in different locations than those associated with the scale of oil production. Internal surfaces of pipes and other equipment in gas treatment plants are often contaminated with 210Pb-rich deposits in the form of thin layers, some of which cannot be detected by visual inspection [30].

5.4.3 CESIUM-137

Cesium-137 or radiocesium is a radioactive isotope created by the fission of Uranium235 in nuclear power plants. It can also be composed of a certain amount of the radioactive element Uranium238. It is moderately short-lived, with a half-life of around 30 years. It has a low boiling point (671 C). For example, the decay modes and energy values in Table 5.1 also show that when a very high temperature Cesium137 leak occurred in the Chernobyl nuclear power plant accident, it was immediately found to be volatile. It can travel long distances in the air. When it is collected in soils on the earth, it has the characteristics of being able to move and spread very easily, since it is very well dissolved in water by means of salt (it is a compound of cesium).

Some usage areas of Cesium137 source:

It is used in the calibration of some radiation instruments. It is used in radiotherapy in the field of nuclear medicine. It is also used in industry for density, thickness and flow measurements [31].

Decay Modes	Decay Energies
Gamma (γ)	*0,6617 MeV*
Beta (β)	*0,512 MeV*

Table 5. 1: *Decay modes and energies of the Cs-137 radiation source.*

5.4.4 COBALT-60

Cobalt-60 (Co-60) radioisotope is the most preferred among radioactive sources in medical applications of radiation and industrial radiation technologies. In addition, in the event of a nuclear accident, the risk of radiation pollution in the environment, radioactive contamination and nuclear pollution in nuclear facilities is minimal compared to Cobalt-60 in terms of nuclear safety and nuclear safety, compared to Cesium-137 (Cs-137). Although there is an advantage for Cs-137 in terms of radioactive half-life, the gamma radiation energy of Co-60 is twice as high. Therefore, the dose rate of Co-60 is higher than that of Cs-137. The high energy of gamma radiation is of great importance in terms of interaction mechanisms and irradiation times of ionizing radiations.

In parallel with the first years of nuclear research, transuranium elements, that is, transuranium radioisotopes, as well as cobalt-59 (Co-59) irradiation in reactors, completely artificial radioisotope and artificial radiation source cobalt-60 (Co-60) were found.

Co-59, which is irradiated with neutrons in stainless steel rods through nuclear power reactors, takes 1 neutron and turns into a Co-60 radioisotope in about a year, thanks to nuclear transmutation, nuclear transformation and nuclear transformation.

Cobalt-60; It is certainly not a radioactive waste produced by the nuclear power industry. At the same time, Co-60, which is not a by-product in the content of nuclear fission and nuclear reactions in the nuclear industry sector, is in the category of completely man-made artificial radioisotopes and artificial radioactive sources or among radioactive elements. Cobalt-60 gamma irradiation sources; It is widely used in the medical industry for the treatment of cancer diseases, sterilization of disposable medical materials, killing microorganisms in pharmaceuticals and cosmetic products [32].

As can be seen from Table 5.2, after Cobalt60 undergoes 99.88% beta decay with an energy of 0.31 MeV, it transforms into a Nickel60 nucleus and then emits two gamma rays. The energies of these rays are 1.173 and 1.332 MeV. Here, the decay equation is:

$$_{27}\mathrm{Co}^{60} \rightarrow {}_{28}\mathrm{Ni}^{60*} + \beta + v \tag{26}$$

$$_{28}\mathrm{Ni}^{60*} \rightarrow {}_{28}\mathrm{Ni}^{60*} + \gamma(1{,}173\ MeV) \tag{26.1}$$

$$_{28}\mathrm{Ni}^{60*} \rightarrow {}_{28}\mathrm{Ni}^{60} + \gamma(1{,}332\ MeV) \tag{26.2}$$

$$_{27}\mathrm{Co}^{60} \rightarrow {}_{28}\mathrm{Ni}^{60} + \gamma(1{,}173\ MeV) + \gamma(1{,}332\ MeV) \tag{26.3}$$

Gamma Energies	**Percent Per Decay**	**Half-Life**
1173,2 keV	*% 99,85*	*5,26 Year*
1332,5 keV	*% 99,98*	*5,26 Year*

Table 5. 2: *Decay energies, decay percentages and half-life of a Cobalt-60 radiation source.*

5.4.5 STRONTIUM-90

The natural element Strontium is not radioactive properties, however its isotope Strontium90 has a very high radioactivity Sr90 transforms into the Yttrium90 isotope by beta decay at 0.546 MeV energy and releases an electron and an antineutrino [33].

The decay equation of Strontium-90 is as follows;

$$_{35}Br^{90} \rightarrow {}_{36}Kr^{90} \rightarrow {}_{37}Rb^{90} + n \rightarrow {}_{\mathbf{38}}\mathbf{Sr^{90}} \rightarrow {}_{39}Y^{90} + {}_{-1}e^{0} \qquad (27)$$

Some properties and usage areas of Strontium90 are as follows:

- It is similar to the element lead and is silver in color.
- It just beta decays. Therefore, it is a very good beta source.
- Its half-life is 28.8 years.
- It is quite dangerous for human health when taken with water or food.
- It can cause diseases such as leukemia and cancer, as well as damage the bone marrow tissue.
- During the Chernobyl and Fukushima nuclear power plant accidents, it was emitted in large quantities to nature.
- It is used in nuclear medicine, radiotherapy and cancer treatments.
- It can also be used in the industry to measure the weight and thickness of some materials.
- It can also be used in generators for a long time, as it emits a lot of heat during its decomposition.

5.4.6 AMERICIUM-241

Americium (Symbol Am) is a man-made radioactive metal that is solid under normal conditions. Americium is produced when plutonium absorbs neutrons in nuclear reactors or during nuclear weapons tests. Americium-241 is the most common form of Americium. The decay equation of the radioactive isotope Am-241, which is a very important source of alpha particles, is as follows:

$$_{95}Am^{241} \rightarrow {}_{2}\alpha^{4} + {}_{93}Np^{237} \qquad (28)$$

Some basic properties and areas of use of Americium241 are as follows:

- Although it emits a very low amount of gamma, it is known as an alpha source in the literature.
- It is silver in color and has a density of 13.67 g/cm^3.
- It must be mixed with Beryllium in order to be used as a neutron source.
- Americium241 can also be used as a smoke detector by making use of the ionization chamber and photoelectric effects.
- It is also used in industry to measure the thickness of some plastics, papers and metals and the densities of fluid materials [34].

5.5 Scintillation Materials Used In The Thesis Project

5.5.1 CsI

Cesium Iodide is colorless crystal or crystalline powder and is light sensitive. Almost insoluble in methanol and water. The relative density is 4.5. Its melting point is 621 C. Its refractive index is 1.7876. Cesium Iodide CsI is a kind of inorganic compound, often used as the fluorescent agent of x-ray image multiplier tube and other fluorescent imaging devices. CsI cathode tube has high detection efficiency for its strong ultraviolet band. CsI crystal is often used as the scintillator material of electromagnetic calorimeter in particle physics experiments. Pure cesium iodine is a fast, high-density scintillator material with relatively high luminescence. Emitted light has two main components: 310 nm and 460 nm in the near ultraviolet region. The disadvantages of Cesium Iodide are its effects under high temperature and slight hygroscopicity. Cesium iodide is used as a spectroscopy in Fourier transform spectroscopy. Compared with the more commonly used KBr spectroscope, Cesium Iodide has a wider light transmission range and can be extended to the far infrared.

Cesium Iodide has higher density and higher gamma ray stopping power than NaI crystal, and it is highly preferred in the 52ort he52re because it is a more economical and less hygroscopic material than NaI crystal. And also, due to its softness, it can be easily processed in different ways. However, the degradation time is less than 1 microsecond compared to other scintillators. CsI scintillator can also be used for particle separation and pulse shape analysis [35].

5.5.2 ZnS(Ag)

ZincSulfide is a mineral consisting of the element zinc as an inorganic compound. And this mineral, which is in its state, can be used in some optical fields. It has the phosphorescence feature introduced by Nikola Tesla, that is, the feature of making a lot of shine. Depending on the activator material it is used with, it can cause glitters in different colors. The melting temperature of this material, which has a density of 4.090 g/cm3, is around 1.850 °C. The refractive index is 2.3677 [36].

5.5.3 EJ212

EJ212 scintillator material, which is used as a good beta particle detector in the industry, is used as a shield in medical devices used in nuclear medicine and is widely preferred in scientific studies, especially in measurements in the field of nuclear physics.

In terms of scintillation efficiency, it has the ability to take 10,000 counts per 1 MeV photon.

Its density is 1.023 g/cm3 and the relevant temperature range is -20°C to 60°C. Rise time, decay time, and Pulse Width (FWHM) are 0.9 ns, 2.4 ns, and 2.7 ns, respectively [37].

5.5.4 LaBr

Lanthanum Bromide crystal appears with its very high efficiency, stopping power and energy resolution, as can be seen in the studies. With a time interval of 200 picoseconds and an energy of 662 keV, it offers a resolution of around 2.7%. Considering the efficiency of scintillation, it provides a count of around 63000 per photon with 1 MeV energy. Its linearity under temperature maintains its position as a separate advantage. Since it is a hygroscopic material, contact with water should be avoided and it is a self-activating material with an energy range of 1500-2750 keV [38].

5.6 Dose Calculation with Water Phantom on Gate Simulation

New features related to radiotherapy were added to the v6 version of the GATE simulation program in 2010, and with a recent update, the modeling of computed tomography and radiotherapy systems was facilitated in the GATE v8.0 version. The higher version of it, v9.1, was used in this study. The following steps has used for radiotherapy simulations and dosimetry calculations:

- *Description of the world where the event took place, dimensions, shape, material (WORLD),*
- *Defining the geometry of the phantom to be used,*
- *Identification of the type, location and distance of the source,*
- *Determining the physical processes to be used in the simulation,*
- *Defining the inputs for the simulation,*
- *Determination of simulation outputs (dose distribution, actor concept, etc.).*

In order to obtain dose values or images in the simulation performed in parallel with the experimental measurements, the following arrangements has made in the files created:

- *Adding and editing the main.mac file to the folder,*
- *defining the target volume in the main.mac file,*
- *main.mac. Defining the dose actor for dose calculation, energy storage, statistical uncertainty calculation in the file,*
- *Editing the physic.mac file where the interactions are carried out, introducing it to the main.mac file,*
- *Introducing the visu.mac file to the main.mac file in order to activate the visualization,*
- *Running the simulation with 5 million particles in order to see the image prepared in the main.mac file and get output.*

Monte-Carlo data has some statistical and systematic uncertainties. Systematic uncertainty often arises from the data in the MC code and the methods used to model interactions. Statistical uncertainty can be calculated for each voxel. Statistical uncertainty is obtained by using the standard deviation of the mean value of the dose stored in each voxel in the GATE program. It is used to calculate statistical uncertainty. The dose actor file defined in GATE gives information about the dose, the square of the dose, the uncertainty of the dose, the energy stored, the square of the stored energy, the uncertainty in the stored energy, and the number of particles arriving in each voxel [28].

Some terms and definitions used in the literature for dose distributions are given below.

The concept of the quality of any beam encountered in dose calculations is directly related to the power of that beam to penetrate the relevant material. And the energy spectrum of the beam shows us this quality. So the graphic value of each photon at each energy is important here. Although there are many factors affecting this beam quality, the most important one is whether the nuclide is the source of the beam or whether it is caused by the braking beam. The energy classifications of photons are given in the literature as follows: Surface (10-100 keV), Orthovoltage (100-500 keV) and Megavoltage (1 MeV and above).

The concept of percent depth dose is very important when defining the photon dose(%PDD). As can be seen in Figure 5.6, The concept defines the normal dose value relative to the maximum dose value as a function of the depth of the phantom. Its basic features include Maximum Dose Depth (dmax), Dose Fall Off (Fall Off) and Skin Protection (Buildup Region). It can be seen these concepts in the Table 5.3 below [39].

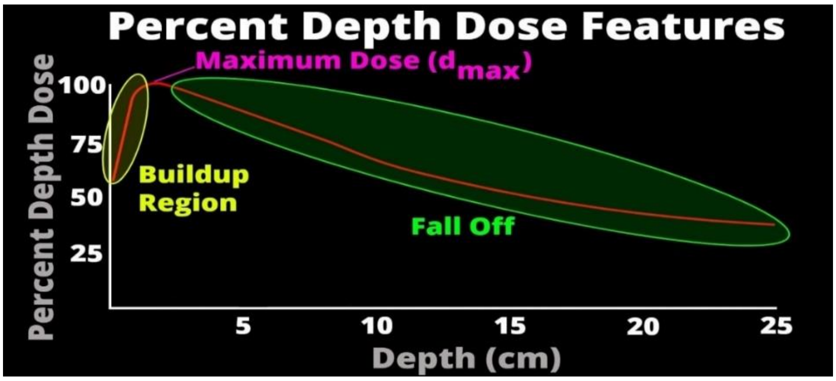

Figure 5. 6: *Plot of Percent depth dose (%PDD) distributions giving dose as a function of depth relative to maximum dose. Adapted from Ref. [39].*

Quantity	Definition	Formula and Unit
Absorbed Dose	*The average energy* $(d_\in)$ *transferred by the ionizing radiation to the unit mass* (d_m) *of an irradiated substance is called the absorbed dose* D.	$D = \frac{d_\in}{d_m}, Gray\ (Gy)$
Kerma	*It is the total kinetic energy of the uncharged particles and all charged particles emitted at the beginning divided by the unit mass* (d_m) *of the relevant area.* dE_{tr} *initial energy of secondary charged particles.*	$K = \frac{dE_{tr}}{d_m}, Jkg^{-1}$
Equivalent Dose	T *is the type of tissue,* D_T *represents the absorbed dose in the tissue, and* Q *represents the quality factor that defines the damage depending on the type of radiation.*	$H_T = D_T\ x\ Q, Sievert\ (Sv)$
Effective Dose	*It is the sum of the doses obtained as a result of multiplying the equivalent dose calculated for the irradiated tissue or organ by the weight factor of the tissue.*	$E = \sum H_T\ x\ W_T, Sievert\ (Sv)$

Table 5. 3: *Dosimetric Quantities (from ICRP 2010).*

It is the percentage $(\boldsymbol{D_{max}} = \%\mathbf{100})$ *of the ratio of the dose measured at any point on the central axis to the dose* $(\boldsymbol{z_{max}})$ *measured at the maximum dose depth:*

$$\boldsymbol{PDD = 100\ x\ \frac{D}{D_{max}}} \tag{29}$$

Here, $\boldsymbol{D}$ is the dose absorbed at any depth, and $\boldsymbol{D_{max}}$ is the maximum dose absorbed at the depth above the central axis.

In radiotherapy, $(\boldsymbol{PDD},\ Percent\ depth\ dose)$ is usually obtained at a certain area size and at a predetermined distance. In clinical practice, $\boldsymbol{PDD}$ measurements are usually made in various field sizes from $2x2\ cm^2$ to $40x40\ cm^2$ and the source-to-surface distance $(\boldsymbol{SSD}$, $Source\ to\ Surface\ Distance)$ is 100 cm. $\boldsymbol{PDD}$ measurements are made during the acceptance tests at the installation stage of the LINAC device, and the difference between the values defined for the device and the measurements is expected to be around 2%.

The maximum dose depth and surface dose depend on the beam energy. The greater the beam energy, the greater the maximum dose depth and the lower the surface dose. While lateral scattering is high in low-energy photons (the penetrating capacity of photons in the tissue decreases due to scattering at low energies and photons scatter sideways, not forwards), forward scattering is dominant in high-energy photons. As the penetration of the photon increases, the surface dose decreases while the maximum dose depth increases. Since the energy of secondary electrons formed at high energies is high, the $\boldsymbol{d_{max}}$ depth will increase. The build-up area is between the surface and the maximum dose depth. An accumulation occurs in the medium due to the electrons ejected from the later layers and the surface. These electrons store their energy at a distance from the origin (Saeedi 2009, Khan 2009).

Through the interaction of electrons and positrons with subatomic particles with the Coulomb force, information is obtained about the behavior of the dose values of these particles (electron and positron) depending on the phantom depth. In applications in medicine, electrons and positrons show a larger surface dose and faster dose reduction compared to photons, and therefore the percent dose depth is also changed [40, 41].

As can be seen in Figure 5.7, some changes are seen when the energy of the electron and positron is increased over the percent dose depth distribution. These;

- There is an increase in the skin dose.
- The maximum dose depth increases.
- Acuity decreases with dose reduction.
- Bremsstrahlung tail increases.

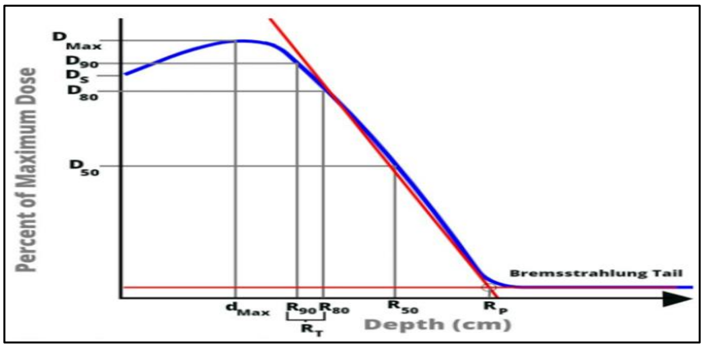

Figure 5. 7: *Depth dependent behavior of electron and positron dose distributions. Adapted from Ref. [40].*

As can be seen in Figure 5.8, a water phantom of certain dimensions ***(50×50×50 mm^3)*** was created using the Gate simulation program, the relevant steps of which were explained above. Because while calculating the dose, a dose calculation is made proportional to water, the water phantom is taken as the basis. Then, dose calculations were made using 5 different energy values (6, 12, 15, 18 and 20 MeV) from 4 different radioactive sources placed right next to this phantom. These sources consist of monoenergetic gamma, electron, positron and alpha particles. As it can be understood from the literature, it has been deemed appropriate to calculate the dose in these energy values, which are frequently used in many areas. These energies were recorded as 6, 12, 15, 18 and 20 MeV in the simulation program. Dose calculations were made for each energy value by taking measurements every 1 mm from the 50 mm long phantom and the energy values stored in the phantom were obtained. From the tables in results and discussion chapter, you can see the dose values in Gray(Gy) according to each energy value and phantom depth. It can be also accessed depth charts and tables against these dose values. All graphs in results and discussion unit has drawn at 5 different energy values and measured at 1 mm intervals.

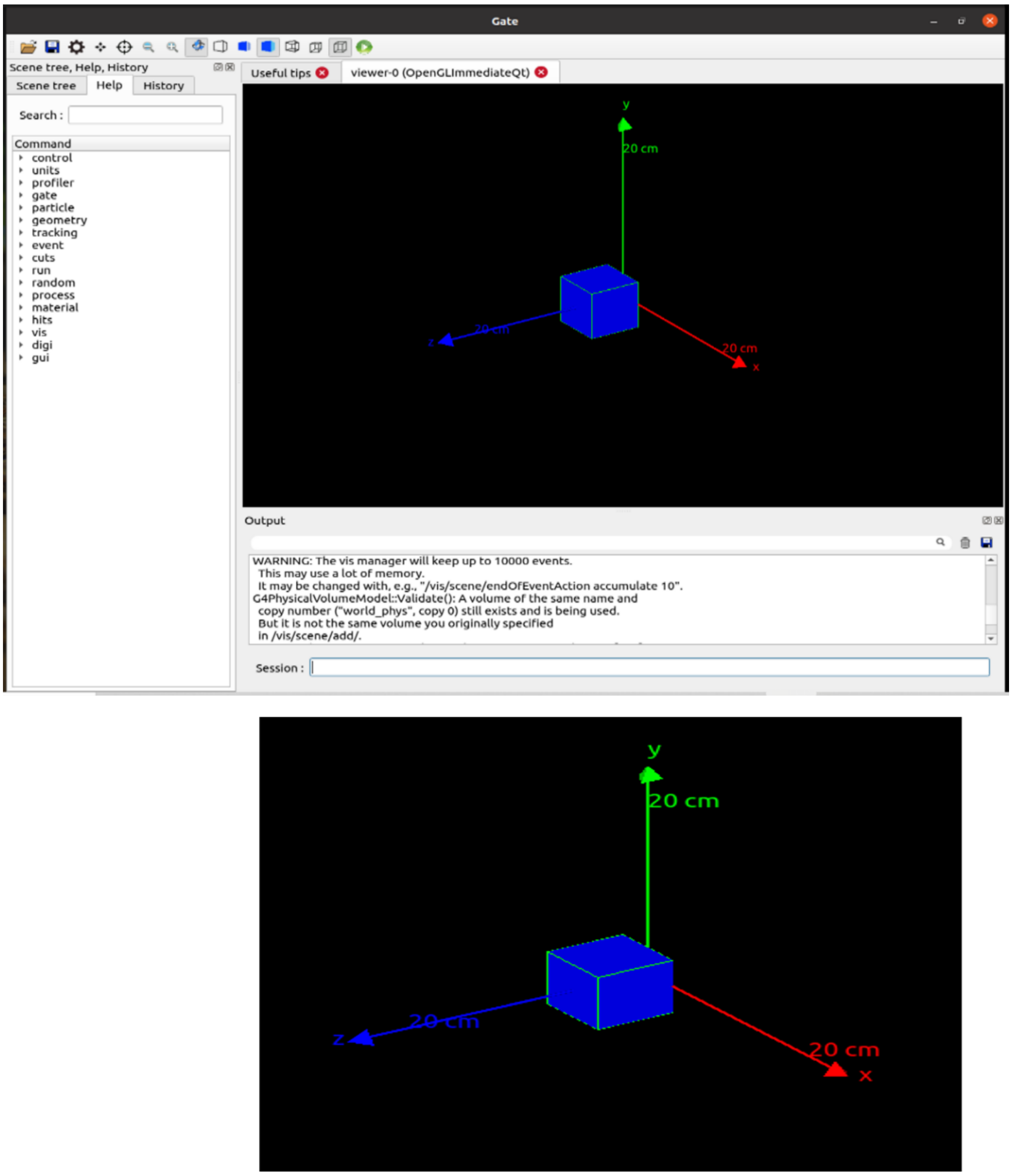

```
WARNING: The vis manager will keep up to 10000 events.
  This may use a lot of memory.
  It may be changed with, e.g., "/vis/scene/endOfEventAction accumulate 10".
G4PhysicalVolumeModel::Validate(): A volume of the same name and
  copy number ("world_phys", copy 0) still exists and is being used.
  But it is not the same volume you originally specified
  in /vis/scene/add/.
```

Figure 5. 8: *Water phantom output coded with Gate simulation program.*

5.7 Detection of Co-60 Emission by a CsI Detector on GEANT4

Using the Cobalt60 radiation source, gamma rays emitted from this source were simulated by the Geant4 simulation program by interacting with the Cesium Iodide scintillation crystal. The gamma ray spectroscopies obtained as a result of this simulation were examined and the interaction types and energy losses were examined.

The detector simulation shown below is a Cesium Iodide (CsI) crystal and a Co-60 radiation source. A gamma ray entering the detector is de-energized by processes mentioned in the previous sections, such as the photoelectric effect, component scattering, and pair formation. After the excitation of the orbital electrons of the Cesium Iodide crystal by photons, some photons are produced in the visible region. Then, these photons were converted into signals by means of the relevant photosensors and examined in a multi-channel analyzer (MCA) by means of electrons.

In the simulation, the Cobalt60 source was placed at a distance of 45.72 cm (18 inches) from the detector as shown in Figure 5.9. Data were recorded both at the detector center and from 16 different angles.

As can be seen in Figure 5.9, measurement of gamma emissions of Co-60 was simulated with a ***1.27x2.54x15.24 cm³ (0.5x1.0x6.0 inch)*** CsI detector. Different source positions were simulated at 17 different angles, including the detector centre - all ***45.72 cm (18 inches)*** from the detector centre.

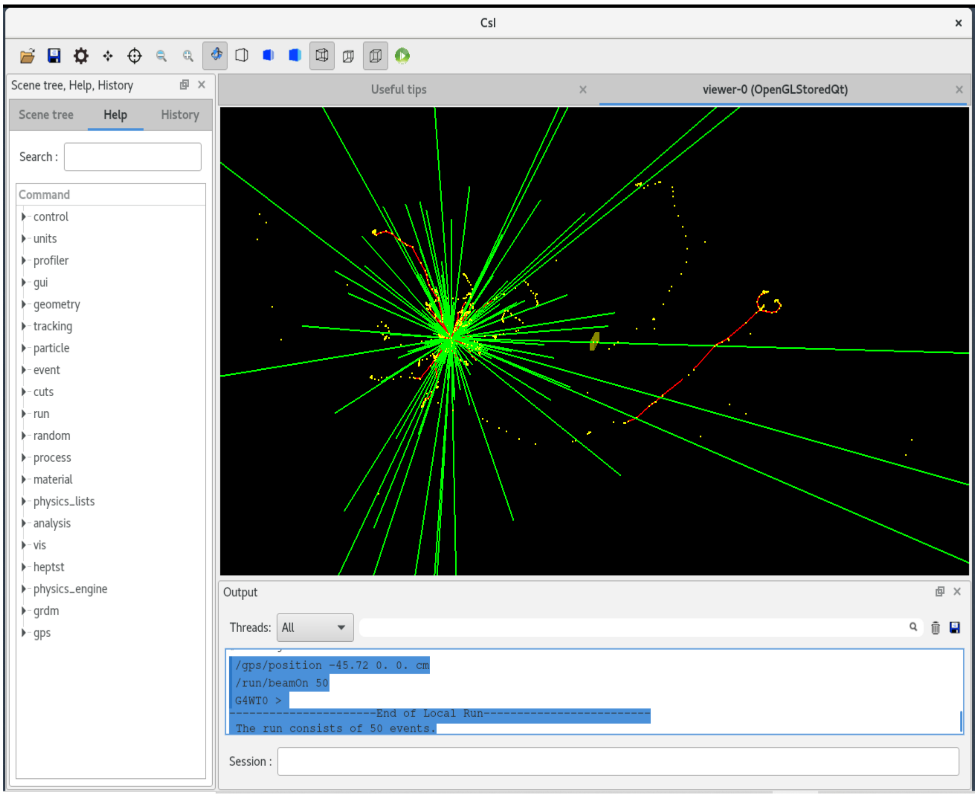

```
/gps/position -45.72 0. 0. cm
/run/beamOn 50
G4WT0 >
----------------------End of Local Run-------------------------
 The run consists of 50 events.
```

__Figure 5. 9:__ Geant4 simulation program output showing the interaction of the cobalt-60 radiation source with the CsI crystal. Green colors represent Gamma-Rays and red colors represent the tracks of the Electron.

5.8 Phoswich Detector System On Gate Simulation

A three-layer detector framework that can calculate alpha particles, beta particles and gamma rays simultaneously and with high sensitivity has been developed by using the Gate simulation program developed for use in medical applications. In this study, Am-241 radiation sources were used for alpha particle source, Sr-90 for beta particle source and Cs-137 radiation sources were used for gamma rays source. In order to detect these radiation sources with high sensitivity, ZnS crystal for the detection of alpha particles in the innermost layer, EJ212 crystal for the detection of beta particles in the middle layer and a new generation LaBr scintillation crystal for the detection of gamma rays in the outermost layer are used. The detector system has been developed in a cylindrical form in order to provide convenience in industrial and medical applications. In the Figure 5.10 below, you can see some outputs of this detector system in the Gate simulation program.

In this three-layer detector system, the ZnS crystal in the innermost layer was chosen with a thickness of 0.05 mm, a length of 50 mm and a radius of 30 mm. The EJ212 crystal in the middle was chosen with a thickness of 3.15 mm, a length of 50 mm and a radius of 30.05 mm. The LaBr crystal in the outermost layer is simulated with a thickness of 5 mm, a length of 50 mm and a radius of 33.2 mm. Some data were obtained from the Gate simulation program by placing Am241, Sr90 and Cs137 radiation sources in the center of the detector system, and some results were obtained according to these data. Some comments and evaluations were made within the framework of these results.

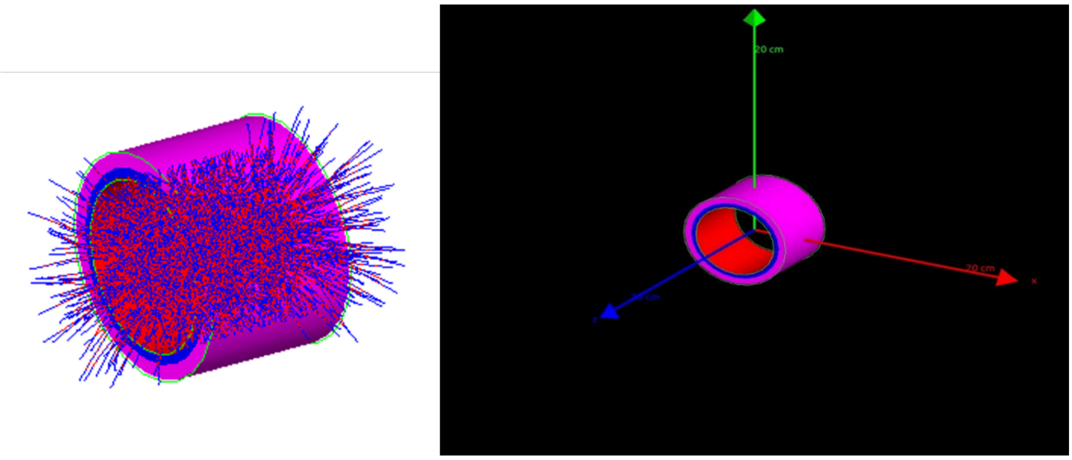

Figure 5. 10: *Outputs of the Gate simulation program showing the three-layer detector system and its interaction with radiation sources.*

5.8.1 Comparison of Phoswich Detector Systems For NORM In Nuclear and Oil/Gas Pipeworks

The following two simulation studies, developed for use in nuclear decommissioning and installations and Oil/Gas installations, developed a new type of three-layer detector system using Naturally Occurring Radiation Sources to measure alpha particles, beta particles and gamma rays.

In this study, Pb-210 radiation source for alpha particles, Sr-90 radiation source for beta particles and K-40 radiation source for gamma rays were used. To detect these radiation sources with high sensitivity, LaBr crystal to detect gamma rays in the innermost layer, EJ212 crystal to detect beta particles in the middle layer and ZnS scintillation crystal to detect alpha particles in the outermost layer are used. These detector systems, unlike other studies above, use natural radiation sources and are also formed in a cylindrical form and in a form suitable for pipe diameters to facilitate their use in pipes in nuclear and oil/gas installations [42]. Figure 5.11 below shows some outputs of these detector systems.

In this three-layer detector system, the LaBr crystal in the innermost layer is 10 mm thick for the pipes in nuclear facilities and 40 mm thick for the pipes in oil/gas installations, while the EJ212 crystal in the middle is 10.05 mm for nuclear installations and 40.05 mm for oil/gas installations. The ZnS crystal in the outermost layer was designed with the same thickness, ie 0.05 mm, for both areas. All scintillators are 50 mm long for nuclear plants and 150 mm for oil/gas applications. In these studies, while the K-40 radiation source was placed inside the detector systems, the Pb-210 and Sr-90 radiation sources were placed outside the detector system, and the following data were obtained from the Gate simulation program and some results were obtained according to these data. The study was completed by making some comments and evaluations regarding the results.

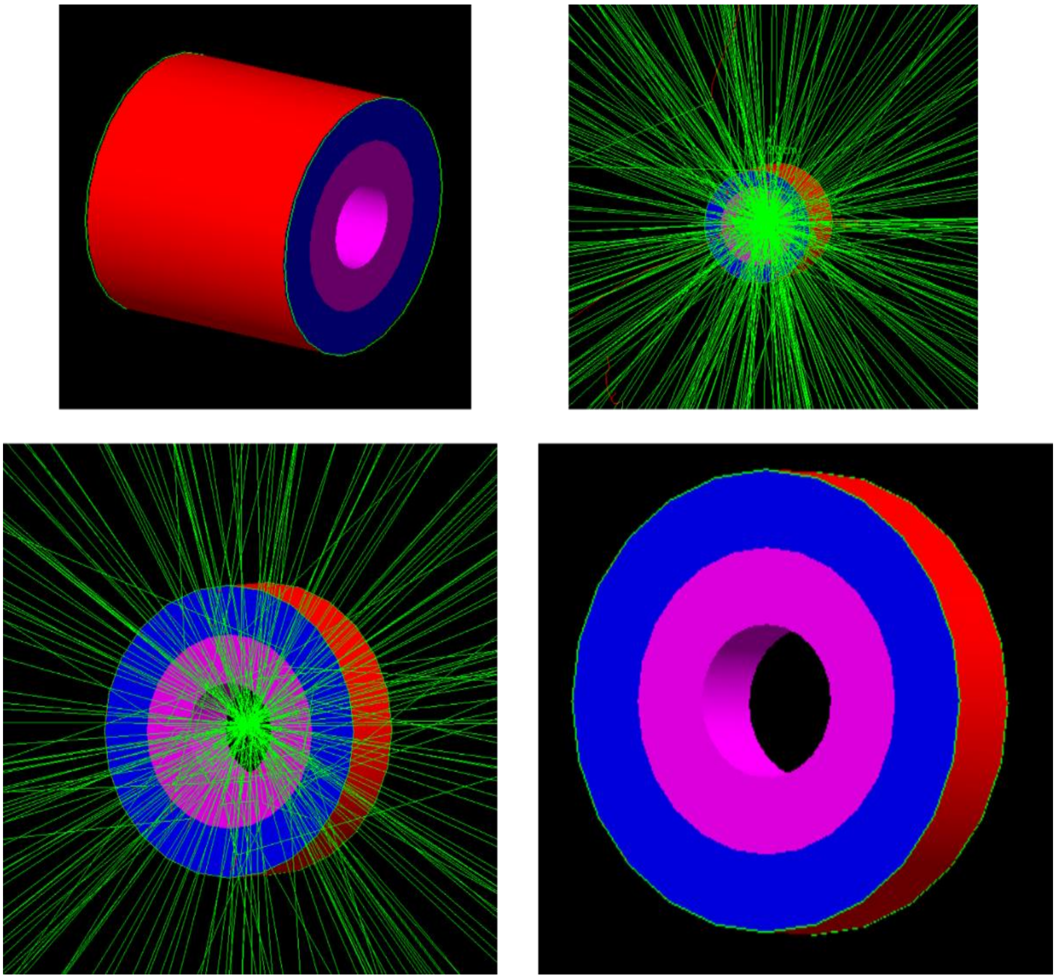

Figure 5. 11: *Outputs of the Gate simulation program showing the three-layer detector system and its interaction with radiation sources. The left side is the simulations for the nuclear pipes and the right ones are the simulations for the oil/gas pipes.*

Chapter 6

6 RESULTS AND DISCUSSIONS

6.1 Results and Some Discussions of Dose Calculation with Water Phantom on Gate Simulation

In Table 6.1 below, dose values of Gamma Rays with 5 different energies (6, 12, 15, 18, 20 MeV) obtained with the Gate simulation program are given at each 1 mm depth of 50 mm^3 Water phantom. Dose values were calculated in Gray. Another Table 6.2 shows the energy-deposited in the water phantom of Gamma rays with different energies. Based on these tables, the Dose values of Gamma rays depending on the depth of the phantom (mm) and the graphs of the Energy deposited in the phantom are presented as can be seen in Figures 6.1 and 6.2.

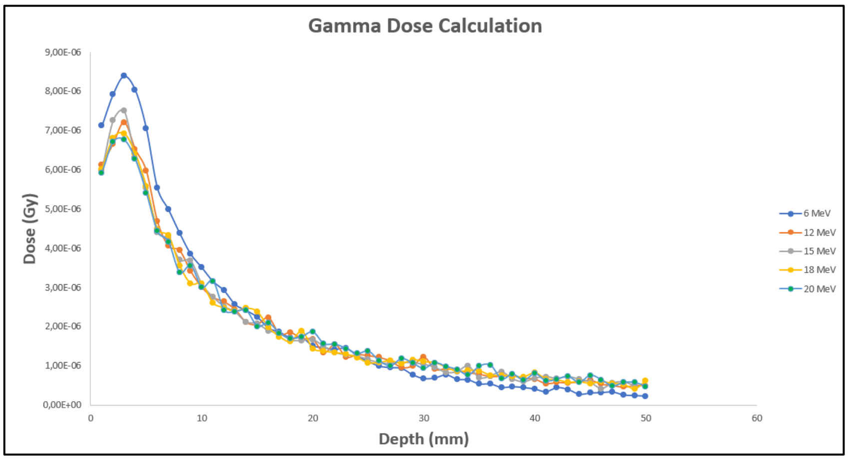

Figure 6. 1: *Dose (Gy) calculation based on depth (mm) at different energy values (MeV) for Gamma Rays in the water phantom.*

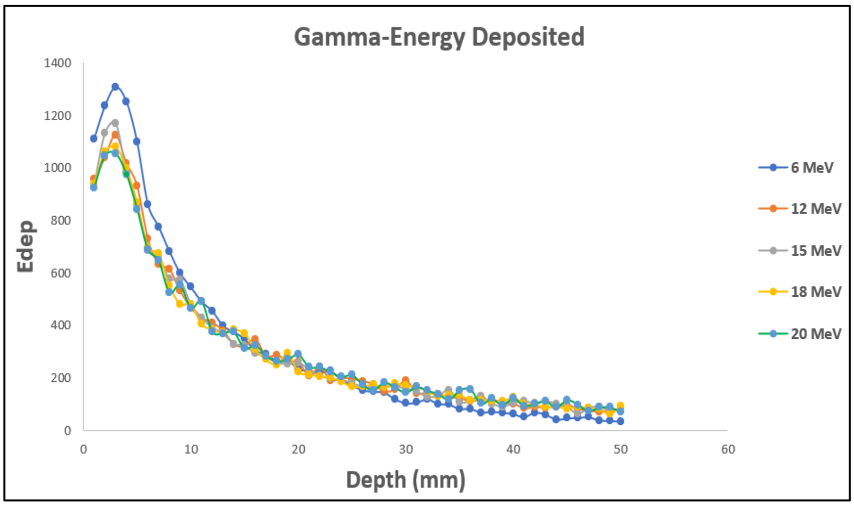

Figure 6. 2: *Energy Deposited calculation based on depth (mm) at different energy values (MeV) for Gamma Rays in the water phantom.*

DEPTH	6 MeV	12 MeV	15 MeV	18 MeV	20 MeV
1	7,1206x10^{-6}	6,13086x10^{-6}	5,98301 x10^{-6}	6,01253 x10^{-6}	5,92195 x10^{-6}
2	7,9208x10^{-6}	6,65996x10^{-6}	7,25339x10^{-6}	6,80492x10^{-6}	6,70956x10^{-6}
3	8,39324x10^{-6}	7,20862x10^{-6}	7,50855x10^{-6}	6,92497x10^{-6}	6,76174x10^{-6}
4	8,03846x10^{-6}	6,52554x10^{-6}	6,32124x10^{-6}	6,41334x10^{-6}	6,26867x10^{-6}
5	7,054x10^{-6}	5,969x10^{-6}	5,53037x10^{-6}	5,57004x10^{-6}	5,41087x10^{-6}
6	5,5311x10^{-6}	4,68095x10^{-6}	4,4092x10^{-6}	4,481x10^{-6}	4,43392x10^{-6}
7	4,98389x10^{-6}	4,05364x10^{-6}	4,24632x10^{-6}	4,31901x10^{-6}	4,15337x10^{-6}
8	4,38585x10^{-6}	3,9413x10^{-6}	3,70493x10^{-6}	3,55198x10^{-6}	3,3759x10^{-6}
9	3,85014x10^{-6}	3,40927x10^{-6}	3,67904x10^{-6}	3,09299x10^{-6}	3,55788x10^{-6}
10	3,50616x10^{-6}	3,00258x10^{-6}	3,0807x10^{-6}	3,08794x10^{-6}	2,99835x10^{-6}
11	3,15466x10^{-6}	2,74676x10^{-6}	2,75145x10^{-6}	2,5997x10^{-6}	3,15976x10^{-6}
12	2,92163x10^{-6}	2,63534x10^{-6}	2,51327x10^{-6}	2,47647x10^{-6}	2,41633x10^{-6}
13	2,56199x10^{-6}	2,43676x10^{-6}	2,37095x10^{-6}	2,3888x10^{-6}	2,38012x10^{-6}
14	2,41116x10^{-6}	2,11058x10^{-6}	2,11211x10^{-6}	2,46447x10^{-6}	2,40914x10^{-6}
15	2,24219x10^{-6}	2,05777x10^{-6}	2,07431x10^{-6}	2,37383x10^{-6}	2,00275x10^{-6}
16	1,9651x10^{-6}	2,23172x10^{-6}	1,8893x10^{-6}	1,97751x10^{-6}	2,09113x10^{-6}
17	1,85814x10^{-6}	1,81017x10^{-6}	1,82679x10^{-6}	1,73774x10^{-6}	1,82618x10^{-6}
18	1,71289x10^{-6}	1,849x10^{-6}	1,65232x10^{-6}	1,6116x10^{-6}	1,69361x10^{-6}
19	1,72533x10^{-6}	1,69668x10^{-6}	1,64135x10^{-6}	1,88101x10^{-6}	1,73892x10^{-6}
20	1,50983x10^{-6}	1,67277x10^{-6}	1,66247x10^{-6}	1,43603x10^{-6}	1,85942x10^{-6}
21	1,46414x10^{-6}	1,33388x10^{-6}	1,48965x10^{-6}	1,37018x10^{-6}	1,55954x10^{-6}
22	1,41623x10^{-6}	1,54909x10^{-6}	1,33703x10^{-6}	1,32894x10^{-6}	1,54793x10^{-6}
23	1,45339x10^{-6}	1,22589x10^{-6}	1,27366x10^{-6}	1,2925x10^{-6}	1,43811x10^{-6}
24	1,25243x10^{-6}	1,28507x10^{-6}	1,23984x10^{-6}	1,20364x10^{-6}	1,30801x10^{-6}
25	1,10898x10^{-6}	1,25869x10^{-6}	1,15506x10^{-6}	1,06946x10^{-6}	1,36843x10^{-6}
26	9,90194x10^{-7}	1,21184x10^{-6}	1,06923x10^{-6}	1,08164x10^{-6}	1,12022x10^{-6}
27	9,5537x10^{-7}	1,12383x10^{-6}	1,06172x10^{-6}	1,1259x10^{-6}	9,94675x10^{-7}
28	9,34838x10^{-7}	9,59123x10^{-7}	1,0777x10^{-6}	1,05475x10^{-6}	1,18157x10^{-6}
29	7,68718x10^{-7}	9,9842x10^{-7}	1,07237x10^{-6}	1,1498x10^{-6}	1,06198x10^{-6}
30	6,75787x10^{-7}	1,22489x10^{-6}	1,03229x10^{-6}	1,10002x10^{-6}	9,31326x10^{-7}
31	6,89599x10^{-7}	9,10242x10^{-7}	9,56889x10^{-7}	1,07713x10^{-6}	1,07467x10^{-6}
32	7,71075x10^{-7}	9,27477x10^{-7}	8,24157x10^{-7}	9,57783x10^{-7}	9,80914x10^{-7}
33	6,57682x10^{-7}	8,88424x10^{-7}	8,46265x10^{-7}	8,53088x10^{-7}	9,01018x10^{-7}
34	6,41129x10^{-7}	8,23574x10^{-7}	9,87953x10^{-7}	8,7229x10^{-7}	7,61196x10^{-7}
35	5,36411x10^{-7}	7,86618x10^{-7}	6,88049x10^{-7}	8,66645x10^{-7}	9,89574x10^{-7}
36	5,36844x10^{-7}	7,27621x10^{-7}	7,35723x10^{-7}	7,5243x10^{-7}	1,0137x10^{-6}
37	4,47325x10^{-7}	7,36963x10^{-7}	8,41083x10^{-7}	7,5293x10^{-7}	6,6379x10^{-7}
38	4,66007x10^{-7}	7,50611x10^{-7}	6,58711x10^{-7}	7,30377x10^{-7}	7,84162x10^{-7}
39	4,44787x10^{-7}	6,87408x10^{-7}	5,87293x10^{-7}	7,13145x10^{-7}	6,27422x10^{-7}
40	4,05939x10^{-7}	6,60158x10^{-7}	6,75554x10^{-7}	8,16746x10^{-7}	7,97446x10^{-7}
41	3,39426x10^{-7}	5,47937x10^{-7}	7,17956x10^{-7}	6,59636x10^{-7}	6,11887x10^{-7}
42	4,44601x10^{-7}	5,75579x10^{-7}	6,7113x10^{-7}	6,37952x10^{-7}	6,57954x10^{-7}
43	3,95289x10^{-7}	5,65637x10^{-7}	7,19054x10^{-7}	5,73461x10^{-7}	7,26827x10^{-7}
44	2,75049x10^{-7}	5,88898x10^{-7}	6,50457x10^{-7}	5,89356x10^{-7}	5,722x10^{-7}
45	3,06226x10^{-7}	6,31528x10^{-7}	5,74021x10^{-7}	5,42438x10^{-7}	7,56786x10^{-7}
46	3,16378x10^{-7}	5,32151x10^{-7}	4,11663x10^{-7}	5,89887x10^{-7}	6,39301x10^{-7}
47	3,31413x10^{-7}	4,99927x10^{-7}	5,52541x10^{-7}	5,44197x10^{-7}	4,81032x10^{-7}
48	2,57111x10^{-7}	4,56156x10^{-7}	5,83453x10^{-7}	5,22814x10^{-7}	5,71821x10^{-7}
49	2,41611x10^{-7}	4,99738x10^{-7}	4,80784x10^{-7}	4,05982x10^{-7}	5,7203x10^{-7}
50	2,27124x10^{-7}	4,91302x10^{-7}	5,06127x10^{-7}	6,15512x10^{-7}	4,67679x10^{-7}

Table 6. 1: *Depth dependent dose values for each energy value for Gamma rays in the water phantom.*

DEPTH	6 MeV	12 MeV	15 MeV	18 MeV	20 MeV
1	1111,082	956,64583	933,57474	938,18229	924,0478
2	1235,944	1039,2055	1131,8031	1061,824	1046,945
3	1309,663	1124,8175	1171,6178	1080,5564	1055,0863
4	1254,303	1018,2304	986,35138	1000,7228	978,14903
5	1100,691	931,38886	862,94696	869,13563	844,29975
6	863,0601	730,40462	688,00081	699,20453	691,85898
7	777,6746	632,52136	662,58569	673,92827	648,08226
8	684,3588	614,99182	578,10899	554,24271	526,76724
9	600,7675	531,97528	574,06892	482,62348	555,16398
10	547,0926	468,51584	480,70502	481,83581	467,85613
11	492,2458	428,59808	429,33074	405,65134	493,04135
12	455,8844	411,21301	392,16488	386,42277	377,03849
13	399,7674	380,22722	369,95759	372,74219	371,38927
14	376,2314	329,33035	329,56821	384,55106	375,91709
15	349,8664	321,08986	323,67047	370,40638	312,50528
16	306,6292	348,23305	294,80256	308,56643	326,29464
17	289,9406	282,45431	285,04742	271,15367	284,95335
18	267,2756	288,51371	257,82436	251,46967	264,26715
19	269,2168	264,74608	256,11305	293,50913	271,33771
20	235,591	261,01571	259,40742	224,0748	290,14009
21	228,4607	208,13565	232,44084	213,79934	243,34663
22	220,9858	241,71614	208,62714	207,36468	241,53483
23	226,7831	191,28451	198,73831	201,67869	224,39926
24	195,4256	200,52001	193,46191	187,8138	204,09891
25	173,0432	196,40321	180,23352	166,87669	213,52653
26	154,5076	189,09302	166,84071	168,77714	174,79628
27	149,0738	175,36057	165,66766	175,68259	155,20686
28	145,87	149,65937	168,16155	164,58153	184,37007
29	119,9489	155,79123	167,33015	179,41162	165,70858
30	105,4482	191,12887	161,07584	171,64498	145,32203
31	107,6034	142,0321	149,31082	168,07301	167,68835
32	120,3168	144,72138	128,59959	149,45023	153,05967
33	102,6232	138,62772	132,04921	133,1139	140,59286
34	100,0403	128,50863	154,15794	136,11017	118,77528
35	83,70028	122,74212	107,36167	135,22939	154,41087
36	83,76793	113,53637	114,80055	117,40754	158,17556
37	69,79957	114,99396	131,24067	117,48546	103,57633
38	72,71473	117,12369	102,78382	113,96638	122,35886
39	69,40362	107,2616	91,639895	111,27751	97,901442
40	63,34182	103,00952	105,41185	127,44321	124,43163
41	52,9632	85,498844	112,02825	102,92816	95,477381
42	69,37453	89,812043	104,72163	99,544613	102,66569
43	61,67999	88,260726	112,19962	89,481489	113,41239
44	42,918	91,890302	101,49585	91,961708	89,28471
45	47,78274	98,542121	89,568981	84,640722	118,08712
46	49,36696	83,035697	64,234928	92,044579	99,755002
47	51,713	78,007514	86,217232	84,915315	75,059077
48	40,11905	71,177621	91,040704	81,578735	89,22561
49	37,70037	77,978006	75,020376	63,348432	89,258227
50	35,43984	76,661597	78,97491	96,043045	72,97555

Table 6. 2: *Depth dependent energy deposited values for each energy value for Gamma rays in the water phantom.*

In Table 6.3 below, Dose values of Electrons with 5 different energies (6, 12, 15, 18, 20 MeV) obtained with the Gate simulation program obtained at each 1 mm depth of 50 mm^3 Water phantom are given. Dose values were calculated in Gray. Another Table 6.4 shows the energy values stored in the water phantom of Electrons with different energy values. Based on these tables, the Dose values of Electrons depending on the depth of the phantom (mm) and the graphs of the Energy deposited in the phantom are presented in Figures 6.3 and 6.4 [43,44].

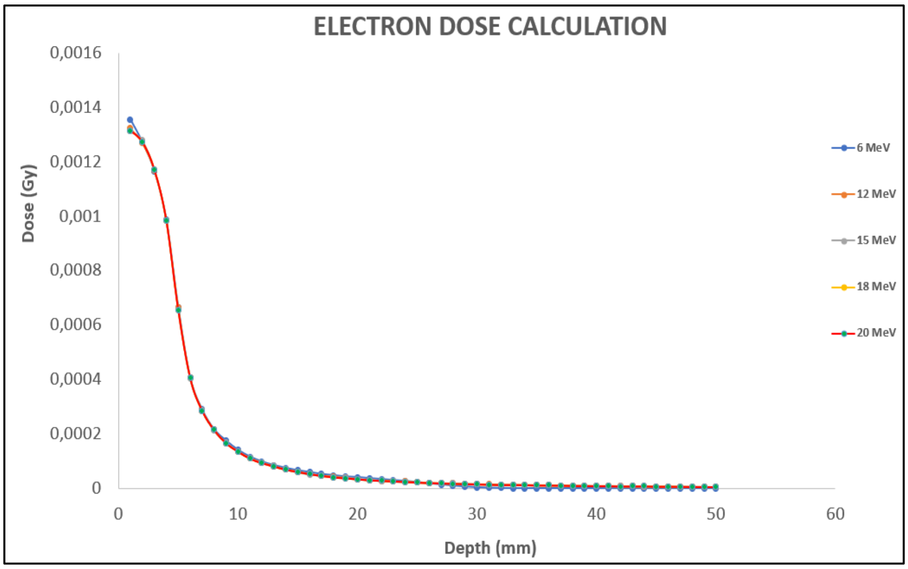

***Figure 6. 3:** Dose (Gy) calculation based on depth (mm) at different energy values (MeV) for Electrons in the water phantom.*

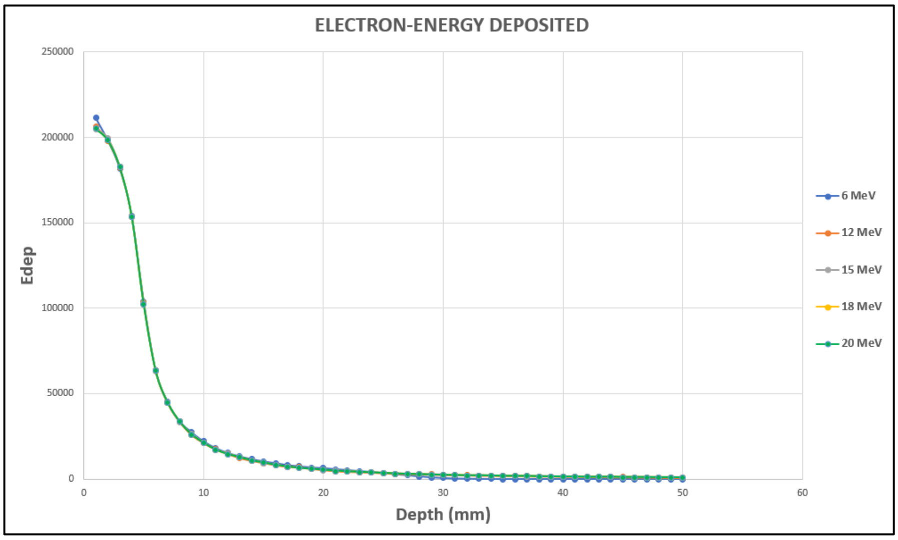

***Figure 6. 4:** Energy Deposited calculation based on depth (mm) at different energy values (MeV) for Electrons in the water phantom.*

DEPTH	6 MeV	12 MeV	15 MeV	18 MeV	20 MeV
1	135,42x10^{-5}	132,31x10^{-5}	131,31x10^{-5}	131,4x10^{-5}	131,4x10^{-5}
2	127,07x10^{-5}	126,91x10^{-5}	127,77x10^{-5}	127,1x10^{-5}	127,1x10^{-5}
3	116,51x10^{-5}	116,87x10^{-5}	117,13x10^{-5}	117,01x10^{-5}	117,01x10^{-5}
4	98,73x10^{-5}	98,39x10^{-5}	98,47x10^{-5}	98,47x10^{-5}	98,47x10^{-5}
5	66,61x10^{-5}	66,32x10^{-5}	65,87x10^{-5}	65,49x10^{-5}	65,49x10^{-5}
6	40,74x10^{-5}	40,62x10^{-5}	40,36x10^{-5}	40,59x10^{-5}	40,59x10^{-5}
7	28,95x10^{-5}	28,55x10^{-5}	28,76x10^{-5}	28,55x10^{-5}	28,55x10^{-5}
8	21,67x10^{-5}	21,47x10^{-5}	21,22x10^{-5}	21,52x10^{-5}	21,52x10^{-5}
9	17,49x10^{-5}	16,59x10^{-5}	16,92x10^{-5}	16,66x10^{-5}	16,66x10^{-5}
10	14,09x10^{-5}	13,53x10^{-5}	13,53x10^{-5}	13,53x10^{-5}	13,53x10^{-5}
11	11,6x10^{-5}	11,09x10^{-5}	11,01x10^{-5}	10,97x10^{-5}	10,97x10^{-5}
12	9,80x10^{-5}	9,50x10^{-5}	9,52x10^{-5}	9,30x10^{-5}	9,30x10^{-5}
13	8,49x10^{-5}	7,91x10^{-5}	8,23x10^{-5}	8,14x10^{-5}	8,14x10^{-5}
14	7,43x10^{-5}	6,87x10^{-5}	6,91x10^{-5}	6,91x10^{-5}	6,91x10^{-5}
15	6,56x10^{-5}	6,03x10^{-5}	5,87x10^{-5}	6,09x10^{-5}	6,09x10^{-5}
16	5,94x10^{-5}	5,26x10^{-5}	5,14x10^{-5}	5,25x10^{-5}	5,25x10^{-5}
17	5,21x10^{-5}	4,61x10^{-5}	4,68x10^{-5}	4,63x10^{-5}	4,63x10^{-5}
18	4,78x10^{-5}	4,38x10^{-5}	4,08x10^{-5}	4,07x10^{-5}	4,07x10^{-5}
19	4,30x10^{-5}	3,89x10^{-5}	3,80x10^{-5}	3,74x10^{-5}	3,74x10^{-5}
20	4,08x10^{-5}	3,39x10^{-5}	3,30x10^{-5}	3,39x10^{-5}	3,39x10^{-5}
21	3,67x10^{-5}	3,00x10^{-5}	3,06x10^{-5}	3,02x10^{-5}	3,02x10^{-5}
22	3,35x10^{-5}	2,76x10^{-5}	2,73x10^{-5}	2,83x10^{-5}	2,83x10^{-5}
23	2,97x10^{-5}	2,60x10^{-5}	2,52x10^{-5}	2,61x10^{-5}	2,61x10^{-5}
24	2,66x10^{-5}	2,47x10^{-5}	2,39x10^{-5}	2,41x10^{-5}	2,41x10^{-5}
25	2,26x10^{-5}	2,20x10^{-5}	2,14x10^{-5}	2,20x10^{-5}	2,20x10^{-5}
26	1,78x10^{-5}	1,99x10^{-5}	2,00x10^{-5}	2,01x10^{-5}	2,01x10^{-5}
27	1,40x10^{-5}	1,90x10^{-5}	1,83x10^{-5}	1,86x10^{-5}	1,86x10^{-5}
28	9,71x10^{-6}	1,81x10^{-5}	1,85x10^{-5}	1,73x10^{-5}	1,73x10^{-5}
29	6,30x10^{-6}	1,71x10^{-5}	1,65x10^{-5}	1,59x10^{-5}	1,59x10^{-5}
30	3,50x10^{-6}	1,53x10^{-5}	1,59x10^{-5}	1,48x10^{-5}	1,48x10^{-5}
31	1,81x10^{-6}	1,49x10^{-5}	1,42x10^{-5}	1,40x10^{-5}	1,40x10^{-5}
32	8,98x10^{-7}	1,39x10^{-5}	1,31x10^{-5}	1,27x10^{-5}	1,27x10^{-5}
33	3,83x10^{-7}	1,29x10^{-5}	1,30x10^{-5}	1,29x10^{-5}	1,29x10^{-5}
34	1,13x10^{-7}	1,27x10^{-5}	1,22x10^{-5}	1,23x10^{-5}	1,23x10^{-5}
35	3,70x10^{-8}	1,19x10^{-5}	1,10x10^{-5}	1,10x10^{-5}	1,10x10^{-5}
36	2,64x10^{-8}	1,14x10^{-5}	1,09x10^{-5}	1,09x10^{-5}	1,09x10^{-5}
37	1,39x10^{-8}	1,08x10^{-5}	9,97x10^{-6}	1,05x10^{-5}	1,05x10^{-5}
38	9,99x10^{-9}	9,89x10^{-6}	1,00x10^{-5}	9,42x10^{-6}	9,42x10^{-6}
39	1,44x10^{-8}	9,97x10^{-6}	9,15x10^{-6}	8,86x10^{-6}	8,86x10^{-6}
40	2,20x10^{-8}	8,64x10^{-6}	8,71x10^{-6}	8,40x10^{-6}	8,40x10^{-6}
41	2,02x10^{-8}	8,94x10^{-6}	7,70x10^{-6}	8,46x10^{-6}	8,46x10^{-6}
42	1,52x10^{-8}	8,16x10^{-6}	7,82x10^{-6}	7,35x10^{-6}	7,35x10^{-6}
43	1,31x10^{-8}	7,88x10^{-6}	7,48x10^{-6}	7,42x10^{-6}	7,42x10^{-6}
44	5,90x10^{-9}	7,14x10^{-6}	6,85x10^{-6}	7,85x10^{-6}	7,85x10^{-6}
45	1,17x10^{-8}	6,92x10^{-6}	6,76x10^{-6}	6,44x10^{-6}	6,44x10^{-6}
46	9,40x10^{-9}	6,27x10^{-6}	6,37x10^{-6}	6,68x10^{-6}	6,68x10^{-6}
47	6,78x10^{-9}	5,93x10^{-6}	6,19x10^{-6}	6,26x10^{-6}	6,26x10^{-6}
48	7,26x10^{-9}	5,35x10^{-6}	5,76x10^{-6}	5,74x10^{-6}	5,74x10^{-6}
49	7,68x10^{-9}	4,67x10^{-6}	5,63x10^{-6}	5,53x10^{-6}	5,53x10^{-6}
50	1,36x10^{-8}	4,54x10^{-6}	5,16x10^{-6}	5,31x10^{-6}	5,31x10^{-6}

Table 6. 3: *Depth dependent dose values for each energy value for Electrons in the water phantom.*

DEPTH	6 MeV	12 MeV	15 MeV	18 MeV	20 MeV
1	211298,7	206450,9	204890,02	205038,9	205038,87
2	198277,8	198027,34	199381,923	198326,5	198326,497
3	181792,4	182361,94	182775,233	182582,6	182582,567
4	154050,4	153536,53	153658,648	153643,9	153643,935
5	103929,4	103480,78	102789,162	102195,7	102195,744
6	63572,34	63384,579	62989,6324	63328,67	63328,669
7	45166,61	44545,725	44884,7676	44550,13	44550,1306
8	33804,62	33502,251	33118,3304	33573,15	33573,1522
9	27287,71	25883,419	26405,1777	25994,27	25994,2745
10	21995,37	21117,047	21112,8001	21113,49	21113,4867
11	18100,97	17298,383	17178,1526	17111,28	17111,2764
12	15283,92	14824,397	14853,3874	14515,34	14515,3379
13	13253,33	12334,825	12843,4312	12705,26	12705,2566
14	11600,11	10720,698	10787,4108	10777,16	10777,1589
15	10242,56	9406,1805	9152,21446	9507,906	9507,90622
16	9268,687	8208,163	8025,75168	8195,593	8195,59291
17	8133,951	7199,9122	7302,35529	7224,644	7224,64441
18	7460,86	6834,3239	6359,71852	6343,331	6343,33108
19	6712,706	6069,2961	5932,13414	5840,596	5840,59632
20	6366,731	5286,7601	5152,3326	5296,468	5296,46848
21	5730,437	4680,5756	4777,37894	4712,97	4712,97034
22	5224,665	4310,6694	4255,96407	4408,728	4408,72801
23	4638,168	4055,3287	3934,5174	4066,832	4066,83191
24	4150,523	3850,919	3734,33686	3753,174	3753,1736
25	3525,518	3434,887	3338,95312	3435,596	3435,59587
26	2782,391	3103,197	3123,87734	3129,497	3129,49747
27	2187,151	2961,541	2849,31894	2902,7	2902,69985
28	1514,406	2818,2019	2885,77961	2704,826	2704,82602
29	983,3313	2671,3923	2570,84677	2481,162	2481,16174
30	546,433	2390,0851	2482,3663	2315,179	2315,17883
31	281,9148	2332,3468	2208,2008	2181,379	2181,37891
32	140,1763	2164,8133	2039,71463	1985,148	1985,14831
33	59,77701	2018,907	2033,68008	2020,008	2020,00803
34	17,70921	1988,6851	1905,8309	1921,614	1921,6141
35	5,769316	1854,9073	1717,50909	1709,896	1709,89561
36	4,125349	1779,341	1693,69785	1698,042	1698,04186
37	2,172195	1677,8912	1556,29331	1641,367	1641,36709
38	1,558873	1542,7974	1566,16666	1469,443	1469,4426
39	2,24058	1556,1398	1428,18691	1382,755	1382,75457
40	3,433746	1347,6294	1359,59027	1311,2	1311,20026
41	3,150336	1395,5615	1201,93923	1320,823	1320,8232
42	2,37076	1272,7069	1219,67511	1147,184	1147,18419
43	2,04239	1229,831	1166,78348	1158,301	1158,30127
44	0,919945	1114,1168	1069,1118	1225,041	1225,04115
45	1,8269	1080,2148	1054,3689	1004,555	1004,55478
46	1,466541	978,43176	993,373925	1042,463	1042,46273
47	1,058355	925,3411	966,129926	976,4285	976,428545
48	1,133201	835,50659	898,410334	895,0503	895,05026
49	1,197935	728,91824	878,740608	862,8135	862,813452
50	2,12113	708,65669	805,729295	828,0409	828,040868

Table 6. 4: *Depth dependent energy deposited values for each energy value for Electrons in the water phantom.*

Here it can be seen the dose values formed in the water phantom by using positrons of different energies as well as electrons. In Table 6.5 below, the Dose values of the Positrons of 5 different energy values (6, 12, 15, 18, 20 MeV) obtained with the Gate simulation program obtained at each 1 mm depth of 50 mm^3 Water phantom are given. Dose values were calculated in Gray. Another Table 6.6 shows the energy values stored in the water phantom of Positrons with different energy values. Based on these tables, the Energy Stored in the Phantom and the Dose of Positrons depending on the depth (mm) of the phantom are presented in Figures 6.5 and 6.6.

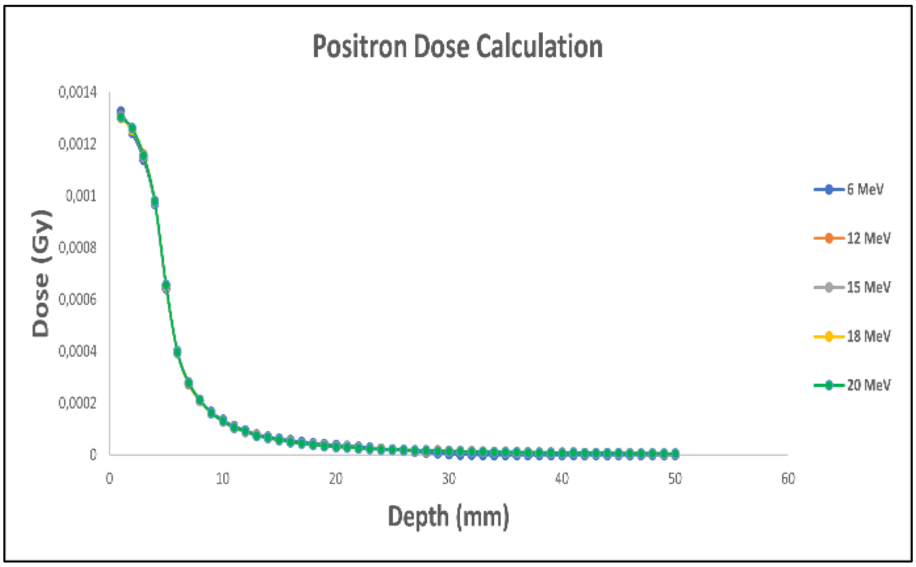

Figure 6. 5: *Dose (Gy) calculation based on depth (mm) at different energy values (MeV) for Positrons in the water phantom.*

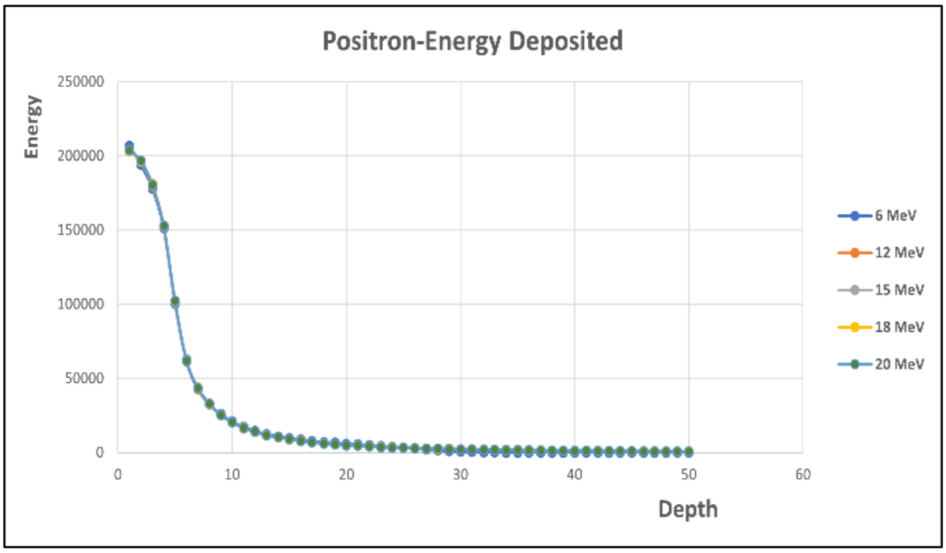

Figure 6. 6: *Energy Deposited calculation based on depth (mm) at different energy values (MeV) for Positrons in the water phantom.*

DEPTH	6 MeV	12 MeV	15 MeV	18 MeV	20 MeV
1	132,59x10^{-5}	130,73x10^{-5}	130,31x10^{-5}	130,16x10^{-5}	130,49x10^{-5}
2	124,38x10^{-5}	125,69x10^{-5}	125,83x10^{-5}	125,51x10^{-5}	126,14x10^{-5}
3	114,09x10^{-5}	115,02x10^{-5}	115,45x10^{-5}	116,1x10^{-5}	115,66x10^{-5}
4	96,96x10^{-5}	97,59x10^{-5}	97,46x10^{-5}	98,14x10^{-5}	97,94x10^{-5}
5	64,34x10^{-5}	64,92x10^{-5}	65,02x10^{-5}	65,33x10^{-5}	65,64x10^{-5}
6	39,43x10^{-5}	39,73x10^{-5}	40,22x10^{-5}	39,59x10^{-5}	39,77x10^{-5}
7	27,43x10^{-5}	27,43x10^{-5}	27,96x10^{-5}	28,13x10^{-5}	27,94x10^{-5}
8	20,88x10^{-5}	20,82x10^{-5}	20,97x10^{-5}	20,83x10^{-5}	21,19x10^{-5}
9	16,66x10^{-5}	16,24x10^{-5}	16,12x10^{-5}	16,32x10^{-5}	16,21x10^{-5}
10	13,46x10^{-5}	13,03x10^{-5}	13,06x10^{-5}	13,23x10^{-5}	13,15x10^{-5}
11	11,16x10^{-5}	10,54x10^{-5}	10,63x10^{-5}	10,77x10^{-5}	10,67x10^{-5}
12	9,40x10^{-5}	9,09x10^{-5}	8,90x10^{-5}	9,06x10^{-5}	9,21x10^{-5}
13	7,97x10^{-5}	7,64x10^{-5}	7,68x10^{-5}	7,50x10^{-5}	7,41x10^{-5}
14	7,00x10^{-5}	6,63x10^{-5}	6,55x10^{-5}	6,62x10^{-5}	6,67x10^{-5}
15	6,21x10^{-5}	5,76x10^{-5}	5,75x10^{-5}	5,77x10^{-5}	5,89x10^{-5}
16	5,60x10^{-5}	5,13x10^{-5}	4,98x10^{-5}	5,08x10^{-5}	5,00x10^{-5}
17	5,05x10^{-5}	4,45x10^{-5}	4,44x10^{-5}	4,47x10^{-5}	4,43x10^{-5}
18	4,51x10^{-5}	4,06x10^{-5}	4,03x10^{-5}	3,90x10^{-5}	3,89x10^{-5}
19	4,16x10^{-5}	3,50x10^{-5}	3,53x10^{-5}	3,59x10^{-5}	3,46x10^{-5}
20	3,77x10^{-5}	3,23x10^{-5}	3,09x10^{-5}	3,17x10^{-5}	3,16x10^{-5}
21	3,45x10^{-5}	2,98x10^{-5}	3,06x10^{-5}	3,06x10^{-5}	2,99x10^{-5}
22	3,19x10^{-5}	2,69x10^{-5}	2,63x10^{-5}	2,65x10^{-5}	2,64x10^{-5}
23	2,81x10^{-5}	2,37x10^{-5}	2,46x10^{-5}	2,38x10^{-5}	2,36x10^{-5}
24	2,44x10^{-5}	2,34x10^{-5}	2,18x10^{-5}	2,26x10^{-5}	2,13x10^{-5}
25	2,15x10^{-5}	2,06x10^{-5}	2,04x10^{-5}	2,04x10^{-5}	2,12x10^{-5}
26	1,81x10^{-5}	1,94x10^{-5}	1,89x10^{-5}	1,93x10^{-5}	1,96x10^{-5}
27	1,42x10^{-5}	1,77x10^{-5}	1,80x10^{-5}	1,71x10^{-5}	1,73x10^{-5}
28	1,00x10^{-5}	1,73x10^{-5}	1,62x10^{-5}	1,60x10^{-5}	1,67x10^{-5}
29	7,09x10^{-6}	1,67x10^{-5}	1,59x10^{-5}	1,57x10^{-5}	1,47x10^{-5}
30	4,51x10^{-6}	1,48x10^{-5}	1,39x10^{-5}	1,46x10^{-5}	1,43x10^{-5}
31	2,43x10^{-6}	1,37x10^{-5}	1,33x10^{-5}	1,38x10^{-5}	1,34x10^{-5}
32	1,30x10^{-6}	1,32x10^{-5}	1,32x10^{-5}	1,19x10^{-5}	1,23x10^{-5}
33	6,22x10^{-7}	1,24x10^{-5}	1,24x10^{-5}	1,25x10^{-5}	1,15x10^{-5}
34	3,50x10^{-7}	1,13x10^{-5}	1,08x10^{-5}	1,08x10^{-5}	1,11x10^{-5}
35	2,60x10^{-7}	1,14x10^{-5}	1,04x10^{-5}	1,03x10^{-5}	1,08x10^{-5}
36	1,87x10^{-7}	1,04x10^{-5}	9,96x10^{-6}	9,39x10^{-6}	1,02x10^{-5}
37	1,50x10^{-7}	1,02x10^{-5}	9,37x10^{-6}	9,76x10^{-6}	9,17x10^{-6}
38	1,76x10^{-7}	9,28x10^{-6}	9,04x10^{-6}	8,93x10^{-6}	8,75x10^{-6}
39	1,30x10^{-7}	9,05x10^{-6}	8,03x10^{-6}	8,13x10^{-6}	8,53x10^{-6}
40	1,21x10^{-7}	8,63x10^{-6}	7,94x10^{-6}	7,65x10^{-6}	7,62x10^{-6}
41	1,23x10^{-7}	8,36x10^{-6}	8,14x10^{-6}	8,11x10^{-6}	8,03x10^{-6}
42	1,22x10^{-7}	7,77x10^{-6}	7,49x10^{-6}	7,49x10^{-6}	7,03x10^{-6}
43	1,14x10^{-7}	7,62x10^{-6}	7,25x10^{-6}	7,28x10^{-6}	6,82x10^{-6}
44	1,13x10^{-7}	7,22x10^{-6}	7,08x10^{-6}	7,07x10^{-6}	6,37x10^{-6}
45	8,75x10^{-8}	6,40x10^{-6}	6,00x10^{-6}	6,70x10^{-6}	6,30x10^{-6}
46	8,69x10^{-8}	6,16x10^{-6}	6,58x10^{-6}	6,39x10^{-6}	5,51x10^{-6}
47	1,03x10^{-7}	5,44x10^{-6}	5,41x10^{-6}	6,20x10^{-6}	5,90x10^{-6}
48	1,01x10^{-7}	5,32x10^{-6}	5,54x10^{-6}	5,89x10^{-6}	5,74x10^{-6}
49	6,36x10^{-8}	4,46x10^{-6}	5,51x10^{-6}	4,84x10^{-6}	4,87x10^{-6}
50	5,67x10^{-8}	4,29x10^{-6}	5,07x10^{-6}	5,27x10^{-6}	4,68x10^{-6}

Table 6. 5: *Depth dependent dose values for each energy value for Positrons in the water phantom.*

DEPTH	6 MeV	12 MeV	15 MeV	18 MeV	20 MeV
1	206886,32	203988,83	203337,18	203101,31	203621,53
2	194092,24	196136,56	196340,51	195845,58	196825,88
3	178035,24	179480,25	180151,47	181160,08	180475,92
4	151300,26	152290,27	152079,95	153134,9	152819,53
5	100394,75	101300,23	101428,22	101946,65	102411,98
6	61527,013	61986,242	62760,526	61772,983	62051,771
7	42794,385	42801,764	43623,933	43894,97	43595,24
8	32586,757	32486,631	32724,128	32509,242	33072,764
9	25991,896	25341,784	25147,085	25472,272	25292,557
10	20998,976	20332,739	20380,291	20643,071	20521,152
11	17418,813	16443,035	16592,781	16808,775	16647,545
12	14660,163	14183,1	13894,744	14140,942	14369,042
13	12436,36	11927,232	11984,046	11709,396	11562,066
14	10927,378	10350,186	10224,824	10330,579	10405,701
15	9686,5519	8985,2764	8971,2451	8997,2649	9192,8276
16	8744,691	8010,7787	7774,9766	7924,9352	7800,3601
17	7877,0991	6943,3543	6920,9919	6980,9019	6915,1225
18	7031,4291	6331,5149	6288,1748	6078,5434	6064,2425
19	6492,1968	5463,0184	5513,1387	5597,1144	5392,6359
20	5887,8207	5040,1247	4819,198	4939,8707	4935,8851
21	5385,3721	4642,8192	4774,2988	4776,1629	4666,9688
22	4974,8005	4194,2083	4107,4359	4130,8748	4122,7751
23	4382,63	3690,6973	3838,8043	3718,998	3679,5847
24	3806,6247	3644,1774	3405,7209	3528,6783	3316,6055
25	3357,965	3217,9199	3188,3789	3187,8521	3300,3976
26	2827,8309	3031,6579	2956,0399	3012,9857	3063,2957
27	2210,4122	2756,2678	2816,0856	2661,7265	2704,2425
28	1562,4679	2692,7503	2533,6816	2489,4467	2612,2326
29	1105,6416	2604,316	2487,3695	2450,2529	2294,5862
30	703,44936	2317,1288	2170,7628	2273,4506	2238,1806
31	378,50133	2143,4704	2072,2358	2145,899	2083,4329
32	203,37532	2052,2348	2060,7735	1858,235	1925,0688
33	96,992194	1939,4871	1933,7861	1944,6709	1789,3913
34	54,630178	1766,8817	1691,9461	1692,3378	1729,0679
35	40,615461	1783,0587	1617,8975	1605,4286	1687,3441
36	29,198037	1615,8145	1553,9915	1465,5546	1594,4393
37	23,418537	1584,667	1461,5272	1523,4049	1430,1264
38	27,529389	1447,6342	1411,1561	1393,357	1365,6218
39	20,299258	1412,0426	1253,6361	1268,7623	1330,5068
40	18,841304	1346,817	1238,9504	1193,21	1189,7843
41	19,148994	1305,201	1269,8527	1265,5605	1252,3305
42	19,001499	1211,7791	1169,4257	1168,9086	1097,546
43	17,728527	1188,907	1131,1493	1135,7081	1063,4699
44	17,597236	1126,6604	1104,4805	1102,6195	994,71372
45	13,647005	998,28927	935,5266	1045,8414	982,74675
46	13,558325	960,99998	1026,5249	997,35231	860,54323
47	16,087392	848,76683	844,01607	968,09939	920,0345
48	15,757554	830,73683	864,46473	919,83836	895,70073
49	9,9187597	695,72549	859,24137	755,56057	759,53536
50	8,8491034	668,80647	790,88536	821,76787	729,73087

Table 6. 6: *Depth dependent energy deposited values for each energy value for Positrons in the water phantom.*

In this section, after photons, electrons and positrons, dose values of alpha particles (with different energies) in the water phantom are presented, provided dose calculations are made for different particles. Compared with all the other particles above, very different results were obtained [29, 30]. In Table 6.7 below, Dose values of Alpha particles with 5 different energy values (6, 12, 15, 18, 20 MeV) obtained by the Gate simulation program are given at each 1 mm depth of 50 mm^3 Water phantom. Dose values were calculated in Gray. Another Table 6.8 shows the energy values stored in the water phantom of Alpha particles with different energy values. Based on these tables, the Dose values of Alpha particles depending on the depth (mm) of the phantom and the graphs of the Energy Stored in the phantom are presented in Figures 6.7 and 6.8 [45,46].

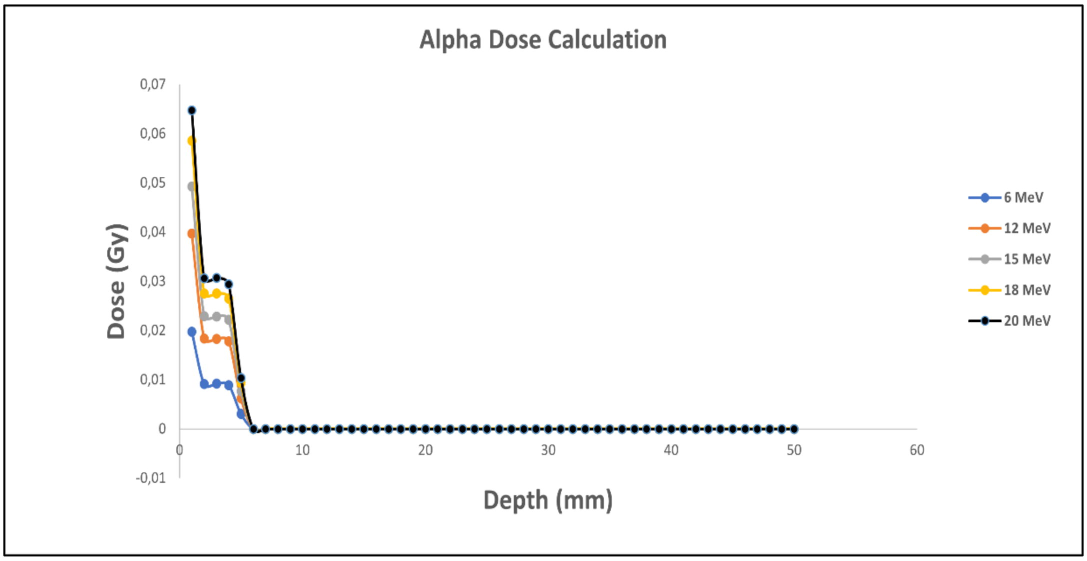

Figure 6. 7: *Dose (Gy) calculation based on depth (mm) at different energy values (MeV) for Alpha Particles in the water phantom.*

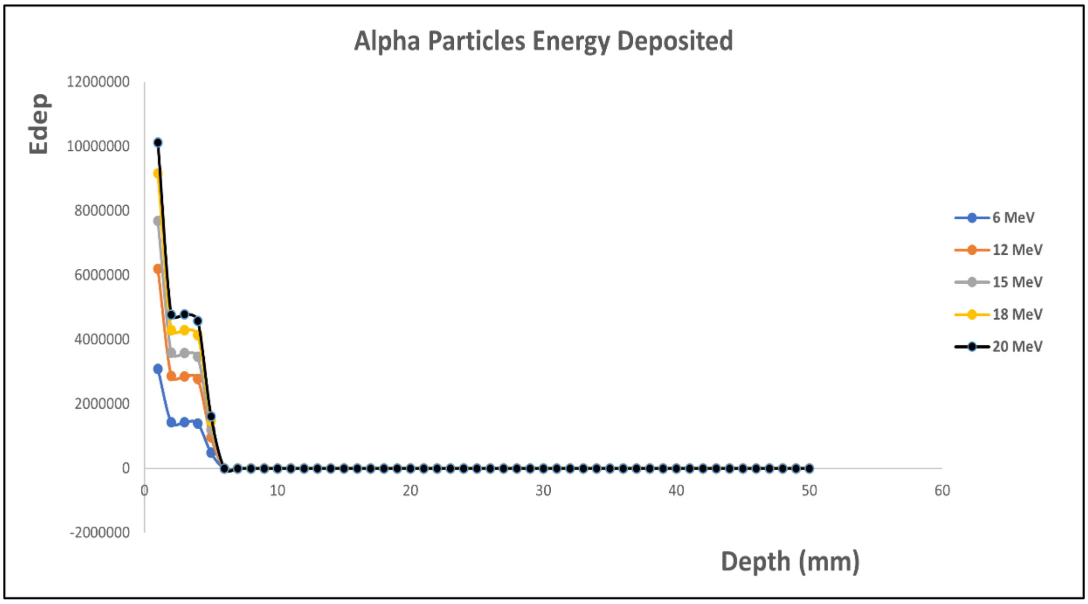

Figure 6. 8: *Energy Deposited calculation based on depth (mm) at different energy values (MeV) for Alpha Particles in the water phantom.*

DEPTH	6 MeV	12 MeV	15 MeV	18 MeV	20 MeV
1	0,01977638	0,039697891	0,049275279	0,058673157	0,064834842
2	0,009159439	0,01835453	0,022992526	0,027546643	0,03059481
3	0,009190931	0,018304061	0,022908602	0,027508267	0,030696442
4	0,008891619	0,017784599	0,022202359	0,02652121	0,029373208
5	0,00307764	0,006169841	0,007699809	0,009355433	0,010373951
6	0	0	0	$1,45x10^{-7}$	$1,77x10^{-6}$
7	0	0	0	0	0
8	0	0	0	0	0
9	0	0	0	0	0
10	0	0	0	0	0
11	0	0	0	0	0
12	0	0	0	0	0
13	0	0	0	0	0
14	0	0	0	0	0
15	0	0	0	0	0
16	0	0	0	0	0
17	0	0	0	0	0
18	0	0	0	0	0
19	0	0	0	0	0
20	0	0	0	0	0
21	0	0	0	0	0
22	0	0	0	0	0
23	0	0	0	0	0
24	0	0	0	0	0
25	0	0	0	0	0
26	0	0	0	0	0
27	0	0	0	0	0
28	0	0	0	0	0
29	0	0	0	0	0
30	0	0	0	0	0
31	0	0	0	0	0
32	0	0	0	0	0
33	0	0	0	0	0
34	0	0	0	0	0
35	0	0	0	0	0
36	0	0	0	0	0
37	0	0	0	0	0
38	0	0	0	0	0
39	0	0	0	0	0
40	0	0	0	0	0
41	0	0	0	0	0
42	0	0	0	0	0
43	0	0	0	0	0
44	0	0	0	0	0
45	0	0	0	0	0
46	0	0	0	0	0
47	0	0	0	0	0
48	0	0	0	0	0
49	0	0	0	0	0
50	0	0	0	0	0

Table 6. 7: *Depth dependent dose values for each energy value for Alpha Particles in the water phantom.*

DEPTH	6 MeV	12 MeV	15 MeV	18 MeV	20 MeV
1	3085861,447	6194369	7688802,58	9.155.226,11	10116681,43
2	1429218	2863999	3587701,45	4.298.316	4773944,618
3	1434132	2856124	3574606,23	4.292.327,41	4789802,987
4	1387428	2775068	3464405,57	4138309,313	4583328,671
5	480228	962727,9	1201460,65	1459800,519	1618727,706
6	0	0	0	22,69818697	275,5408065
7	0	0	0	0	0
8	0	0	0	0	0
9	0	0	0	0	0
10	0	0	0	0	0
11	0	0	0	0	0
12	0	0	0	0	0
13	0	0	0	0	0
14	0	0	0	0	0
15	0	0	0	0	0
16	0	0	0	0	0
17	0	0	0	0	0
18	0	0	0	0	0
19	0	0	0	0	0
20	0	0	0	0	0
21	0	0	0	0	0
22	0	0	0	0	0
23	0	0	0	0	0
24	0	0	0	0	0
25	0	0	0	0	0
26	0	0	0	0	0
27	0	0	0	0	0
28	0	0	0	0	0
29	0	0	0	0	0
30	0	0	0	0	0
31	0	0	0	0	0
32	0	0	0	0	0
33	0	0	0	0	0
34	0	0	0	0	0
35	0	0	0	0	0
36	0	0	0	0	0
37	0	0	0	0	0
38	0	0	0	0	0
39	0	0	0	0	0
40	0	0	0	0	0
41	0	0	0	0	0
42	0	0	0	0	0
43	0	0	0	0	0
44	0	0	0	0	0
45	0	0	0	0	0
46	0	0	0	0	0
47	0	0	0	0	0
48	0	0	0	0	0
49	0	0	0	0	0
50	0	0	0	0	0

Table 6. 8: *Depth dependent energy deposited values for each energy value for Alpha Particles in the water phantom.*

All numerical values in these above tables were calculated one by one in simulation studies. Each value corresponds to the corresponding water phantom depth. Because each value gives the exact results of certain points of the phantom. Compared to these values, the above graphs were drawn and as can be seen from the graphs, these numerical values were found to be in agreement with the studies in the literature.

In the light of all the tables and graphics above, the study of dose calculations with the water equivalent phantom showed us that gamma rays have a much longer range than all particles, they have the lowest dose and the lowest stored energy values. It interacts much less with the water phantom and from the first moment, very low values were calculated in terms of dose and deposited energy values compared to other particles. However, this situation continued until the midpoint of the water phantom, that is, around 25 mm. After this point, due to the range length and chain reaction, higher dose and stored energy values were obtained than all other particles in dose and stored energy values. This high dose and accumulated energy values continued to show its effect until the end of the phantom.

Likewise, it has been observed that there are general similarities in the dose values of electrons and positrons in the water equivalent phantom. The reason for this is that these two particle types, which have all the same properties except their charges, show the same properties while moving in the phantom, and therefore have dose and stored energy values close to each other. It has been observed that these particles, which are much lighter than alpha particles, can go all the way to the end of the water phantom and therefore have dose and stored energy values even at 50 mm. When the depth dependent dose values table for these two particles were examined, very close dose and stored energy values were obtained almost any energy value. This shows that even if the energy values of these particles are increased, they interact with water molecules at the same rate.

Due to the range of the heaviest particles, Alpha particles, high dose values cause them to suddenly drop to zero by losing all their energy at the shortest distance. Since alpha particles are very heavy compared to other particles, it has been observed that they lose all their energy in the first 5 mm depth inside the phantom. In the experiment performed at different energy ranges, it was observed that there was a parallel increase in dose values as the energy values increased. In addition, higher energy values were obtained in the energy values stored in the water phantom compared to all other particles.

6.2 Results and Some Discussions of Detection of Co-60 Emission by a CsI Detector on GEANT4

A simulation program was run to examine the interaction of the Cobalt-60 radiation source with the Cesium Iodide (CsI) scintillation crystal according to the criteria in Figure 5.9. The numerical data obtained as a result of this simulation are presented in Table 6.9. After the outputs, relevant comments and evaluations are included within the framework of all these results.

Degree	**Positions (cm)**			**Entries**	**Counts**	**% Resolution**	**% Resolution**	**Number of**	
	x	**y**	**z**			***1173.2 keV***	***1332.5 keV***	**Photoelectric Effect**	**Compton Scattering**
0°	0	0	-45.72	2952	56	0.01797	0.01613	2250	2000
1°	0.8	0	-45.71	3006	70	0.01916	0.0248	2300	1950
2°	1.6	0	-45.70	3199	60	0.0227	0.0169	2400	2150
3°	2.4	0	-45.66	3441	56	0.0211	0.0219	2600	2350
4°	3.2	0	-45.61	3739	64	0.0189	0.0180	2900	2600
5°	3.9	0	-45.55	3872	72	0.0215	0.0183	2950	2650
6°	4.8	0	-45.47	4171	72	0.0233	0.0189	3400	2850
8°	6.4	0	-45.27	4469	72	0.0228	0.0175	3500	3000
10°	7.9	0	-45.02	4892	102	0.0236	0.0181	3500	3500
15°	11.8	0	-44.16	5750	98	0.0212	0.0208	4800	4000
20°	15.6	0	-42.96	6373	95	0.0198	0.0141	4850	4500
30°	22.86	0	-39.59	6653	110	0.0183	0.0137	5050	4700
40°	29.39	0	-35.02	7112	105	0.0194	0.0173	5400	5000
45°	32.33	0	-32.33	7168	110	0.02256	0.02032	5400	5000
60°	39.59	0	-22.86	7349	120	0.0177	0.0169	5600	5300
90°	45.72	0	0	7401	128	0.0183	0.0144	5650	5400
Detector Center	0	0	0	$1x10^{7}$	$35x10^{3}$	0.0191	0.0167	$86x10^{5}$	$56,5x10^{4}$

Table 6. 9: *Numerical data obtained from the interaction of the Cobalt60 radiation source with the CsI scintillation crystal at different angles.*

Table 6.9 above shows us the amount of radiation coming to the detector from the radioactive source at different angles, that is, at different positions, during the interaction of the gamma rays emitted from the Co-60 radiation source with the CsI crystal. It has been observed that the amount of radiation coming to the detector increases significantly depending on the location of the relevant radioactive source. Cobalt60 source has two peak energies. These are 1.1732 MeV and 1.3325 MeV. By using the relevant photosensors, the electrical signals generated by the Photoelectric effect and Compton scattering are illuminated. By means of these signals, it is seen that the detector resolution and efficiency increase at almost the same rate depending on the change in angles. The figures below 6.13, 6.14 and 6.15 show the variation of both the resolution and efficiency of the CsI scintillation crystal depending on the angles. And at the same time, as a result of a more in-depth approach, it has been tried to show in these graphs which type of interaction is dominant and larger at which angle.

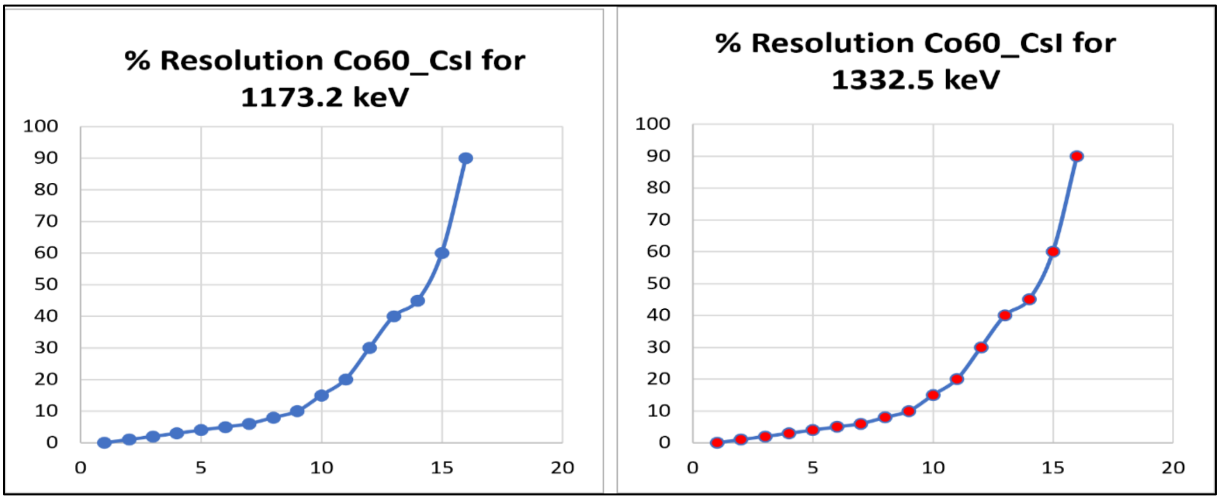

Figure 6. 9: *The Spectrum Resolution values depending on the respective Angles in the Co-60 source and the CsI crystal detector system.*

This Figure 6.9 gives some information about the detector resolution. The resolution of the CsI scintillation detector depending on the angles of the two energy peaks of the Cobalt60 source is shown. The spectrum resolution values in Table 6.9 were calculated based on the Full-Width Half Maximum (FWHM) values of the spectra. It was observed that the resolution increased as the angle value increased in both energy peaks. In this way, it is thought that the solubility of the CsI crystal can be further improved. Because as the resolution increases, the results that a detector can give in the areas where the detector is used will be more sensitive and close to certain.

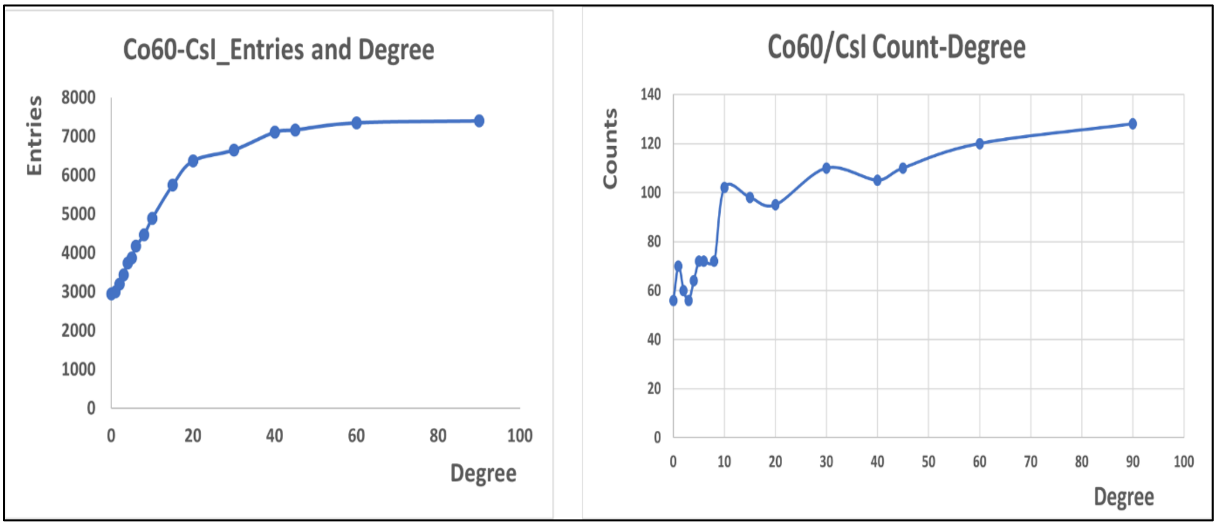

Figure 6. 10: *The Entries and Count values related to the respective Angles in the CsI crystal detector system with the Co-60 source.*

Figure 6.10 shows the variation of the number of gamma rays entering the detector depending on the angles. It is seen that the number of photons interacting with the CsI crystal increases as the position of the Cobalt-60 radiation source is changed at certain angles. By increasing the angle value, providing interaction with the wider surface of the detector made it easier for more particles to enter the detector. It is aimed that more photons in the scintillation crystal reach the relevant photosensors, so that more beautiful and smooth electrical signals are received.

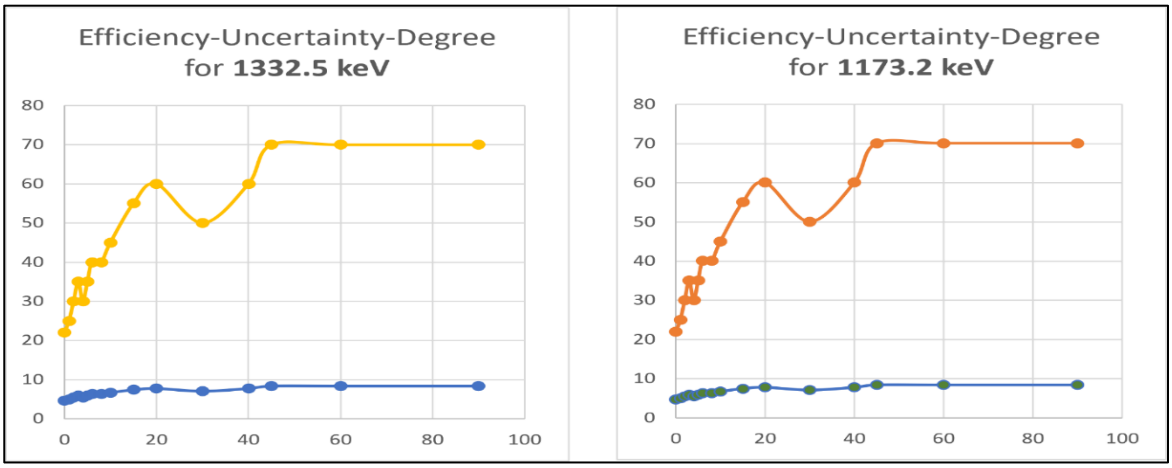

Figure 6. 11: *Graphs of the Efficiency and Uncertainty values depending on the respective Angles in the Co-60 source and the CsI crystal detector system.*

Figure 6.11 above shows the changes in detector efficiency and hence uncertainty in both energy peaks depending on the angles. The efficiency of the scintillation crystal is actually how suitable the electrical signal obtained from the crystal is. It is seen that as the efficiency of the CsI crystal increases, the electrical signal efficiency increases at the same rate. Except for the reductions in only 4 and 30 degrees, of course. And it has been observed that the amount of uncertainty remains below 10 percent and does not change very, very little depending on the angles. The existence of this uncertainty constancy shows us that the working capacity of the detector does not change easily and it is kind of durable.

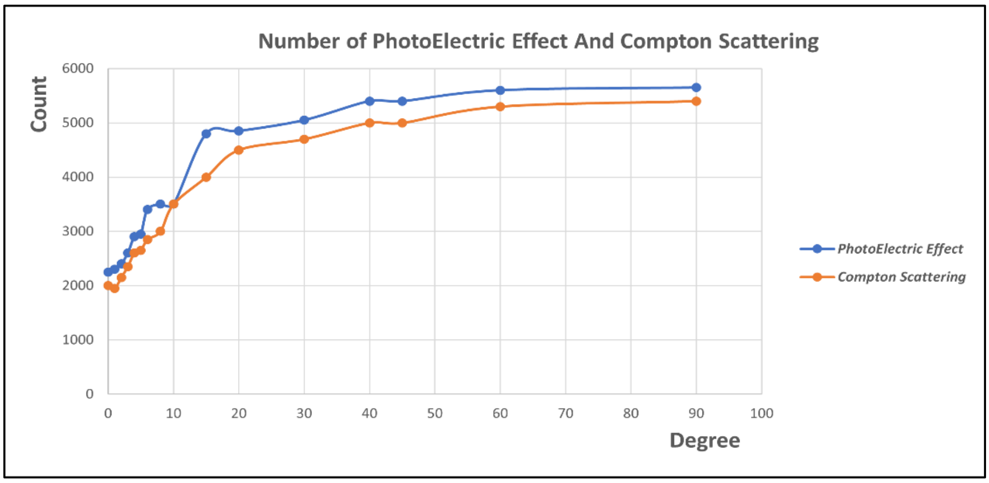

Figure 6. 12: *Number of interaction types of Gamma rays occurring in the CsI scintillation crystal. The Blue one is Photoelectric Effect and the Brown one is Compton Scattering.*

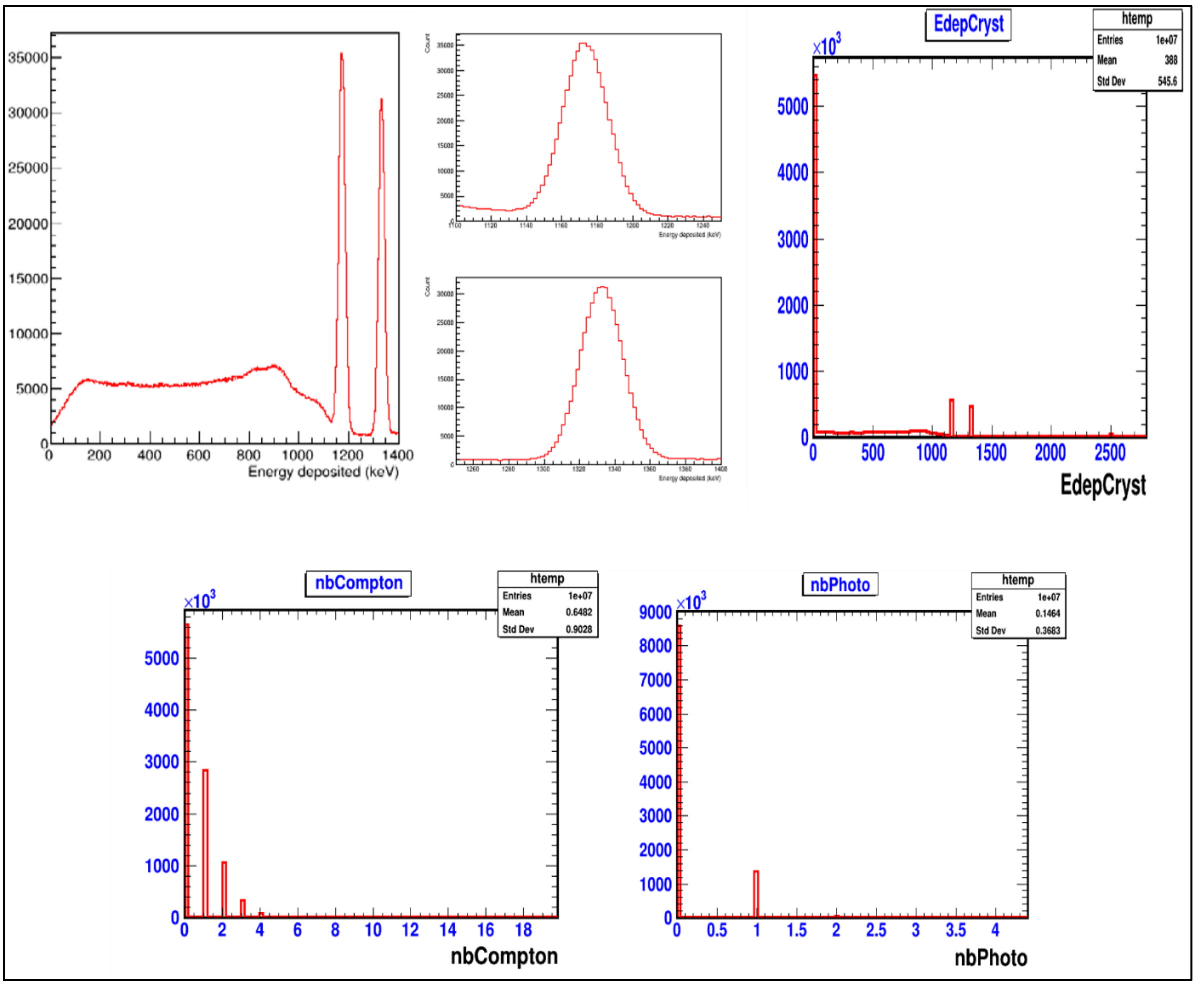

Figure 6. 13: *Energy deposited in the CsI crystal with the Co-60 source* ***at the Detector Center (top)*** *and the number of* ***Photoelectric Absorption*** *and* ***Compton Scattering (bottom).***

Figure 6.13 above is made to see what consequences the radiation source can have when interacting with the highest and most likely scintillation crystal. Here, the interactions that the Cobalt60 radiation source can make with the scintillation material while it is inside and in the center of the detector, and the possibilities, efficiency and signal resolutions of these interactions are examined. Theoretically, the best signal efficiency is obtained this way, which is natural and expected. Because the largest number of particles interacted, and as a result, the number of photoelectric and Compton events made by photons was obtained in very large quantities. And here, even in the first moments, it is easily seen from the relevant graph that both types of interaction show themselves at the same time. All other charts below include the effects of the radiation source's propagation outside the detector and at different points, so that they can be used in real work and operations.

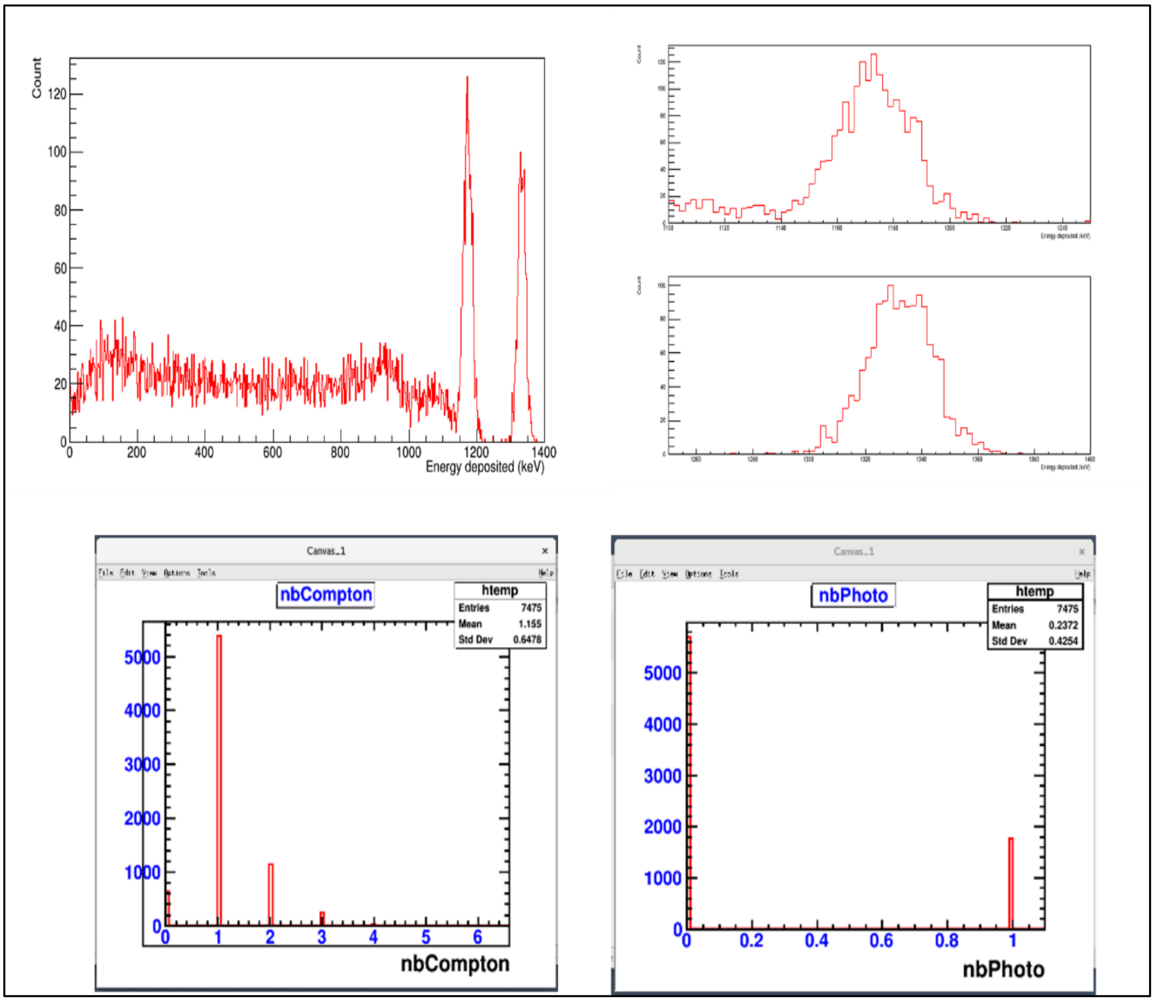

Figure 6. 14: *Energy deposited in the CsI crystal with the Co 60 source positioned* ***at 90 degree*** *and* ***18 inches*** *from the detector (above) and the number of* ***Photoelectric Absorption*** *and* ***Compton Scattering (below).***

The Cobalt-60 radiation source, which is positioned at an angle to see the widest surface of the rectangular prism-shaped CsI scintillation crystal, is provided to interact with the crystal at an angle of 90 degrees. Figure 6.14 shows the top two photoelectric energy peaks and the length of the Compton scattering. Below is the numerical equivalent of these two interaction types. Here, it is seen in which energies the photoelectric effect is very dominant at the first moment and then in which energy ranges the Compton scattering and the Compton edge exist. After it was seen that the intensity of interactions in the crystal was the largest at this angle, the most efficient of the obtained signal was obtained through this point.

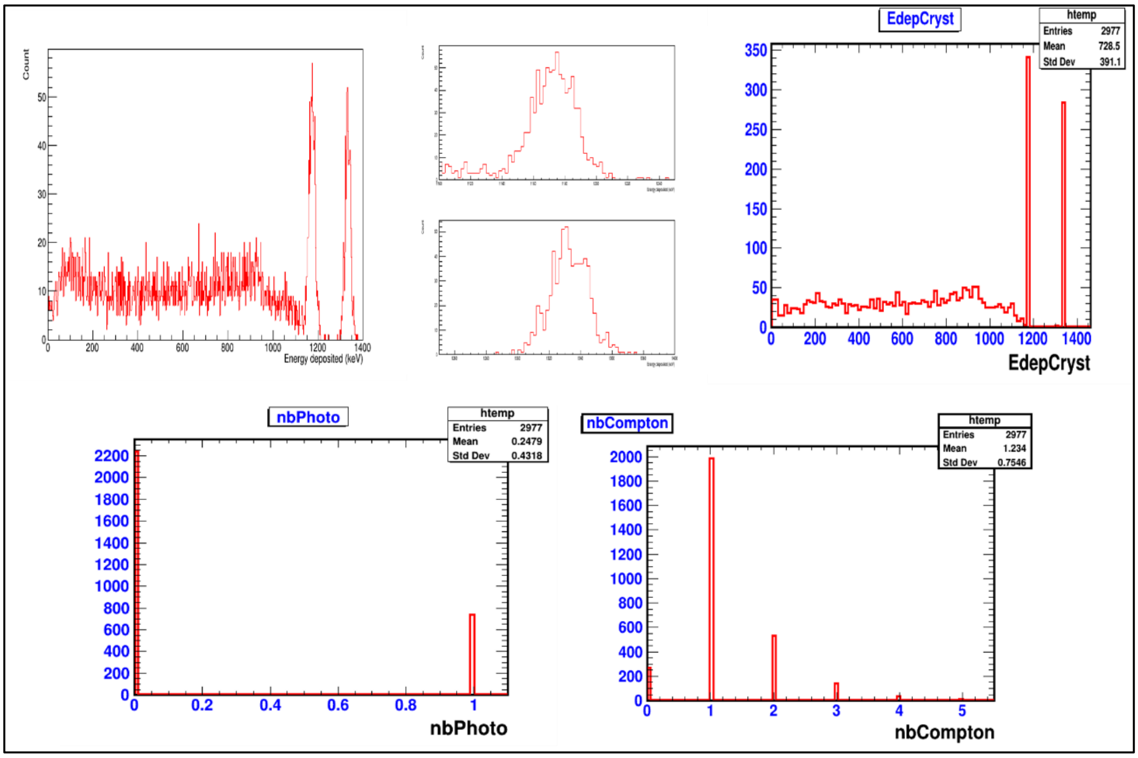

Figure 6. 15: *Energy deposited in the CsI crystal with the Co 60 source positioned at* ***0 degree*** *and* ***18 inches*** *from the detector (above) and* ***the number of Photoelectric Absorption*** *and* ***Compton Scattering (below).***

With this different study, using the Cobalt-60 radiation source, which is frequently used in the treatment of diseases such as tumors and cancer in radiotherapy and in many other fields, and the CsI scintillation crystal, which is frequently encountered in nuclear physics and nuclear medicine, more accurate measurements have been achieved, and these measurements have become a source for many fields in the literature is intended to.

Looking at the work done in this way, the values in Table 6.9 show a large increase in the number of particles entering the detector as the angle value increases (from zero to ninety degrees). Here, it is meant to show that the detector surface area increases by increasing the angle value. Obtaining the highest number of particles in the simulation performed at the detector center is an expected result. Because almost all of the radiation interacts with the scintillation material. It has been observed that the lowest particle number interacts with the detector material when the radiation source is positioned at zero angle with the detector. When the angle values are increased, more particle numbers are seen in the simulation. At ninety degrees, the highest number of particles reaches the detector.

Considering the spectrum resolution, the position of the source positioned at certain angles with respect to the detector is of great importance in the spectrum resolution. Because it gives important information about the detector resolution. It has been observed that when the angle values are increased from 0 degrees to 90 degrees, the detector resolution also increases due to the changing position of the radiation source. In the interpretation of the respective energy spectra, the energy peaks indicate that the photoelectric effect is very dominant. The increase in the detector surface area with the incidence angle of the radiation and the density of the detector crystal cause this photoelectric interaction. Compton scattering is dominant in low energy regions.

Each graph shows at what angles and positions this dominant effect occurs, and at what particle count it occurs. It is also aimed to play a guiding role in areas that can be used depending on the dominance of interaction types. It is thought that it will contribute to the determination of the appropriate position and amount of radiation for patients in radiotherapy, and to more accurate and sensitive measurement of radiation dose amounts needed by the pharmaceutical industry in the industry.

6.3 Results and Some Discussions of Phoswich Detector System On Gate Simulation

Gate simulation program was run to examine the three-layer (ZnS, EJ212, LaBr) scintillation detector system using three different (Am241, Sr90 and Cs137) radiation sources and some outputs were obtained as shown in Figure 5.10. The numerical data obtained as a result of this simulation are also presented in Table 6.10. On the other hand, in this Table 6.10, it is aimed to show how much better results this study gave by making comparisons with previous studies in the literature. Each of the related graphs are counts vs. energy graphs of Alpha, Beta, and Gamma particles. Based on the tables and graphics, some comments and evaluations are included in the conclusion chapter within the framework of all these results.

Layers	**(Yamamato S.)**	**(Jenkins D., Yavuzkanat N.)**	**(Present work with different geometry and material)**	**Percentages (%)**
Inner Layer (ZnS)	*93.5*	*99.87*	***98.64***	**Percentage of Alpha Particles**
Middle Layer (EJ212)	*6.1*	*0.13*	*0.95*	
Outer Layer (LaBr)	*0.4*	*0*	*0.41*	
Inner Layer (ZnS)	*0.4*	*1.85*	*7.6*	**Percentage of Beta Particles**
Middle Layer (EJ212)	*87.7*	*90.02*	***84.18***	
Outer Layer (LaBr)	*11.9*	*8.13*	*8.1*	
Inner Layer (ZnS)	*0.6*	*1.65*	*1.44*	**Gamma Rays Percentage**
Middle Layer (EJ212)	*60.0*	*19.74*	*16.0*	
Outer Layer (LaBr)	*39.4*	*78.61*	***82.55***	

Table 6. 10: *Comparison of the results obtained after examining different materials, geometries and thicknesses for each layer in our Latest Simulation with the work of Yamamato S. and Jenkins D., Yavuzkanat N.*

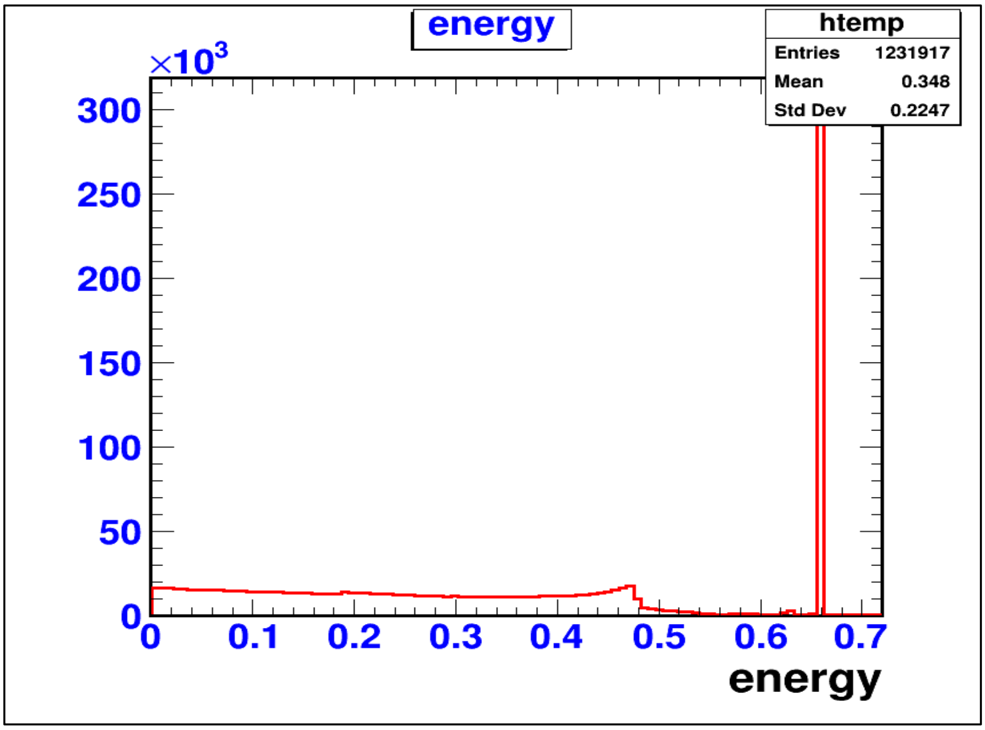

Figure 6. 16: *Count-Energy Deposited plot of Gamma rays with 662 keV energy and 370 kBq activity emitted from the Cs-137 source.*

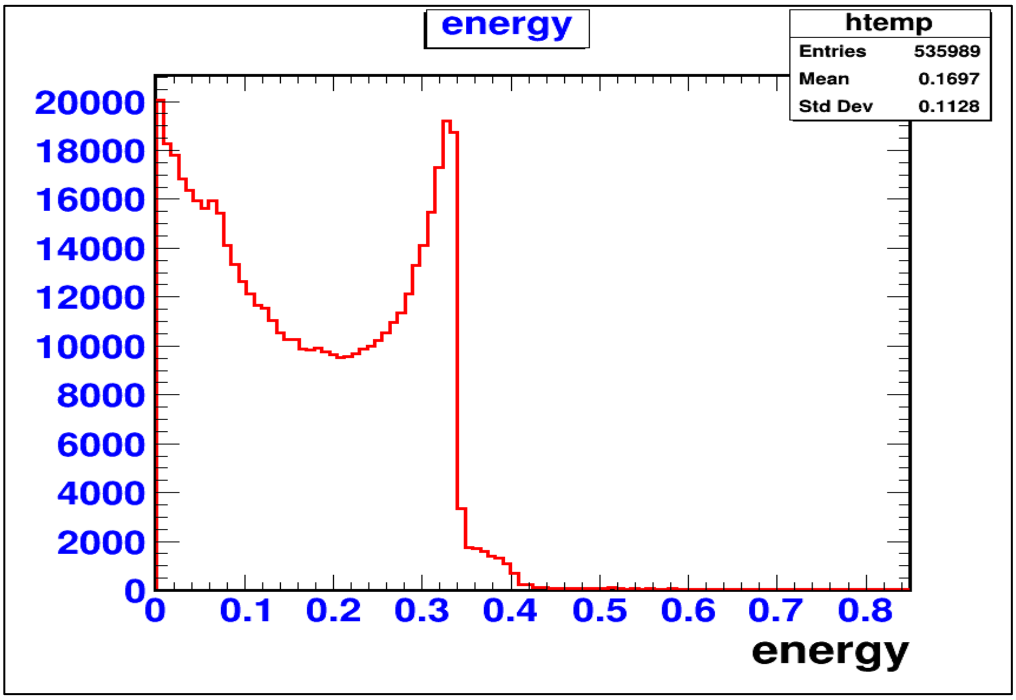

Figure 6. 17: *Energy Deposited-Count graph of Beta particles with 100 Bq activity emitted from the Strontium-90 source.*

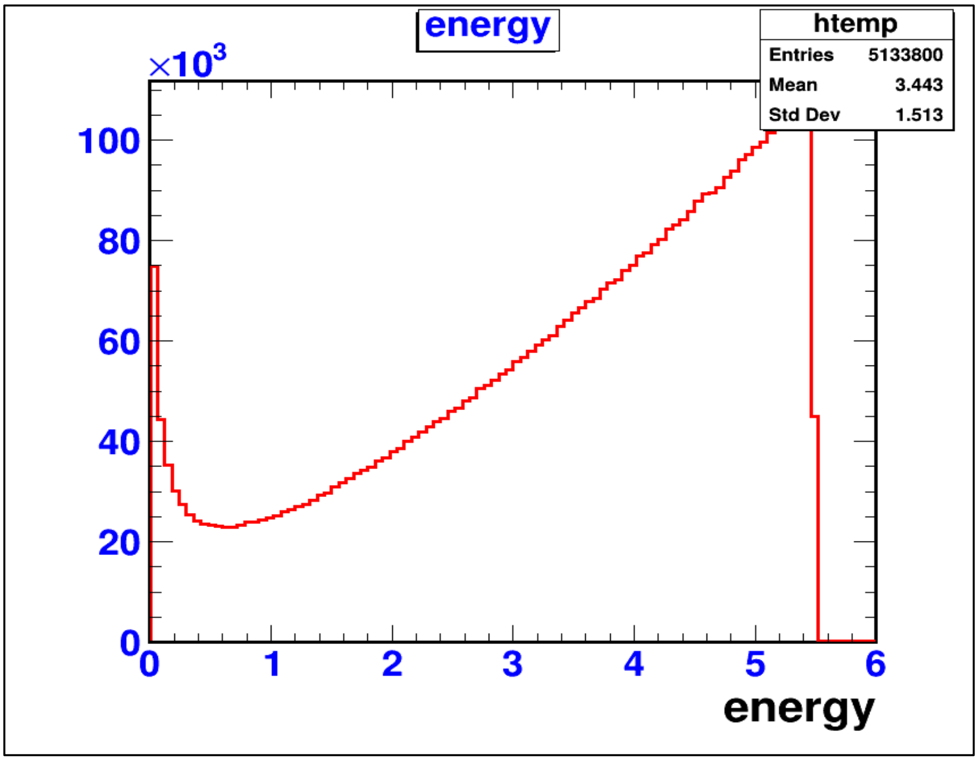

Figure 6. 18: *Energy Deposited-Count graph of 5.5 MeV energy Alpha particles with 2 kBq activity emitted from the Am-241 source.*

The 3-layer alpha, beta, gamma detector system above is designed with certain thicknesses and a cylindrical geometry. Cesium-137 as a gamma source, Strontium-90 as a beta source, and Americium-241 radiation sources, which are frequently used in applications, were used for Alpha particles. These radiation sources have an important place in nuclear medicine and nuclear physics applications. Silver-doped ZnS(Ag), which can detect alpha particles with high sensitivity, as scintillation material, EJ212 scintillation material to detect beta particles, and LaBr scintillation crystal to detect gamma rays were used. These scintillation crystals are designed with optimal thickness and geometry to achieve the highest signal efficiency. Designed to eliminate the environmental damage caused by nuclear power plant accidents in the fastest and optimum time, this system can simultaneously detect alpha, beta and gamma particles. Since it can be easily integrated into medical imaging systems, it is aimed to be used more sensitively in radiotherapy procedures.

Compared to previous studies, it can be easily seen from Table 6.10 that higher precision measurements were taken. Because while all previous studies have a square detector design, this study is designed in a cylindrical form, making it much easier to use in nuclear facilities and medical applications. Simultaneously, simulation studies were carried out using different and more advanced state-of-the-art scintillation materials.

This detector system, designed using the Geant4-based Gate simulation program, can be developed in different geometries and dimensions according to the purpose of the application area in accordance with the relevant area.

6.3.1 Results and Some Discussions of Comparison of Phoswich Detector Systems For NORM in Nuclear and Oil/Gas Pipeworks

In this study, the gate simulation program is used to create a detector system with ZnS, EJ212 and LaBr scintillation crystals using naturally occurring radiation sources such as Pb-210, Sr-90 and K-40, which are frequently encountered in both nuclear facilities and oil/gas applications. Some outputs have been obtained as shown in Figure 5.11 [47]. The numerical data obtained as a result of this simulation are also presented in Table 6.11. The data in this table shows the interaction percentage of each particle in each layer. Count-energy graphs of these particles during the simulation are shown below. Within the framework of these results, some comments and evaluations are also included in the conclusion section.

Nuclear Pipeworks - 2 inches	*Oil/Gas Pipeworks - 6 inches*

	ZnS	EJ212	LaBr	Source Details
ALPHA (%)	*99.98*	0.0075	0.005	Pb-210 5.305 MeV 0.4 Bq
BETA (%)	3	*72.5*	24.5	Sr-90 0.546 MeV 100 Bq
GAMMA (%)	2.26	17.24	*80.49*	K-40 1.45 MeV 31.31 Bq

	ZnS	EJ212	LaBr	Source Details
ALPHA (%)	*99.87*	0.075	0.05	Pb-210 5.305 MeV 0.4 Bq
BETA (%)	1.5	*59.02*	39.48	Sr-90 0.546 MeV 100 Bq
GAMMA (%)	0.55	13.46	*85.99*	K-40 1.45 MeV 31.31 Bq

Table 6. 11: *Detection percentages of Alpha, Beta particles and Gamma rays in each scintillation crystal.*

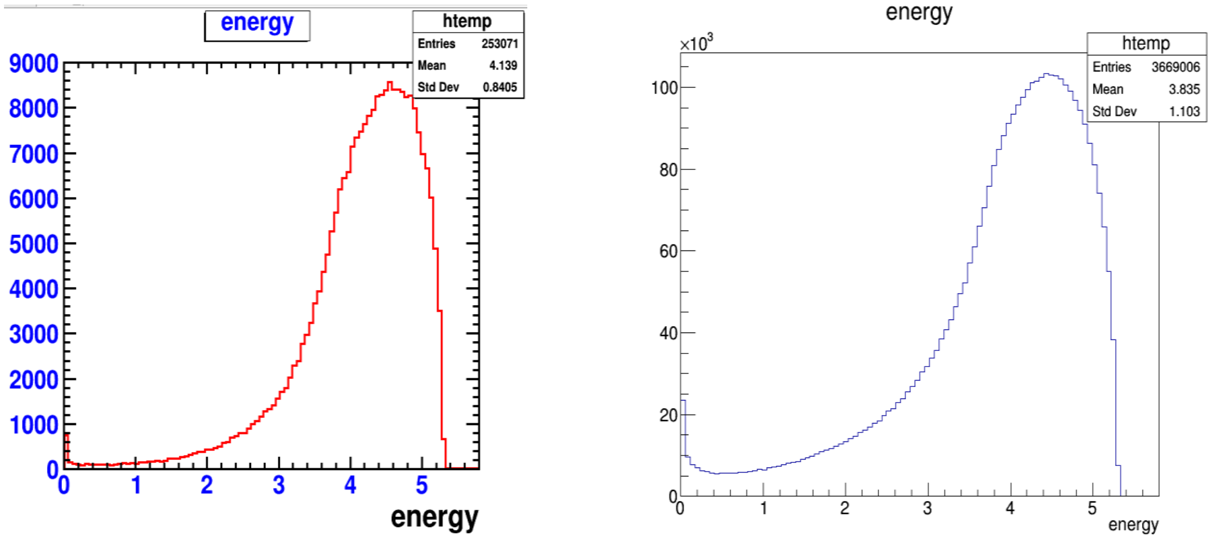

Figure 6. 19: *Energy Deposited-Count graph of 5.305 MeV energy Alpha particles with 0,4 Bq activity emitted from the Pb-210 source.*

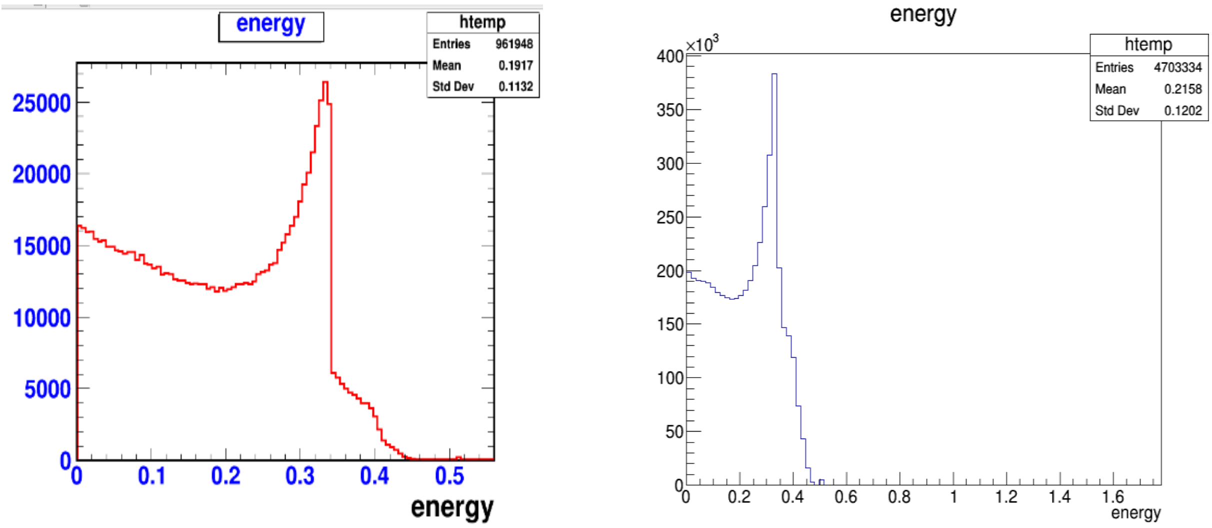

Figure 6. 20: *Energy Deposited-Count graph of 0,546 MeV Beta particles with 100 Bq activity emitted from the Strontium-90 source.*

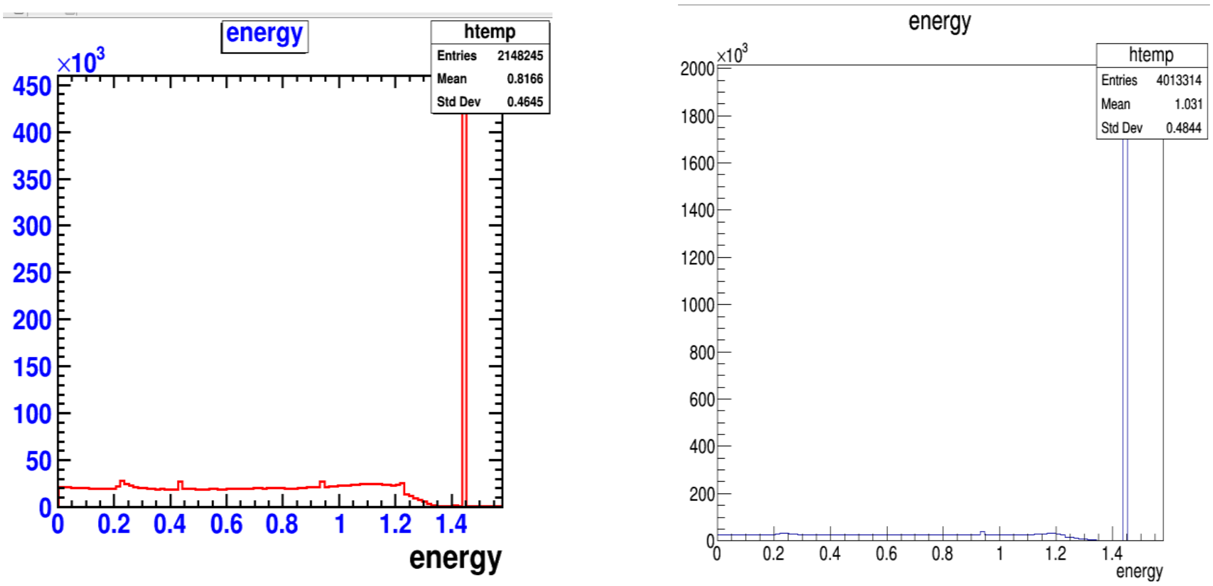

Figure 6. 21: *Count-Energy Deposited plot of Gamma photons with 1,45 MeV energy and 31,31 Bq activity emitted from the K-40 source.*

While both Alpha, Beta, Gamma detector systems above are designed in certain thicknesses and solid cylindrical geometry for both nuclear and oil/gas plants, K-40 radiation source is gamma rays, Sr-90 beta particles and Pb-210 radiation source is alpha particles. used. LaBr scintillation crystals of appropriate thickness were used to detect alpha particles ZnS(Ag), Beta particles EJ212 and Gamma rays. In this way, it is presented as an easily usable system for both nuclear decommissioning and applications in nuclear and oil/gas installations. In addition, they have the ability to detect all kinds of radiation at the same time in cases of radioactive leakage in oil/gas stations in nuclear power plants.

In these studies, it has become possible to make more precise measurements in different areas by using different geometries and scintillation materials compared to previous studies. The relevant percentages are given in Table 5.3 for both nuclear facilities and oil/gas pipes. In this respect, there is no such study in the literature.

As can be seen Table 6.11 and Figures 6.19, 6.20 and 6.21, If both tables are compared, the percent values of the simulation study for nuclear installations do not show much change in alpha particles compared to oil/gas systems, while the detection percentage of beta particles is higher in the nuclear system, while the percentage of gamma rays is higher in the oil/gas system. The reason for this is thought to be related to the geometry of the detector systems and the positions of the radiation sources.

Since the pipes in nuclear facilities are ***2 inches*** in diameter, the design of this detector system has been kept to less than ***2 inches*** so that the detector can easily pass through the pipes. Likewise, since the dimensions of the oil/gas pipes are around ***6 inches***, the detector system is designed with a size of less than ***6 inches*** and the simulations are made within this framework and the results are obtained. The graphs at the bottom of the table are the energy-dependent particle number graphs of Alpha, Beta particles and Gamma rays. Due to the larger size of the detector system, the maximum number of particles occurred in the oil/gas design. By making the most optimum adjustments and geometric designs, it is aimed to facilitate the use in the industry and natural radiation sources, which are known to have a great impact on human health, have been used.

Chapter 7

7 CONCLUSIONS

Since even a very small absorbed energy of radiation energy has enormous biological consequences, the main body of the thesis is devoted to radiation dose and some related application areas. As can be seen from all tables and graphics obtained in the dose calculation study in the thesis, the highest dose values were obtained in alpha particles, and the lowest dose values were obtained in gamma rays. It has been observed that the dose and stored energy values of electrons and positrons are almost in the same ratio. It is thought that the results of the dose and stored energy values in the water equivalent phantom in the tables and graphics will be the source of all clinical studies that can be done based on the water phantom in nuclear medicine. It is also clear that it is the source of operations performed with different methods in patients, pharmaceutical industry and nuclear facilities. The radiation sources used here are monoenergetic Alpha, Beta (electron and positron) and Gamma radiation sources stored in a water-equivalent phantom, and their energies, absorption doses and dose distributions have been investigated in order to be used in radiotherapy studies.

As a result of the radiation dose calculations, in the experimental measurement and simulation model of the interaction of the CsI(Tl) scintillator, which is frequently used in nuclear physics applications, with the Co-60 radioactive source, which is also used in the treatment of cancer in radiotherapy, Co-60 radiation was used to investigate which interaction type is more dominant in a certain energy range. the source is positioned at different angles to the CsI(Tl) detector block. The aim here is to find the ideal angle value and the results of the scattering process are focused. In this way, it has been seen that both the photoelectric effect and the dominance of Compton scattering give important clues about the interaction of the scintillation crystal with radiation. In this way, it has been seen that high Z numbers (with 99.98% sensitivity) for gamma rays and low Z numbers (with 99.9% sensitivity) for beta particles can be used. As a result of this situation, it becomes possible to detect isotopes, that is, to distinguish energy. It has also been demonstrated that it can be used to measure both high and low background environmental radiation levels.

Within the framework of finding the ideal angle value in the interaction of radiation with the material and its results, some new types of detector systems were designed and their effects in different application areas were focused. These areas are focused on radiation leaks in nuclear power plants and the determination of radiation in nuclear installations and oil/gas installations and their effects on human health. The main purpose of 3-layer detector systems, which can be used in molecular imaging systems for these purposes, is to simultaneously detect alpha, beta particles and gamma rays emitted from different radioactive sources (especially NORM-Pb210-K40-Sr90). The importance of such detector systems was first felt at the Fukushima Daichii nuclear power plant accident in Japan. The content of the radiation leak that spread to the environment and the atmosphere as a result of the accident could not be detected very quickly and in a short time. It has been seen that such studies, which will gain more importance in the future, can be used in different fields. For example, it was concluded that it could be used in nuclear installations or decommissioning, oil/gas installations, as well as in the development of Gamma cameras, which are widely used in nuclear medicine, in the diagnosis of cancer in the pharmaceutical industry, or in the determination of drug radiation dose, or in the safety procedures of nuclear power plants. In this thesis, it has become possible to make more precise measurements by using different geometries and new generation different scintillation materials compared to previous studies. Because these radiation sources are widely used in nuclear power plants, nuclear physics and nuclear medicine applications, and they are radiation sources that are known to exist naturally and have great effects on human health.

APPENDIX 1. Dose Calculation with Water Phantom on Gate Simulation

Codes run for the calculation of the Dose and Deposited Energy with different radiation sources using the Water Phantom in the Gate simulation program.

```
#========================================
# VISUALISATION
#========================================
#/vis/open OGLSQt
/vis/open OGLIQt
/vis/viewer/set/viewpointThetaPhi            60 30
/vis/viewer/zoom                             15
#/vis/viewer/set/background                  white
/vis/viewer/set/style surface
/vis/drawVolume
/vis/scene/add/trajectories
#/vis/scene/add/hits
/tracking/storeTrajectory 1
/vis/scene/endOfEventAction accumulate 10000
/vis/viewer/update
#/vis/viewer/refresh
/gate/geometry/setMaterialDatabase   GateMaterials.db
#/vis/disable
#==============================================
#    W O R L D
#==============================================
/gate/world/geometry/setXLength              300 cm
/gate/world/geometry/setYLength              300 cm
/gate/world/geometry/setZLength             300 cm
/vis/scene/add/axes
# ============SCANNER ======================
/gate/world/daughters/name                   scanner
/gate/world/daughters/insert                 box
/gate/scanner/geometry/setXLength                 50 mm
/gate/scanner/geometry/setYLength                 50 mm
/gate/scanner/geometry/setZLength                 50 mm
/gate/scanner/placement/setTranslation      0.0 0.0 25.25 mm
/gate/scanner/setMaterial                                 Air
/gate/scanner/vis/setColor                                   green
/gate/scanner/vis/forceWireframe
/gate/scanner/vis/setVisible                                 1

/gate/scanner/daughters/name                fantom
/gate/scanner/daughters/insert             box
/gate/fantom/geometry/setXLength            50 mm
/gate/fantom/geometry/setYLength            50 mm
/gate/fantom/geometry/setZLength            50 mm
/gate/fantom/placement/setTranslation          0 0 0 mm
/gate/fantom/setMaterial                     Water
/gate/fantom/vis/setColor                    blue
/gate/fantom/vis/forceSolid
/gate/fantom/vis/setVisible                 1
 #ATTACH SYSTEM
/gate/systems/scanner/level1/attach         fantom
# ATTACH LAYER
/gate/fantom/attachCrystalSD
#==============================================
#  P H Y S I C S
/gate/physics/addPhysicsList                 emstandard
#/gate/physics/addProcess         PositronAnnihilation   e+
/gate/physics/processList                    Initialized
/gate/physics/Gamma/SetCutInRegion           scanner 0.1 mm
/gate/physics/Positron/SetCutInRegion        scanner 0.1 mm
/gate/physics/Gamma/SetCutInRegion           fantom 0.1 mm
/gate/physics/Positron/SetCutInRegion        fantom 0.1 mm
#==========================================
#############  SOURCES   ###############
/gate/source/addSource                            Source3
/gate/source/Source3/gps/particle                   alpha
/gate/source/Source3/gps/ene/type                  Mono
/gate/source/Source3/gps/ene/mono          18 MeV
```

```
/gate/source/Source3/gps/ang/type                    iso
/gate/source/Source3/gps/pos/type             Volume
/gate/source/Source3/gps/pos/shape            Sphere
/gate/source/Source3/gps/pos/radius            5 mm
/gate/source/Source3/gps/pos/centre               0. 0. 0 mm
/gate/source/Source3/setActivity      370000 Bq #121040 Bq
/gate/source/Source3/visualize                1000 magenta 2
#####gamma # e- #e+ # alpha different radiation type #####
##### 6, 12, 15, 18, 20 MeV different energy values ######
#============================================
# D A T A   O U T P U T
#/gate/output/root/enable
#/gate/output/root/setFileName         output/dose/alpha.txt
#/gate/output/root/setRootSinglesFlag                  1
#/gate/output/root/setRootOpticalFlag                  0
#/gate/output/root/setRootNtupleFlag                   0
#/gate/output/root/setRootSinglesOpticaladderFlag   0
#/gate/output/root/setRootSinglesReadoutFlag          1
#/gate/output/root/setRootSinglesSpblurringFlag       0
#/gate/output/root/setsetRootSinglesBlurringFlag      0
#/gate/output/root/setRootSinglesThresholderFlag      1
#/gate/output/root/setRootSinglesUpholderFlag         0
#/gate/output/root/setRootRecordFlag                  0
#/gate/output/root/setSaveRndmFlag                    0
#/gate/output/analysis/disable
#/gate/output/fastanalysis/enable
#============================================
#  M E A S U R E M E N T   S E T T I N G S (TimeSlice = for updating geometry for movement)
#============================================
#/gate/application/setTotalNumberOfPrimaries         5000000
#/gate/application/setNumberOfPrimariesPerRun      26883855

#/gate/application/setTimeSlice                          60 s
#/gate/application/setTimeStart                          0 s
#/gate/application/setTimeStop                           60 s
#/gate/output/allowNoOutput
#/gate/application/startDAQ
```

APPENDIX 2. Detection of Co-60 Emission by a CsI Detector on GEANT4

Some codes run for Co-60 radiation source at different angles and positions by using CsI scintillation material in Geant4 simulation program.

```
#include "CsIDetectorConstruction.hh"
#include "G4Material.hh"
#include "G4Element.hh"
#include "G4NistManager.hh"
#include "G4Box.hh"
#include "G4LogicalVolume.hh"
#include "G4PVPlacement.hh"
#include "G4SystemOfUnits.hh"
#include "G4VisAttributes.hh"
#include <math.h>
CsIDetectorConstruction::CsIDetectorConstruction()
{}
CsIDetectorConstruction::~CsIDetectorConstruction()
{}
G4VPhysicalVolume* CsIDetectorConstruction::Construct()
{
        // Useful names
        G4String name, symbol;
        G4bool checkOverlaps = true;
        // Materials
        G4NistManager* nist = G4NistManager::Instance();
        G4Material* air = nist->FindOrBuildMaterial("G4_AIR");
        // Caesium iodide definition
        G4Element* caesium = new G4Element("Caesium", "Cs", 55., 132.90545*g/mole);
        G4Element* iodine = new G4Element("Iodine", "I", 53., 126.904473*g/mole);
        G4Material* CsI = new G4Material("CsI", 4.51*g/cm3, 2);
        CsI->AddElement(caesium, 1);
        CsI->AddElement(iodine, 1);
        // Definition of the volumes (world and cryst)
        // World
        G4VSolid* world = new G4Box("World", 2.*m, 2.*m, 2.*m);
        G4LogicalVolume* world_log = new G4LogicalVolume(world, air, "World");
        G4VPhysicalVolume* physWorld = new G4PVPlacement(G4Transform3D(), world_log,
        "World", 0, false, 0);
        // Definition of the crystal volüme
        G4double crystX = 1.27 * cm;
        G4double crystY = 2.54 * cm;
        G4double crystZ = 15.24 * cm;
        G4VSolid* cryst = new G4Box("Cryst", crystX / 2., crystY / 2., crystZ / 2.);
        G4LogicalVolume* cryst_log = new G4LogicalVolume(cryst, CsI, "Cryst");
        new G4PVPlacement(0, G4ThreeVector(0., 0., 0.), cryst_log, "Cryst", world_log  false, 0, checkOverlaps);
        // For the visualisation
        world_log->SetVisAttributes(G4VisAttributes::GetInvisible());
        G4VisAttributes* cryst_vis = new G4VisAttributes(G4Colour(1., 1., 0., .5));
        cryst_vis->SetDaughtersInvisible(false);
        cryst_vis->SetForceSolid(true);
        cryst_log->SetVisAttributes(cryst_vis);
        return physWorld
```

APPENDIX 3. Phoswich Detector System On Gate Simulation

The codes of the three-layer Alpha, Beta, Gamma detector system run in the Gate simulation program.

```
#==============================================
# VISUALISATION
#==============================================
#/vis/open OGLSQt
/vis/open OGLSQt #IQt
/vis/viewer/set/viewpointThetaPhi              60 30
/vis/viewer/zoom                               15
#/vis/viewer/set/background                    white
#/vis/viewer/set/style surface
/vis/drawVolume
/vis/scene/add/trajectories
/vis/scene/add/hits
#/tracking/storeTrajectory 1
#/vis/scene/endOfEventAction accumulate 10000
/vis/viewer/update
/vis/viewer/refresh
/gate/geometry/setMaterialDatabase  GateMaterials.db
#/vis/disable
#================================================
#    W O R L D
#================================================
/gate/world/geometry/setXLength                300 cm
/gate/world/geometry/setYLength                300 cm
/gate/world/geometry/setZLength               300 cm
/vis/scene/add/axes
#==============================================
#ATTACH SYSTEM
/gate/systems/scanner/level1/attach           det1
/gate/systems/scanner/level2/attach            det2
/gate/systems/scanner/level3/attach            det3
# ATTACH LAYER
#/gate/det1/attachCrystalSD                    #Alpha
#/gate/det2/attachCrystalSD                    #Beta
/gate/det3/attachCrystalSD                     #Gamma
```

```
#================================================
#  P H Y S I C S
#================================================
/gate/physics/addPhysicsList                    emstandard
/gate/physics/addProcess            PositronAnnihilation  e+
/gate/physics/processList                       Initialized
/gate/physics/Gamma/SetCutInRegion              det1 0.1 mm
/gate/physics/Positron/SetCutInRegion           det1 0.1 mm
# I N I T I A L I Z E
/gate/run/initialize
#==============================================
#  Random generator
/gate/random/setEngineSeed                      auto
#==============================================
# DIGITIZER And Photoelectrons
#==============================================
/gate/digitizer/Singles/enable
/gate/digitizer/Singles/insert                  readout
/gate/digitizer/Singles/readout/setDepth        1
############## SOURCES ####################
######## Am241 - Alpha source ###############
#/gate/source/addSource                                  Source1
#/gate/source/Source1/gps/particle                       alpha
#/gate/source/Source1/gps/ene/type                       Mono
#/gate/source/Source1/gps/ene/mono                       5.5 MeV
#/gate/source/Source1/gps/ang/type                      iso
#/gate/source/Source1/gps/pos/type                       Volume
#/gate/source/Source1/gps/pos/shape                      Cylinder
#/gate/source/Source1/gps/pos/radius                      29.9 mm
#/gate/source/Source1/gps/pos/halfz                         25 mm
#/gate/source/Source1/gps/pos/centre                  0. 0. 0. mm
#/gate/source/Source1/setActivity                        2000 Bq
#/gate/source/Source1/visualize                      200 blue 5
```

```
############## Strontium90-Beta Source ##############

#/gate/source/addSource                         beta

#/gate/source/beta/gps/particle                 e+

#/gate/source/beta/setActivity                  100 Bq

#/gate/source/beta/gps/ang/type                             iso

#/gate/source/beta/gps/pos/type                             Volume

#/gate/source/beta/gps/pos/shape                            Cylinder

#/gate/source/beta/gps/pos/radius                           29.5 mm

#/gate/source/beta/gps/pos/halfz                              25 mm

#/gate/source/beta/gps/pos/centre               0. 0. 0.  mm

#/gate/source/beta/setForcedUnstableFlag                    true

#/gate/source/beta/setForcedHalfLife            907921440 s

#/gate/source/beta/visualize                    2000 green 5

#/gate/source/list

#########  Cs137-Gamma photons ##################

/gate/source/addSource                                      Source3

/gate/source/Source3/gps/particle                           gamma

/gate/source/Source3/gps/ene/type                           Mono

/gate/source/Source3/gps/ene/mono                           662 keV

/gate/source/Source3/gps/ang/type                           iso

/gate/source/Source3/gps/pos/type                           Volume

/gate/source/Source3/gps/pos/shape                          Cylinder

/gate/source/Source3/gps/pos/radius                         29.0 mm

/gate/source/Source3/gps/pos/halfz                            25 mm

/gate/source/Source3/gps/pos/centre                   0. 0. 0. mm

/gate/source/Source3/setActivity          370000 Bq #121040 Bq

/gate/source/Source3/visualize                  1000 magenta 2

#==========================================
```

```
# D A T A   O U T P U T

/gate/output/root/enable

/gate/output/root/setFileName          det3_gamma10million

/gate/output/root/setRootSinglesFlag                    1

#/gate/output/root/setRootOpticalFlag                   0

#/gate/output/root/setRootNtupleFlag                    0

#/gate/output/root/setRootSinglesOpticaladderFlag       0

#/gate/output/root/setRootSinglesReadoutFlag            1

#/gate/output/root/setRootSinglesSpblurringFlag         0

#/gate/output/root/setsetRootSinglesBlurringFlag        0

#/gate/output/root/setRootSinglesThresholderFlag        1

#/gate/output/root/setRootSinglesUpholderFlag           0

#/gate/output/root/setRootRecordFlag                    0

#/gate/output/root/setSaveRndmFlag                      0

#/gate/output/analysis/disable

#/gate/output/fastanalysis/enable


#============================================

#   M E A S U R E M E N T   S E T T I N G S (TimeSlice = for
updating geometry for movement)

#/gate/application/setTotalNumberOfPrimaries       100

#/gate/application/setNumberOfPrimariesPerRun    26883855

#/gate/application/setTimeSlice                              60 s

#/gate/application/setTimeStart                         0 s

#/gate/application/setTimeStop                          60 s

#/gate/output/allowNoOutput

#/gate/application/startDAQ
```

APPENDIX 4. Comparison of Phoswich Detector Systems For NORM in Nuclear and Oil/Gas Pipeworks

The codes of the three-layer cylindrical Gamma, Beta, Alpha phoswich detector system run in the Gate simulation program.

```
#=================================================
# VISUALISATION
#=================================================
/vis/open OGLSQt
/vis/open OGLSQt #IQt
/vis/viewer/set/viewpointThetaPhi          60 30
/vis/viewer/zoom                           15
#/vis/viewer/set/background                white
/vis/viewer/set/style surface
/vis/drawVolume
/vis/scene/add/trajectories
/vis/scene/add/hits
/tracking/storeTrajectory 1
/vis/scene/endOfEventAction accumulate 100000
/vis/viewer/update
/vis/viewer/refresh
/gate/geometry/setMaterialDatabase   GateMaterials.db
#/vis/disable
#=================================================
#   P H Y S I C S
#=================================================
/gate/physics/addPhysicsList               emstandard
/gate/physics/addProcess          PositronAnnihilation  e+
/gate/physics/processList                  Initialized
/gate/physics/Gamma/SetCutInRegion         det1 0.1 mm
/gate/physics/Positron/SetCutInRegion      det1 0.1 mm
#==================================================
# I N I T I A L I Z E
/gate/run/initialize
#  Random generator
#=================================================
```

```
/gate/random/setEngineSeed                  auto
#=================================================
# DIGITIZER And Photoelectrons
#=================================================
/gate/digitizer/Singles/enable
/gate/digitizer/Singles/insert                          readout
/gate/digitizer/Singles/readout/setDepth                1
#################### SOURCES ######################
######### 1-Alpha Source ( Pb-210  ) #####################
#/gate/source/addSource                                 Source1
#/gate/source/Source1/gps/particle                      alpha
#/gate/source/Source1/gps/ene/type                      Mono
#/gate/source/Source1/gps/ene/mono          5.305 MeV
#/gate/source/Source1/gps/angtype                      iso
#/gate/source/Source1/gps/pos/type          Volume
#/gate/source/Source1/gps/pos/shape         Cylinder
#/gate/source/Source1/gps/pos/radius                      7.5 mm
#/gate/source/Source1/gps/pos/halfz                       25 mm
#/gate/source/Source1/gps/pos/centre        0. 37.625 0. mm
#/gate/source/Source1/setActivity                       0.4 Bq
#/gate/source/Source1/visualize             200 blue 5
#/gate/source/list
########## 2- Strontium90- Beta Source ##############
#/gate/source/addSource                                 beta
#/gate/source/beta/gps/particle                         e+
#/gate/source/beta/setActivity                          100 Bq
#/gate/source/beta/gps/ang/type                         iso
#/gate/source/beta/gps/pos/type                         Volume
#/gate/source/beta/gps/pos/shape                        Cylinder
#/gate/source/beta/gps/pos/radius                       1 mm
#/gate/source/beta/gps/pos/halfz                          25 mm
```

```
#/gate/source/beta/gps/pos/centre           0. 30.625 0. mm
#/gate/source/beta/setForcedUnstableFlag              true
#/gate/source/beta/setForcedHalfLife        907921440 s
#/gate/source/beta/visualize                2000 green 5
/gate/source/list
##########  3- Gamma Photons (K-40) ##################
/gate/source/addSource                                Source3
/gate/source/Source3/gps/particle                     gamma
/gate/source/Source3/gps/ene/type                     Mono
/gate/source/Source3/gps/ene/mono                     1.45 MeV
/gate/source/Source3/gps/ang/type                     iso
/gate/source/Source3/gps/pos/type                     Volume
/gate/source/Source3/gps/pos/shape                    Cylinder
/gate/source/Source3/gps/pos/radius              0.549 mm
/gate/source/Source3/gps/pos/halfz                     12 mm
/gate/source/Source3/gps/pos/centre         0. 1. 0. mm
/gate/source/Source3/setActivity          31.31 Bq #121040 Bq
/gate/source/Source3/visualize              1000 magenta 2
#=================================================
# D A T A   O U T P U T
#================================================
/gate/output/root/enable
/gate/output/root/setFileName               Det1_K40-GAMMA
/gate/output/root/setRootSinglesFlag                  1
```

```
#/gate/output/root/setRootOpticalFlag                  0
#/gate/output/root/setRootNtupleFlag                   0
#/gate/output/root/setRootSinglesOpticaladderFlag      0
#/gate/output/root/setRootSinglesReadoutFlag           1
#/gate/output/root/setRootSinglesSpblurringFlag        0
#/gate/output/root/setsetRootSinglesBlurringFlag       0
#/gate/output/root/setRootSinglesThresholderFlag       1
#/gate/output/root/setRootSinglesUpholderFlag          0
#/gate/output/root/setRootRecordFlag                   0
#/gate/output/root/setSaveRndmFlag                     0
#/gate/output/analysis/disable
#/gate/output/fastanalysis/enable
#=================================================
#  M E A S U R E M E N T   S E T T I N G S
#=================================================
/gate/application/setTotalNumberOfPrimaries      10000000
#/gate/application/setNumberOfPrimariesPerRun       26883855
#/gate/application/setTimeSlice                             60 s
#/gate/application/setTimeStart                        0 s
#/gate/application/setTimeStop                         60 s
#/gate/output/allowNoOutput
#/gate/application/start
/gate/application/startDAQ
```

Abbreviations

PMTs	PhotoMultiplier Tubes
SiPM	Silicon PhotoMultiplier
APDs	Avalanche PhotoDiodes
MPPC	Multi Pixel Photon Counter
PET	Positron Emission Tomography
CT	Computed Tomography
CAT	Computerized Axial Tomography
SPECT	Single Photon Emission Computed Tomography
GEANT	GEometry ANd Tracking
GATE	Geant4 Application for Tomographic Emission
MCA	Multi Channel Analyser
C++	General-purpose Computer Programming Language
EM	Electro Magnetic
EC	Electron Capture
NORM	Naturally-Occurring Radioactive Material
CZT	Cadmium Zinc Telluride
CsI	Cesium Iodide
LaBr	Lanthanum Bromide
CeBr	Cerium Bromide
HPGe	High Purity Germanium
GSO	Gadolinium OxyorthoSilicate
GAGG	Gadolinium Aluminium Gallium Garnet
BGO	Bismuth Germanium Oxide
MC	Monte-Carlo
FWHM	Full Width Half Maximum
PPD	Percent Depth Dose
SSD	Source to Surface Distance
LINAC	Lineer Accelerator

Bibliography

1. *Flugge, S., Practical Quantum Mechanics, 2nd ed.; Springer-Verlag, Berlin, 1992.*
2. *Newton, R. G., Scattering Theory of Waves and Particles.; Berlin: Springer, 1982.*
3. *Aytekin H., Nuclear Physics Lecture Notes, Z.K.U., 2009.*
4. *Tanyeli B., Nuclear Physics, Ege University Press, 1994.*
5. *S. K. Krane, Introductory Nuclear Physics, S.K. Krane, John Wiley and Sons, Inc., 1988.*
6. *Glenn F. Knoll Radiation Detection and Measuements, 2000.*
7. *D. C. Giancoli, Physics, Prentical Hall, New Jersey 7th edition 2014.*
8. *David Jenkins, Radiation Detection for Nuclear Physics Methods and industrial applications, 2020.*
9. *https://vle.york.ac.uk/webapps/blackboard/content/listContent.jsp?course_id=_101577_1&content_id=_4193155_1&mode=reset*
10. *S. Liu, Z. Pan, NORM exposure in China, in: Naturally Occurring Radioactive Material (NORM VII), Proceedings of an International Symposium Beijing, China, 22–26, April, 2013.*
11. *Q. Wu, Y. Yu, Z. Cao, C. Ma, X. Kong, Radionuclide release from the combustion of coal: a case study, in: Naturally Occurring Radioactive Material (NORM VII), Proceedings of an International Symposium Beijing, China, 22–26 April, 2013.*
12. *INTERNATIONAL ATOMIC ENERGY AGENCY, "Radiation protection and the management of radioactive waste in the oil and gas industry", Training course series No. 40, IAEA, Vienna, 2010.*
13. *IAEA NUCLEAR ENERGY SERIES No. NW-T-2.3, "Decommissioning of small medical, industrial and research facilities: a simplified stepwise approach", IAEA, Vienna, 2011.*
14. *INTERNATIONAL ATOMIC ENERGY AGENCY, "decommissioning of facilities". IAEA SAFETY STANDARDS SERIES No. GSR Part 6, IAEA, Vienna, 55 2014.*
15. *Radionuclide concentrations in food and environment (book edited by M-Pöschl and Leo M.L. Nollet, Taylor and Francis, 2007)*
16. *http://www.world-nuclear.org/information-library/nuclear-fuel-cycle/nuclear-wastes/radioactive-waste-management.aspx.*

17. *M.I. Ojovan, W.E. Lee, An Introduction to Nuclear Waste Immobilization, Elsevier, Amsterdam, 2005.*

18. *2012 Fuel Cycle Technologies, Annual Review Meeting, Transactions Report, Argonne National Laboratory, October 30–31, 2012, Department of Energy.*

19. *Testimony of Robert Meyers Principal deputy Assistant Administrator for the Office of Air and Radiation U.S. Environmental Protection Agency before the subcommitee on Energy and Air Quality Committee on Energy and Commerce U. S. House of Representatives, July 15, 2008.*

20. *'Working with ionising radiation. Ionising Radiations Regulations 2017. Approved Code of Practice and guidance', Health and Safety Executive, Series L121 (Second edition), March 2018, ISBN: 9780717666621.*

21. *The Environmental Permitting (England and Wales) (Amendment) (No.2) Regulations 2018.*

22. *Seiichi Y., Jun H., Development of an alpha/beta/gamma detector for radiation monitoring, Review Of Scientific Instruments, 82 (2011) 1-6, 113503.*

23. *Seiichi Y., Hiroyuk I., Development of at threelayer phoswich alpha–beta–gamma imaging detector, Nuclear Instruments and Methods in Physics Research A, (785) (2015) 129–134.*

24. *Yavuzkanat N., Ertürk S., Investigation of the New Generation Detector System Using in Medical Image, Aksaray University Journal of Science and Engineering, 3(2), (2019) 99-111.*

25. *Yavuzkanat N., Jenkins D., Geant4 investigation of the alpha-beta-gamma detector system used in medical imaging, environmental and nuclear site monitoring, Cumhuriyet Science Journal, 42(1), 2021.*

26. *https://en.wikipedia.org/wiki/Monte_Carlo_method#Physical_sciences*

27. *https://geant4.web.cern.ch/*

28. *http://www.opengatecollaboration.org/*

29. *https://en.wikipedia.org/wiki/Potassium-40*

30. *https://www.researchgate.net/figure/The-decay-chain-210-Pb-210-Bi-210-Po-206-Pb-Within-parentheses-the-half-lives-of_fig1_230904327*

31. *https://en.wikipedia.org/wiki/Caesium-137*

32. *https://en.wikipedia.org/wiki/Cobalt-60*

33. *https://www.chemistrylearner.com/strontium-90.html#:~:text=Natural%20Strontium%20(Sr)%20does%20not,(Yttrium%2D90)%20isotope*

34. *https://www.epa.gov/radiation/radionuclide-basics-americium-241#:~:text= Americium%20(chemical%20symbol%20Am)%20is,most%20common%20form%20of %20Americium.*

35. *https://www.crystals.saint-gobain.com/radiation-detection-scintillators/crystal-scintillators/csi-cesium-iodide*

36. *Karl A. Franz, Wolfgang G. Kehr, Alfred Siggel, Jürgen Wieczoreck, and Waldemar Adam "Luminescent Materials" in Ullmann's Encyclopedia of Industrial Chemistry 2002, Wiley-VCH, Weinheim.*

37. *https://eljentechnology.com/products/plastic-scintillators/ej-200-ej-204-ej-208-ej-212*

38. *Yavuzkanat N., Development of Novel Scintillation Detection Techniques for Use in Nuclear Physics and Medical Applications, Doctor of Philosophy thesis, University of York, 2015.*

39. *https://oncologymedicalphysics.com/photon-dose-distributions/*

40. *https://aapm.onlinelibrary.wiley.com/doi/epdf/10.1118/1.598691*

41. *F. Nielsen, M. Jonsson, Journal of Nuclear Materials 359 (2006) 1–7*

42. *https://pure.york.ac.uk/portal/en/publications/flexible-siliconbased-alphaparticle-detector(904f4ddc-3ef2-4641-8a31-c4bb61073338).html*

43. *https://oncologymedicalphysics.com/electron-therapy-physics/*

44. *https://inis.iaea.org/collection/NCLCollectionStore/Public/20/018/20018529.pdf*

45. *https://www.nature.com/articles/s41529-021-00183-4.pdf*

46. *https://reader.elsevier.com/reader/sd/pii/S2352179120300107?token=77FE6F1CEF59B0CAF32DBF17113B4726813502F7A415801AB38C72DB3D26753A1DF47D1C87E2884F0409A337460EFC97&originRegion=eu-west-1&originCreation=20220423003132*

47. *http://nuclearsafety.gc.ca/eng/resources/radiation/introduction-to-radiation/types-and-sources-of-radiation.cfm*

48. *https://radiopaedia.org/articles/photoelectric-effect*

49. *http://www.futura-sciences.us/dico/d/physics-compton-scattering-50003718/*

50. *http://electrons.wikidot.com/pair-production-and-annihilation*